Eindhoven University of Technology

MASTER

Y/C separation of composite color video signals

Cordes, C.N.

Award date:
2003

Link to publication

Disclaimer
This document contains a student thesis (bachelor's or master's), as authored by a student at Eindhoven University of Technology. Student theses are made available in the TU/e repository upon obtaining the required degree. The grade received is not published on the document as presented in the repository. The required complexity or quality of research of student theses may vary by program, and the required minimum study period may vary in duration.

General rights
Copyright and moral rights for the publications made accessible in the public portal are retained by the authors and/or other copyright owners and it is a condition of accessing publications that users recognise and abide by the legal requirements associated with these rights.

- Users may download and print one copy of any publication from the public portal for the purpose of private study or research.
- You may not further distribute the material or use it for any profit-making activity or commercial gain

Take down policy
If you believe that this document breaches copyright please contact us providing details, and we will remove access to the work immediately and investigate your claim.

Download date: 07. 11月. 2025

TU/e technische universiteit eindhoven

Faculty of Electrical Engineering
Section Design Technology For Electronic Systems (ICS/ES)
ICS-ES 814

Master's Thesis

Y/C SEPARATION OF COMPOSITE COLOR VIDEO SIGNALS.

C.N. Cordes

Coach:	Dr.ing.habil. C. Hentschel (Philips Research)
Supervisor:	prof.dr.ir. G. de Haan
Date:	February 2003

The Faculty of Electrical Engineering of the Eindhoven University of Technology does not accept any responsibility regarding the contents of Master's Theses

Abstract

For analog color television standards such as PAL and NTSC, the requirement of backward compatibility to existing black-and-white televisions dictates that the transmission of color has to take place within the band available for the gray-scales. For that purpose, the color component (C) is modulated onto a subcarrier and added to the gray-scale component (Y), and the resulting composite color video signal is used for transmission.

At the television receiver, the required separation of Y and C can only be imperfect as both components now share the same frequency space. Modern televisions apply so-called comb-filters that exploit the opposite chrominance phase of adjacent samples to separate both components. However, cross-talk artifacts and loss of resolution continue to appear in situations where few samples meet the strict requirements of the used comb-filter kernel.

In this report, a novel comb-filter kernel is proposed that uses samples with non-opposite chrominance phases for Y/C separation. To exploit these additional decoding options, a comb-filter is proposed that locally selects the comb-filter kernel that yields superior results. Subjective and objective evaluations have shown that the proposed comb-filter achieves a significant increase in luminance resolution and reduction of cross-talk artifacts when compared to current high-end comb-filters.

The work described in this report has been carried out within the Video Processing and Visual Perception group of Philips Research Eindhoven, The Netherlands, from April 8th 2002 until January 8th 2003. I am indebted to my supervisors Gerard de Haan and Christian Hentschel, who contributed greatly to my work. Thanks are also due to Hans Puttenstein, Michel Nieuwenhuizen and Matthijs Piek for their critical and careful review of this report. Finally, I would like to thank my group leader, Geert Depovere, for giving me the opportunity to perform this work within his group.

Contents

1 Introduction **6**
- 1.1 Principles of color coding 7
- 1.2 Standard decoder 8

2 Comb-filtering state-of-the-art **12**
- 2.1 Principles of comb-filtering 12
- 2.2 2D adaptive comb-filters 18
- 2.3 3D motion adaptive comb-filters 19
  - 2.3.1 Generic filter structure 19
  - 2.3.2 Filter proposed by Philips 21
- 2.4 3D motion compensated comb-filters 23
  - 2.4.1 PAL filter 23
  - 2.4.2 NTSC filter 29
  - 2.4.3 Conclusions 32
- 2.5 Literature survey 32

3 Novel decoding principle **35**
- 3.1 Principles 35
- 3.2 Identical V-switches 36
- 3.3 Non-identical V-switches 43
- 3.4 Conclusions 44

4 Implementations of the new decoder **47**
- 4.1 Candidate selection 48
  - 4.1.1 Up-sampling 48
  - 4.1.2 Dynamic window resizing 49
  - 4.1.3 Candidate set 50
- 4.2 Penalty calculation 53
  - 4.2.1 Identical V-switches 54
  - 4.2.2 Non-identical V-switches 55
  - 4.2.3 Three sample decoder 57
- 4.3 Decoder configurations 59
  - 4.3.1 Selection techniques 59

4.3.2 Chrominance derived from luminance 61
4.3.3 Luminance derived from chrominance 62
4.3.4 Recursive comb-filtering 63

5 Evaluation of the new decoder 64
5.1 Decoder parameters 67
5.1.1 Up-sampling and window size 67
5.1.2 Dynamic window resizing 68
5.1.3 Individual versus combined comb-filter kernels 69
5.1.4 Median filtering and Y/C derivation 71
5.1.5 Candidate set configurations 73
5.1.6 Recursive comb-filtering 75
5.2 Comparison to reference filters 77
5.2.1 Evaluation of reference filters 79
5.2.2 Comparison on noise-free sequences 81
5.2.3 Comparison on noise-corrupted sequences 83
5.2.4 *Moving zoneplate* comparison 85

6 Conclusions and recommendations 88
6.1 Conclusions 88
6.2 Recommendations 89

A Filters 93

B Decoded *Moving zoneplate* 95

C Literature research 99
C.1 Snowball method 99
C.2 Citation method 101
C.3 Conclusions 102

List of Figures

1.1 Spectrum of the composite PAL video signal. 7
1.2 Simplified block diagram of the PAL encoder. 8
1.3 Simplified block diagram of the standard PAL decoder. 9
1.4 Luminance notch and chrominance band-pass filters for PAL. 9
1.5 Examples of cross-color and cross-luminance artifacts. 10

2.1 Frequency interleaving of luminance and chrominance. 13
2.2 Amplitude frequency response of PAL comb-filter. 14
2.3 Subcarrier phase pattern for PAL and NTSC. 16
2.4 Line, field and frame comb-filters for PAL. 17
2.5 Examples of 2D adaptive comb-filters. 18
2.6 Generic 3D motion adaptive comb-filter. 20
2.7 3D motion adaptive comb-filter developed by Philips PDSL. . 21
2.8 Suitable motion vectors for PAL. 24
2.9 Transv. and recursive motion compensated PAL comb-filters. 26
2.10 Hybrid motion compensated PAL comb-filters. 27
2.11 Motion compensated comb-filter for NTSC. 29
2.12 Possible motion vectors for NTSC. 31

3.1 Addition of noise to represent imperfect correlation. 38
3.2 Varying relative and absolute phases. 39
3.3 Identical V-switches: SNR of Y for relative phases. 41
3.4 Identical V-switches: SNR of Y for absolute phase. 41
3.5 Identical V-switches: SNR of U for absolute phase. 42
3.6 Identical V-switches: SNR of V for absolute phase. 42
3.7 Non-identical V-switches: SNR of Y for relative phases. . . . 45
3.8 Non-identical V-switches: SNR of Y for absolute phase. . . . 45
3.9 Non-identical V-switches: SNR of U for absolute phase. . . . 46
3.10 Non-identical V-switches: SNR of V for absolute phase. . . . 46

4.1 Noise measurement in *Cross-color couple* sequence. 50
4.2 Candidate windows at fixed and motion compensated positions. 51
4.3 Examples of temporal candidate sets. 52
4.4 Phase penalty for samples with identical V-switches. 54

4.5 Phase penalty for samples with non-identical V-switches. . . . 55
4.6 Candidates on a 2D correlation/phase plane. 56
4.7 Flowchart of proposed comb-filter. 57
4.8 Standard decoder with optional luminance median filter. . . . 60
4.9 Decoder configurations using derived Y and C. 62
4.10 Decoder configurations for 2D and 3D recursive comb-filtering. 63

5.1 Calculation of MSE for luminance and chrominance. 65
5.2 Snapshots of the test sequences. 66
5.3 MSE (Y,C) for candidate set size and up-sampling factor. . . 67
5.4 MSE (Y,C) for fixed and dynamic window sizes. 68
5.5 MSE (Y) for individual and combined decoders. 69
5.6 MSE (Y) for standard/median decoder and C_{sub}, Y_{sub}, YC_{sub}. 71
5.7 Examples of artifacts for various decoder configurations. . . . 72
5.8 Relative MSE (Y) for various candidate set configurations. . 74
5.9 Examples of cross-luminance and cross-color artifacts. 76
5.10 MSE (Y) of transversal and recursive 2D and 3D comb-filters. 77
5.11 MSE (Y,C) comparison of reference and proposed comb-filters. 80
5.12 Comparison of decoding artifacts. 82
5.13 Relative MSE (Y) for various comb-filters and noise levels. . 84

A.1 Luminance notch and chrominance band-pass filter. 93
A.2 U and V low-pass filter. 93
A.3 Luminance and chrominance low-pass pre-filter. 94
A.4 CVBS up-sampling low-pass filter. 94

B.1 Location of chrominance components in *Moving zoneplate*. . . 95
B.2 Decoded *Moving zoneplate* of 1D and 2D comb-filters. 96
B.3 Decoded *Moving zoneplate* of field-based 3D comb-filters. . . 97
B.4 Decoded *Moving zoneplate* of frame-based 3D comb-filters. . . 98

C.1 Snowball method 101
C.2 Citation method 103

Chapter 1

Introduction

In analog encoded television signals, the gray-value (Y, luminance) and color (C, chrominance) components share the same frequency space. Therefore, separation of both components can only be imperfect, which results in visible artifacts known as cross-color and cross-luminance. The early PAL/NTSC decoders used a horizontal notch filter in the luminance path to suppress the chrominance components, thereby inherently attenuating the horizontal high-frequency luminance components. In the chrominance path, a band-pass filter passes chrominance and high-frequency luminance components, but suppresses the low-frequency luminance components. Hence, the standard PAL/NTSC decoder suffers from a loss of horizontal luminance resolution and strong cross-luminance and cross-color artifacts.

So called comb-filters aim at an improved Y/C separation by exploiting the opposite chrominance phase of certain vertically or temporally adjacent samples. However, only comb-filtering of highly correlated samples results in satisfactory Y/C separation. Particularly in vertically detailed and/or moving areas, insufficient samples meet the required correlation and chrominance phase, which results in the appearance of cross-talk artifacts and the vertical or temporal loss of resolution. Although comb-filters yield significant improvements in quality over the early decoders, cross-talk artifacts remain due to the strict comb-filter requirements.

In this report, the principles of comb-filtering are introduced in Chapter 2, and followed by the description of the current state-of-the-art comb-filters. In Chapter 3, a novel comb-filter kernel is proposed that is able to use samples with non-opposite chrominance phases for Y/C separation. To exploit these additional decoding options, a comb-filter is proposed in Chapter 4 that adaptively combines multiple comb-filter kernels by locally selecting a kernel that is expected to yield superior results. In Chapter 5, the performance of the proposed filter is evaluated and compared to current high-end comb-filters. Finally, conclusions and recommendations for further developments are given in Chapter 6.

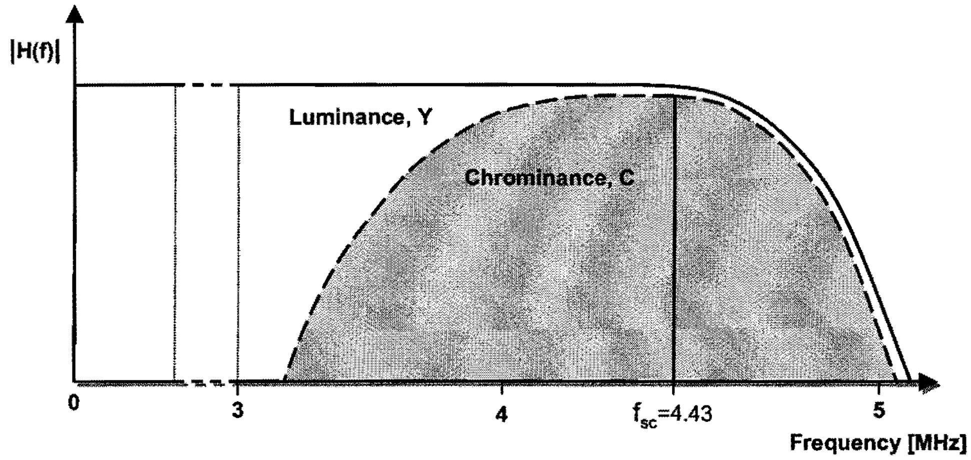

Figure 1.1: Spectrum of the composite PAL video signal.

1.1 Principles of color coding

In order to fully comprehend the problems involved in Y/C separation, one has to understand the standards for the transmission of analog color television signals, such as the PAL, NTSC and SECAM standards described in ITU-R BT.470. For these standards, the requirement of backward compatibility to existing black-and-white televisions dictates that the transmission of color (*chrominance*) has to take place within the band available for the gray-scales (*luminance*). For that purpose, the chrominance, which consists of the chrominance components U and V, is modulated onto a subcarrier F_{sc} and added to the luminance signal Y.

To reduce the required chrominance bandwidth, the chrominance components are bandwidth limited to approximately 1.3MHz prior to encoding. This does not lead to severe quality loss, as the human visual system is less sensitive to chrominance resolution than to luminance resolution. The *modulated chrominance* C now occupies the upper part of the luminance frequency band, but the original signal bandwidth is not extended.

For PAL, the chrominance components U and V are amplitude modulated in quadrature onto a subcarrier frequency of 4.43MHz. The resulting one-dimensional spectrum of the composite PAL video signal is illustrated in Figure 1.1. It can be seen that the chrominance sidebands are of unequal width due to PAL's bandwidth limitation of approximately 5MHz. Furthermore, the sign of the V-component, the so-called *V-switch*, is inverted every other line to reduce the influence of phase errors. If phase errors occur in the modulated chrominance, they will opposite in successive lines (see e.g. [25] pp. 18-19). Therefore, electronic or optical averaging over successive lines will lead to their transformation into less visible amplitude errors.

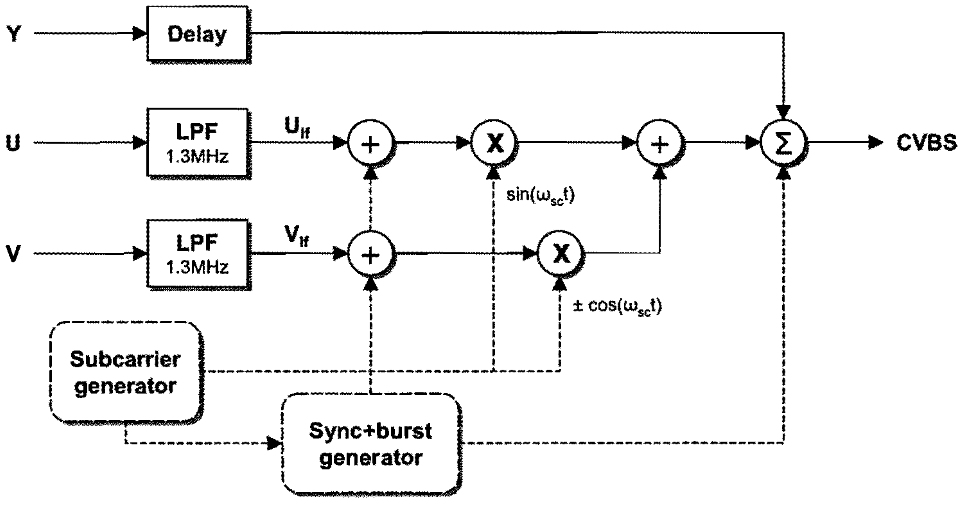

Figure 1.2: Simplified block diagram of the PAL encoder.

More formally, the above is described in Equation 1.1, where $\vec{x}$ indicates the pixel position in a given field n and F_{cvbs} the resulting PAL composite signal. Figure 1.2 shows a simplified block diagram of the PAL encoder.

$$F_{cvbs}(\vec{x},n) = Y(\vec{x},n) + U_{lf}(\vec{x},n)\cdot sin(2\pi F_{sc}t) \pm V_{lf}(\vec{x},n)\cdot cos(2\pi F_{sc}t) \quad (1.1)$$

For NTSC, the somewhat differently defined chrominance components I and Q are amplitude modulated in quadrature onto a subcarrier frequency of 3.58MHz. As no alternating sign is applied to either chrominance component, there is an increased sensitivity to phase errors which can result in an erroneous hue of the decoded picture. The one-dimensional spectrum is similar to that of PAL, except now the available video bandwidth is limited to approximately 4.2MHz. Equation 1.2 formally defines NTSC encoding:

$$F_{cvbs}(\vec{x},n) = Y(\vec{x},n) + I_{lf}(\vec{x},n)\cdot sin(2\pi F_{sc}t) + Q_{lf}(\vec{x},n)\cdot cos(2\pi F_{sc}t) \quad (1.2)$$

For SECAM, frequency modulation is used for the chrominance transmission as opposed to the amplitude modulation used for PAL and NTSC. Furthermore, the chrominance components are transmitted line sequentially. As such, the Y/C separation of SECAM signals differs fundamentally from that of PAL and NTSC, and will not be covered in this report.

1.2 Standard decoder

The standard decoder for PAL and NTSC composite video signals uses two simple one-dimensional horizontal filters to separate luminance and chromi-

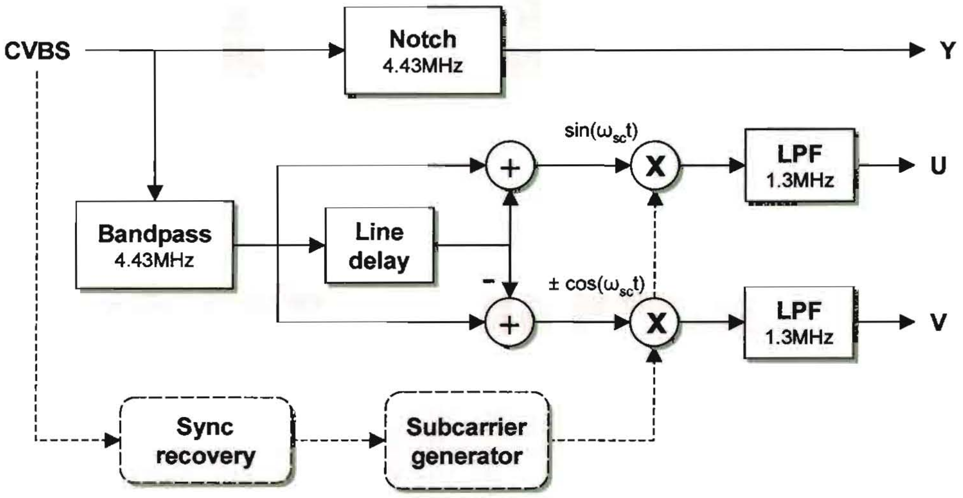
CVBS
Notch
4.43MHz
Y
Bandpass
4.43MHz
Line
delay
+
-
+
sin(ω_sc t)
± cos(ω_sc t)
X
X
LPF
1.3MHz
U
LPF
1.3MHz
V
Sync
recovery
Subcarrier
generator

Figure 1.3: Simplified block diagram of the standard PAL decoder.

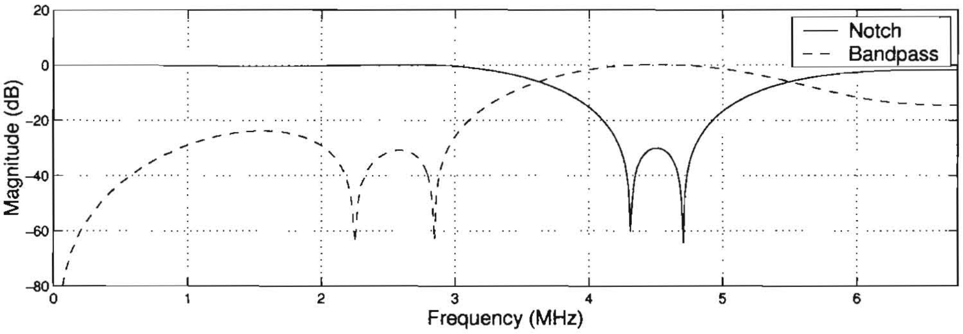

Figure 1.4: Typical PAL luminance notch and chrominance band-pass filters.

nance from the CVBS signal. A simplified block diagram of the standard PAL decoder is shown in Figure 1.3.

In the luminance path, a notch filter suppresses frequencies near the subcarrier frequency to eliminate horizontal chrominance components. The amplitude frequency response of a typical digital PAL notch filter is shown in Figure 1.4. Due to the small stop band of the notch filter, high-frequency chrominance components, as they occur on horizontal colored transitions, will be insufficiently attenuated. This introduces cross-talk from chrominance to luminance, resulting in the so-called *cross-luminance* artifacts. Furthermore, the luminance resolution is significantly reduced, as the notch filter suppresses any luminance components in the stop-band.

An example of a cross-luminance artifact caused by the standard decoder is illustrated in Figure 1.5a, where both the original and the decoded picture

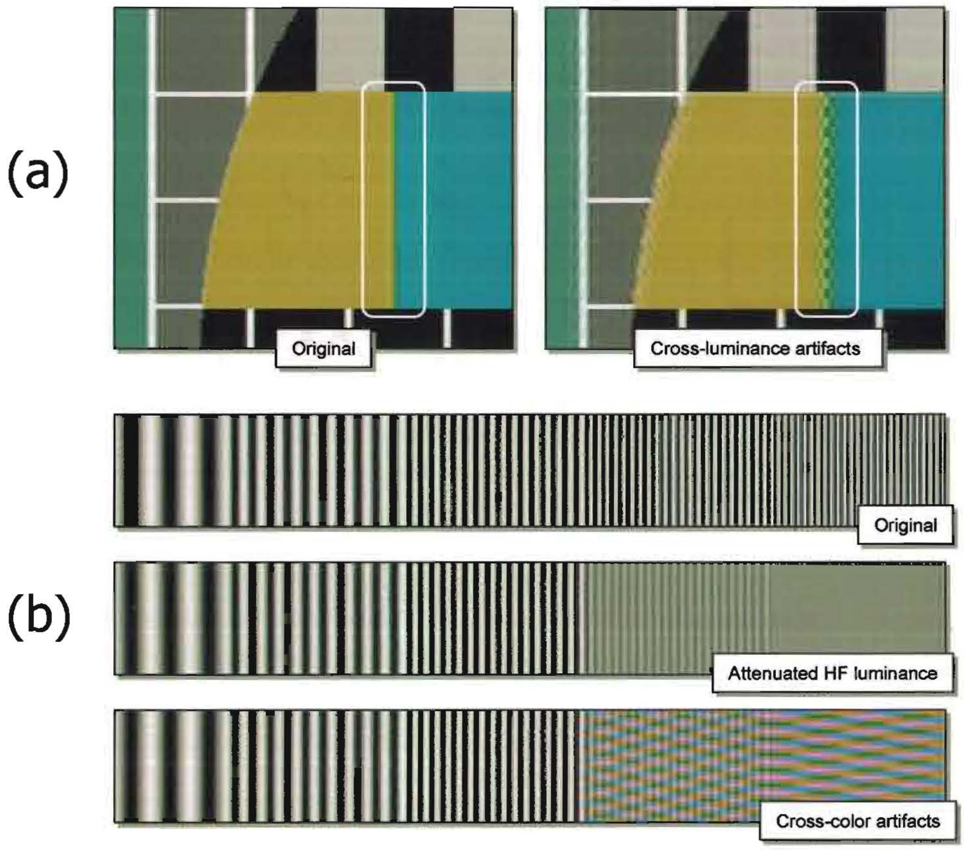

Figure 1.5: Examples of a) cross-luminance artifacts, and b) luminance attenuation and cross-color artifacts (depicted is luminance of increasing frequency from left to right).

are shown. Clearly visible in the highlighted area is the cross-luminance due to cross-talk from the strong horizontal chrominance edge. An example of the reduced luminance resolution is shown in Figure 1.5b, where increasing horizontal luminance frequencies are depicted. Clearly, horizontal high-frequency luminance will be attenuated in the decoded output, as shown in the middle picture.

In the chrominance path, a band-pass filter separates the high frequency components from the composite signal. The amplitude frequency response of a typical PAL band-pass filter is shown in Figure 1.4. It be seen that the notch and band-pass filters are complementary, which enables an implementation using only one filter and the subsequent subtraction from the original CVBS signal.

Although the passband of the band-pass filter contains mostly chrominance information, high-frequency luminance is present as well. Again, cross-talk will occur as the high-frequency luminance will be decoded as chrominance, resulting in the so-called *cross-color* artifacts. In Figure 1.5b, the cross-color artifacts are illustrated in the lower picture. Clearly, high-frequency luminance will be decoded as chrominance, resulting in the depicted cross-color artifacts.

The visibility of these artifacts is somewhat decreased in moving sequences though. Especially the cross-color artifacts, which can be severe in still fields, are attenuated due to the fact that the subcarrier phase changes with each successive field. For example, a red artifact in the current field can change to green in the next field. Due to the temporal integration of the human visual system, these high frequency temporal artifacts will be attenuated.

Furthermore, the amount of cross-talk is highly depended upon the correlation along the horizontal axis. If the luminance and chrominance values of horizontally adjacent samples are identical, the frequency spectrum consists of a luminance component at 0Hz and a chrominance component at the subcarrier frequency. The above band-pass/notch filters now achieve perfect Y/C separation. However, if the correlation along the horizontal axis is insufficient, the frequency spectrum contains high-frequency luminance and/or chrominance components. The horizontal separation is now imperfect and results in severe cross-talk artifacts in the decoded signal.

In Figure 1.3, it can be seen that the band-pass filter in the chrominance path is followed by a so-called *PAL delay line*. Here, the modulated chrominance is separated into the modulated U and V components by the addition and subtraction of two consecutive lines. Because of the alternating V-switch, a phase error occurring in the modulated chrominance will now manifest itself as an amplitude error in the modulated U and V components. This results in a saturation error in the decoded picture instead of the more annoying hue error which is present in NTSC decoding (see [25] pp. 18-19).

A disadvantage of the PAL delay line is the vertical displacement of the chrominance by $\frac{1}{2}$ field line, which is typically not compensated by a corresponding luminance displacement. Furthermore, the vertical chrominance resolution is decreased by the line averaging. The visual impact of both effects, however, is relatively minor due to the human visual system's limited sensitivity to chrominance resolution.

The PAL delay line is followed by the demodulation of the modulated chrominance components. For the V component, the subcarrier is multiplied by the proper sign to cancel the sign alternation. To suppress the double frequency components in the demodulated U and V components, a low-pass filter is applied to the output of the demodulator.

The standard NTSC decoder is highly similar, except that no delay line or sign-alternating demodulation is used. Due to its simplicity, the standard decoder is still in use in low-end and mid-end televisions. However, as it suffers from severe cross-talk and reduced luminance resolution, most high-end televisions nowadays use *comb-filters*, as described in the next chapter.

Chapter 2

Comb-filtering state-of-the-art

The standard decoder described in the previous chapter attempts to separate the luminance and chrominance by applying horizontal band-pass/notch filters to the composite video signal. However, a satisfactory Y/C separation is only obtained in areas with sufficient correlation along the horizontal axis. In areas where horizontally adjacent samples are insufficiently correlated, additional methods for Y/C separation are desirable. For that purpose, so-called *comb-filters* can be used to separate luminance and chrominance along the vertical or temporal axis. Their underlying principles are similar to those of the standard decoder, i.e. passing the desired frequency components and suppressing the undesired frequency components.

2.1 Principles of comb-filtering

To fully understand the principles of comb-filtering, a more detailed view of the composite signal spectrum of PAL and NTSC is required. This can be achieved by imagining a static luminance pattern of identical lines. Within a field, the luminance signal is periodical with period T_h causing harmonics of f_h, i.e. the line frequency, in the spectrum of the signal. Over several fields, the vertical blanking causes a modulation of these harmonics with harmonics of f_v, i.e. the picture frequency. The resulting line spectrum of the luminance signal consists of peaks at $nf_h \pm mf_v$, as shown in Figure 2.1a. Most energy is concentrated at multiples of f_h, with empty spaces in between.

If the color difference signals are modulated onto the subcarrier frequencies of PAL or NTSC, the resulting modulated chrominance signal will have spectral lines at $(n+\frac{1}{2})f_h \pm mf_v$, i.e. between the luminance spectral lines as shown in Figure 2.1b. In turn, the spectral lines of the chrominance components U and V will be located at $(n+\frac{1}{4})f_h \pm mf_v$ and $(n+\frac{3}{4})f_h \pm mf_v$, re-

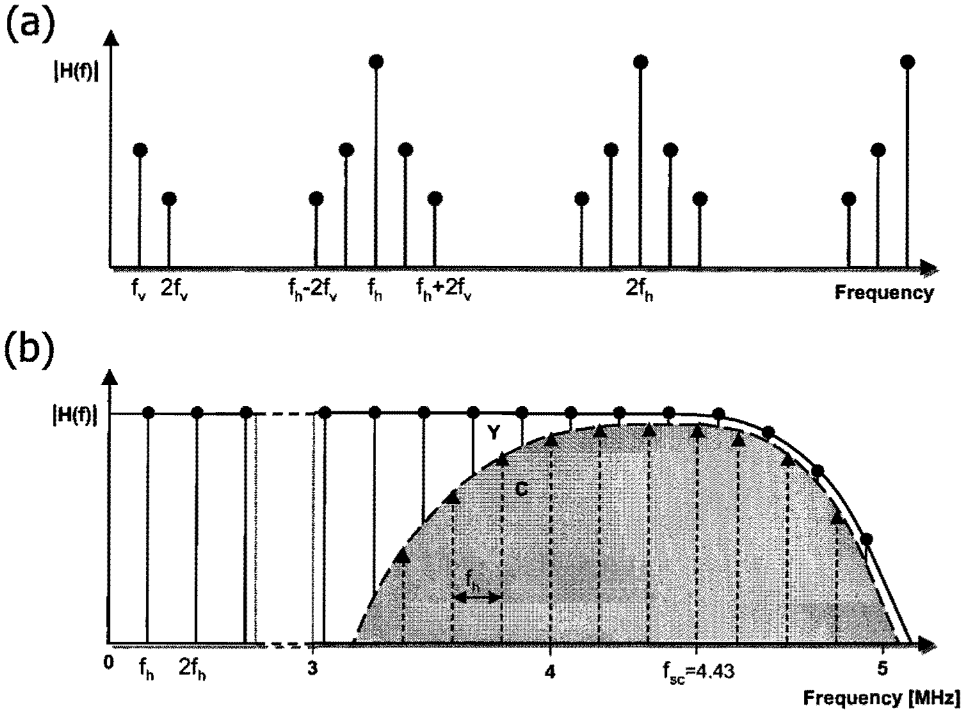

Figure 2.1: a) Luminance line spectrum of a stationary picture, and b) the frequency interleaving of luminance and chrominance.

spectively. This means that for stationary video content, the luminance and chrominance frequency components are interleaved, i.e. non-overlapping, suggesting that perfect separation is possible.

For moving pictures, however, the positions of the spectral lines move along the frequency axis. The new luminance spectral lines are located at $nf_h \pm mf_v + f_m$, where frequency component f_m indicates the amount of motion. For example, if $f_m = \frac{1}{4}f_h = 6.25\text{Hz}$ in the temporal direction, the spectral lines of the luminance now occupy the former positions of the spectral lines of U-component. This means that the frequency lines of the composite signal depend on movements, and even the exchange of the spectral positions of luminance and chrominance is possible.

More elaborate explanations on the one- and multi-dimensional PAL and NTSC spectra can be found in References [19],[20] and [21] of D. Teichner and in References [8] (pp. 99-102) and [25] (pp. 10-25).

Standard comb-filter kernel

The above description of the composite video signal spectrum suggests that, if sufficient correlation is present (i.e. no motion occurs) along a particular

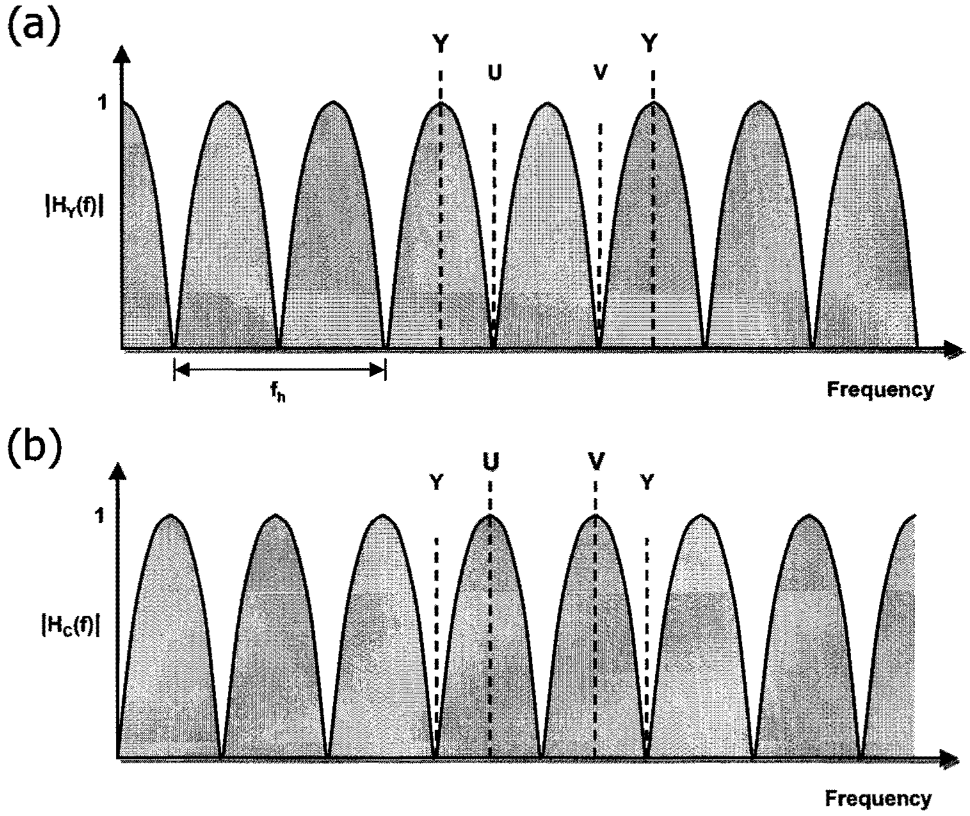

Figure 2.2: Example of the amplitude frequency response of a PAL comb-filter for a) luminance path, and b) chrominance path.

axis, the luminance and chrominance frequency components are interleaved and at fixed positions along that direction. It is possible to exploit this interleaved frequency spectrum by applying a filter that has unity gain at the desired spectral lines and zero gain at the undesired lines, as shown in Figure 2.2 for the luminance and chrominance paths. Filters which exhibit this comb-shaped amplitude frequency response are called *comb-filters*.

The basic principle of comb-filtering is that two samples with opposite relative phases, i.e. having a phase difference of 180°, can be used to separate luminance and chrominance. This can be illustrated by taking a composite sample, F_{cvbs1}, which is encoded at an arbitrary phase ϕ:

$$F_{cvbs1} = Y + U \cdot sin(\phi) + V \cdot cos(\phi)$$

and a second sample F_{cvbs2}, encoded at $\phi + 180°$, of which we assume that it was encoded from identical luminance and chrominance values as F_{cvbs1}:

$$\begin{aligned} F_{cvbs2} &= Y + U \cdot sin(\phi + 180^\circ) + V \cdot cos(\phi + 180^\circ) \\ &= Y - U \cdot sin(\phi) - V \cdot cos(\phi) \end{aligned}$$

Now, the addition of F_{cvbs1} and F_{cvbs2} and subsequent division by two results in the separated luminance Y, whereas the subtraction and subsequent division by two yields the modulated chrominance $U \cdot sin(\phi) + V \cdot cos(\phi)$. The above method can only be applied to PAL if the V-switch of both samples is identical. However, comb-filtering is also possible if the V-switch of both samples differs. In that case, an opposite absolute phase, i.e. $-\phi$, is required for F_{cvbs2}, and again the luminance and chrominance can be separated by an addition and a subtraction:

$$\begin{aligned} F_{cvbs2} &= Y + U \cdot sin(-\phi) - V \cdot cos(-\phi) \\ &= Y - U \cdot sin(\phi) - V \cdot cos(\phi) \end{aligned}$$

However, *perfect* separation is only possible if both CVBS samples were encoded from *identical* Y, U and V values. Only in this case, the positions of the luminance and chrominance frequency components correspond to those of the comb-filter. Therefore, sufficient correlation is required along the comb-filtering direction in order to prevent decoding errors. This is analogous to the horizontal band-pass/notch filters, where sufficient correlation is required along the horizontal axis.

When considering an arbitrary composite sample encoded at phase ϕ, various spatially and/or temporally adjacent samples exhibit the required opposite relative phase $\phi + 180^\circ$. Figures 2.3a and b illustrate the subcarrier phase for PAL and NTSC, respectively, for samples at various vertical and temporal positions. Indicated are pairs of samples that have an opposite phase and thereby represent the three standard comb-filters: the line, field and frame comb-filter. In the following sub-sections, we shall discuss these comb-filters separately in more detail.

Line comb-filter

The so-called *line comb-filter* filters along the vertical axis. For PAL, it uses at least two samples that are separated by one field line. As the resulting comb-filtered values are written back on the original sample grid, a vertical displacement of the decoded output will occur. To avoid such vertical displacement, a line comb-filter is typically implemented as the average of *two* line comb-filter outputs, i.e. a 3-line comb-filter, as illustrated in Figure 2.4a. In NTSC, the line comb-filter is identical except that it operates on directly adjacent lines due to the 180° phase shift from line to line.

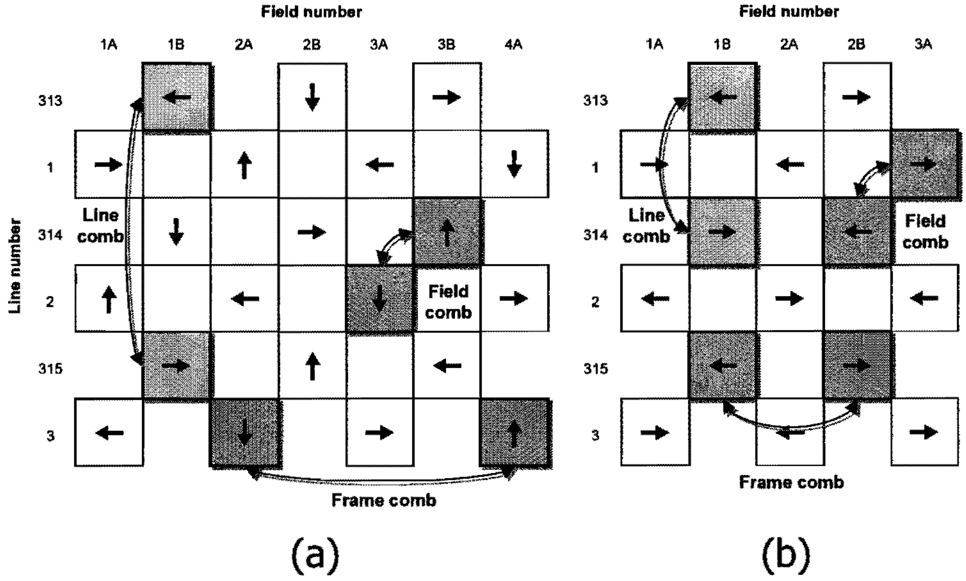

Figure 2.3: Subcarrier phase of samples in adjacent lines for successive fields for a) PAL, and b) NTSC (the horizontal position remains fixed). Here, the arrow equals the subcarrier phase, i.e. pointing up denotes 0°. Indicated are the standard comb-filters: line, field and frame.

As expected, the line comb-filter performs well in absence of vertical detail, as here the luminance and chrominance are highly correlated. In areas of vertical detail, however, blurring will occur due to the low-pass filtering characteristics of the line comb-filter and cross-luminance and cross-color artifacts will appear. The line comb-filter generally performs better in NTSC than in PAL because of the reduced spatial filtering distance, which leads to a higher correlation between the pixels in the filter aperture.

Field and frame comb-filter

For stationary pictures, temporal filtering is preferable over spatial filtering as the samples in successive fields are highly correlated. Two options are available for temporal comb-filtering of PAL signals. The first option is the *field comb-filter*, which uses the current field line and the adjacent line in the previous field. Near-perfect results can be achieved in stationary areas with little vertical detail. However, the correlation between both field lines can be insufficient in areas containing significant vertical detail, which results in a sub-optimal decoding quality.

A *frame comb-filter* can yield perfect separation in these cases, but requires a temporal distance of four fields instead of one, as illustrated in Figure 2.3a. This reduces the temporal correlation, as the chance of image

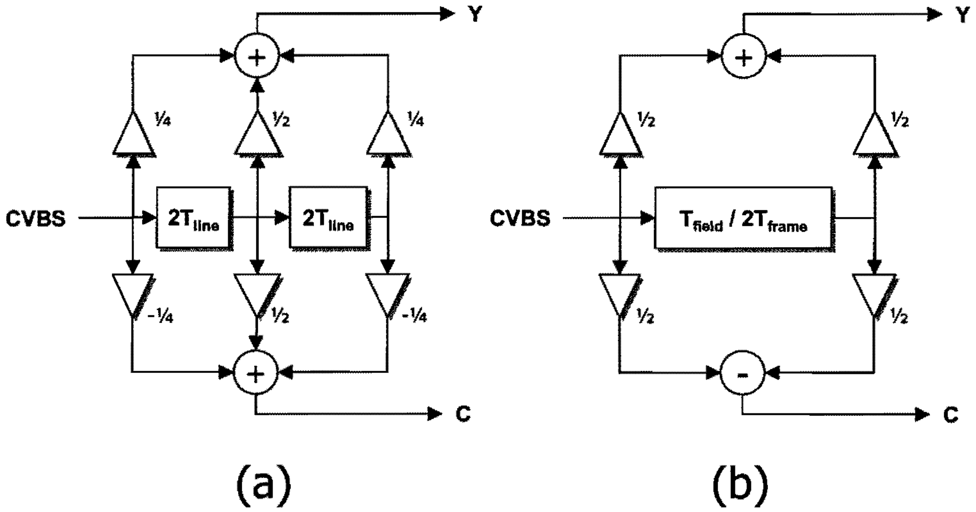

Figure 2.4: PAL comb-filters: a) 3-line comb-filter, and b) field or frame comb-filter. T_{line}, T_{field} and T_{frame} are the line, field and frame delay, respectively.

content remaining stationary decreases for increasing temporal distances. The storage requirements increase as well, as now four field delays are required compared to only one field delay for the field comb-filter. For these reasons, the field comb-filter is typically preferred over the frame comb-filter for PAL decoding, despite its problems in areas of vertical detail.

For NTSC, the frame comb-filter is the preferred temporal filtering option, as it only requires a two field delay. This means that perfect separation is possible in stationary areas, but without the large temporal distance and corresponding storage requirements of the PAL frame comb-filter.

Conclusions

The above comb-filters only yield satisfactory performance if sufficient correlation is present along the filtering direction. Applying one of the comb-filters globally, i.e. on the entire picture, will result in severe artifacts in areas with insufficient correlation along its axis. Therefore, the global application of vertical or temporal comb-filters typically yields no improvement over the standard decoder using horizontal band-pass/notch filters.

So-called *adaptive* filters can, depending upon the local signal characteristics, switch between various comb-filters. By locally selecting the filter that yields superior results, an overall increase in quality is expected over fixed comb-filters. In the remainder of this chapter, we will describe various 2D and 3D adaptive comb-filters, as well as 3D comb-filters using motion compensation.

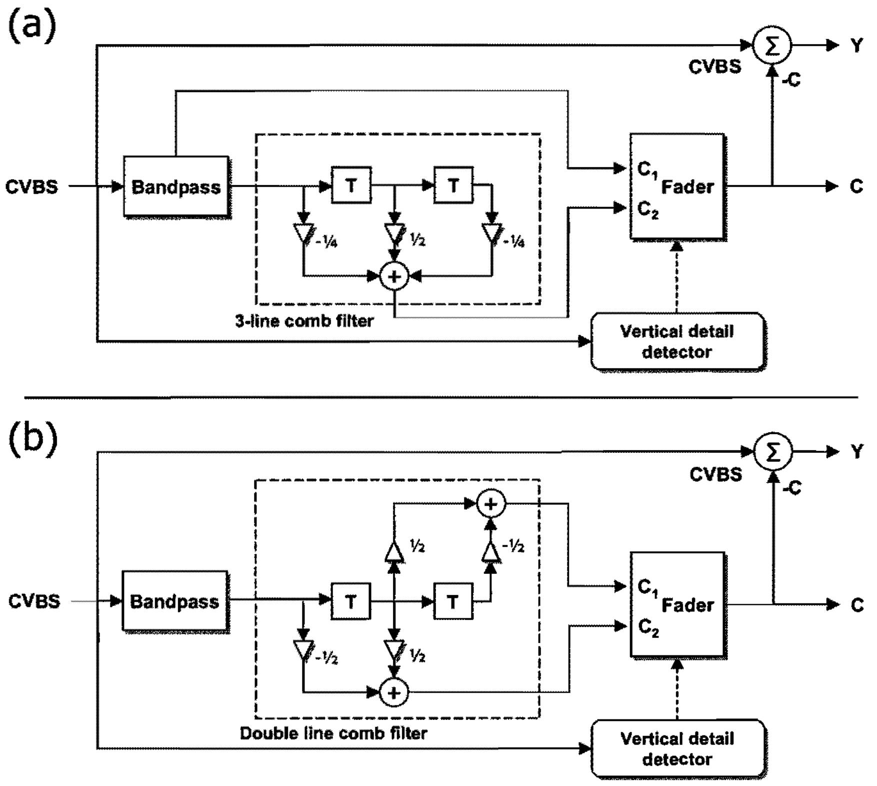
(a)
CVBS
Bandpass
T
T
-¼
½
-¼
+
3-line comb filter
CVBS
Σ
-C
Y
C1
C2
Fader
C
Vertical detail detector
(b)
CVBS
Bandpass
T
T
½
-½
+
-½
½
+
Double line comb filter
CVBS
Σ
-C
Y
C1
C2
Fader
C
Vertical detail detector

Figure 2.5: a) 2D adaptive comb-filter using band-pass and 3-line comb-filter, and b) adaptive double line comb-filter. Here, T equals a 1-line delay for NTSC and a 2-line delay for PAL.

2.2 2D adaptive comb-filters

The 2D adaptive comb-filters aim at an improved Y/C separation by adaptively combining the output of various spatial (comb-)filters. Figure 2.5a depicts a typical configuration that uses a standard decoder and a line comb-filter. This enables the comb-filtering along the horizontal and vertical axis, respectively.

Per default, the line comb-filter will be used to decode the composite video signal. However, if the vertical correlation is determined to be insufficient, as e.g. around vertical edges, the filter reverts back to the standard decoder. Artifacts in the decoded signal are thereby avoided that otherwise would have been caused by the line comb-filter in these areas.

Furthermore, the filter gradually fades between the standard decoder and the line comb-filter to avoid artifacts due to sudden switching. The fading ratio itself is determined by the amount of vertical detail. Lastly, as the filter shown operates on the chrominance only, and the luminance is generated by subtracting the decoded chrominance from the composite video signal.

Another approach to 2D adaptive comb-filtering is the adaptive double line comb-filter shown in Figure 2.5b. This filter is similar to the 3-line comb-filter previously depicted in Figure 2.4a. However, instead of averaging both outputs, the output of the adaptive double line comb-filter is determined by the individual line comb-filter of which the samples in its filter aperture exhibit the highest correlation. This results in a reduction of artifacts in areas of vertical detail.

Various other 2D adaptive comb-filter configurations exist nowadays, as e.g. presented in References [8] (pp. 112-115) and [20]. However, the overall performance of 2D comb-filters is considered to be insufficient for present-day high-end applications, as illustrated by the increasing trend toward 3D comb-filters.

2.3 3D motion adaptive comb-filters

A distinct drawback of 2D comb-filters is that situations can occur where temporally adjacent samples exhibit a higher correlation to the current sample than spatially adjacent samples. This is particularly the case in non-moving areas. A 2D adaptive comb-filter, which is restricted to spatial filtering, will yield sub-optimal results in these areas. A 3D adaptive comb-filter, however, can exploit above fact by switching to temporal filtering instead of spatial filtering. By locally selecting the filter that yields superior results, a gain in decoding quality can be achieved over 2D filters.

The most commonly used method to determine the temporal correlation is the detection of movement. This is based upon the fact that in stationary areas, temporally adjacent samples are highly similar and therefore highly correlated [1]. Temporal filtering will therefore yield better results than spatial filter in these areas. Filters using motion detection to determine whether to use spatial or temporal filtering are referred to as 3D *motion adaptive* comb-filters.

2.3.1 Generic filter structure

A generic version of the 3D motion adaptive comb-filter is shown in Figure 2.6a, as it was previously described by D. Teichner in References [19], [20] and [21]. It consists of a spatial (comb) filter and a temporal comb-filter that are combined by a fader. Depending upon the local amount of motion, the fading ratio between spatial and temporal filtering is adjusted.

The spatial filter is either a basic filter, as e.g. the standard decoder or line comb-filter, or a more elaborate 2D adaptive filter. Naturally, the latter

---

[1] In practice, however, interlacing can reduce the temporal correlation of adjacent fields, especially in areas with vertical detail.

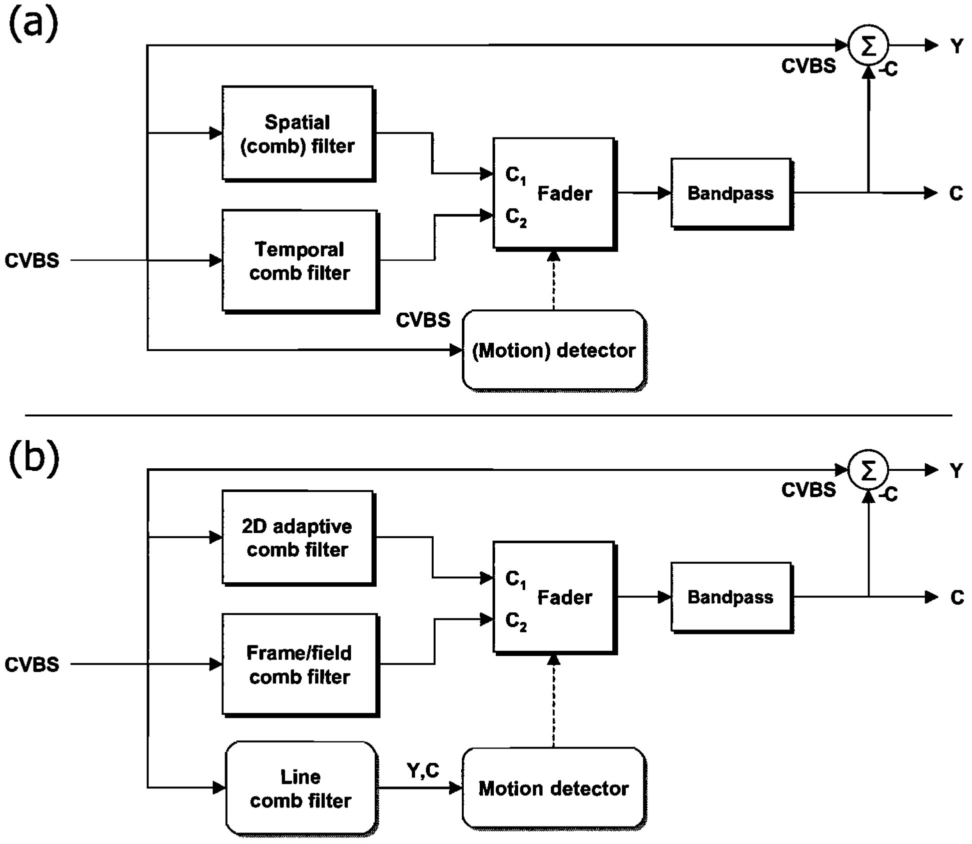
(a)
CVBS
Spatial (comb) filter
Temporal comb filter
CVBS
(Motion) detector
C1
C2
Fader
Bandpass
CVBS
Σ
-C
Y
C
(b)
CVBS
2D adaptive comb filter
Frame/field comb filter
Line comb filter
Y,C
Motion detector
C1
C2
Fader
Bandpass
CVBS
Σ
-C
Y
C

Figure 2.6: a) Generic 3D motion adaptive comb-filter, and b) possible configuration using 2D adaptive spatial filtering and motion detection on initially separated luminance and chrominance by a line comb-filter.

will yield superior decoding quality at the expense of higher implementation costs. For PAL, the field or the frame comb-filter can be used for temporal filtering. For NTSC, however, the frame comb-filter is the preferred filter as the field comb-filter yields unsatisfactory results.

The motion is typically determined on the luminance and/or chrominance signal separated by a basic (comb) filter. This so-called initial separation prevents the field-by-field changes in subcarrier pattern from being erroneously interpreted as movement. The motion detector itself can vary in complexity, but usually consists of the summed pixel value differences of samples in the current and previous field.

A possible configuration of the 3D motion adaptive comb-filter is shown in Figure 2.6b. Here, a line comb-filter is applied to the composite video signal as an initial separation of the luminance and chrominance, enabling the detection of both moving luminance and chrominance. Furthermore,

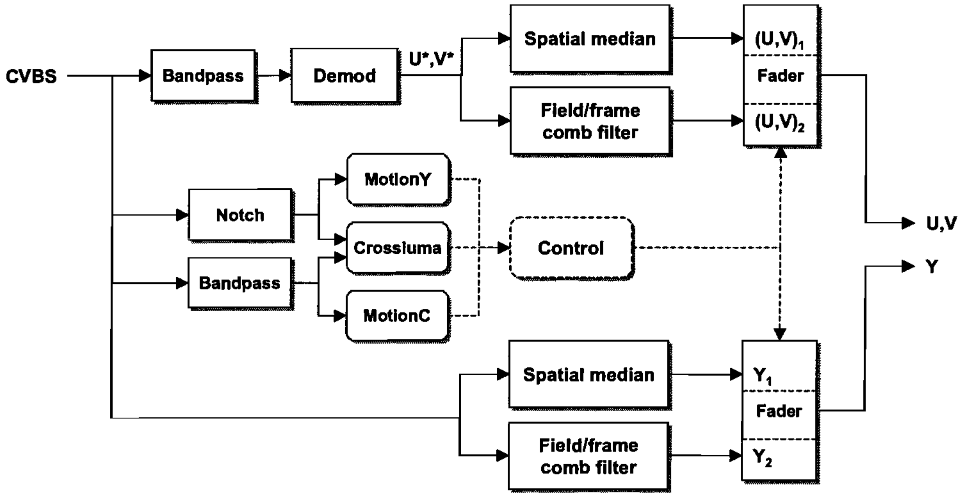
CVBS
Bandpass
Demod
U*,V*
Spatial median
Field/frame comb filter
(U,V)₁
Fader
(U,V)₂
Notch
Bandpass
MotionY
Crossluma
MotionC
Control
Spatial median
Field/frame comb filter
Y₁
Fader
Y₂
U,V
Y

Figure 2.7: 3D motion adaptive comb-filter developed by Philips PDSL.

a 2D adaptive comb-filter is used for spatial filtering, and a field or frame comb-filter for temporal filtering.

The 3D motion adaptive comb-filter is the most commonly used 3D comb-filter, and is considered to be the most advanced comb-filter actually in use in present day consumer electronics products. A significant improvement in decoding quality can be achieved compared to spatial filters, thereby replacing them in an increasing number of applications. We will continue with the description of an enhanced 3D motion adaptive comb-filter that was recently developed by Philips Consumer Electronics.

2.3.2 Filter proposed by Philips

This 3D motion adaptive comb-filter was originally proposed by C. Hentschel, and subsequently improved upon and implemented at Philips CE-PSDL by M. Nieuwenhuizen and others. Reference [8] (pp. 115-118) describes the original algorithm, whereas Reference [13] describes its implementation. Only a general overview will be given, as an extensive description is available in above references.

A simplified block diagram is shown in Figure 2.7. Here, the general concept of a 3D motion adaptive comb-filter can be recognized, as the filter fades between spatial and temporal filtering depending upon the detected motion.

Motion detection

The motion detection consists of two parts, i.e. the luminance and the chrominance motion detection. The luminance motion detector operates on the notch filtered input signal in order to attenuate any cross-talk from the chrominance subcarrier. Depending upon the temporal filtering mode, motion is detected between the current field n and the previous field $n-1$ or previous frame $n-2$ for NTSC and $n-4$ for PAL.

Situations exist where chrominance movement occurs without an accompanying movement in the luminance. In order to prevent artifacts due to temporal filtering in these cases, the chrominance motion is detected as well. The chrominance motion detector operates on the band-pass filtered input signal, and incorporates various methods to attenuate high-frequency luminance components as well as noise.

In some instances of temporal filtering, a cross-luminance artifact called *hanging dots* or *dot crawl* can occur along saturated chrominance edges. In order to avoid this artifact, a cross-luminance detection has been implemented which determines the temporal correlation of both the notch filtered luminance inputs and the band-pass filtered chrominance. If both correlations are lower than a certain threshold, the filter reverts to spatial filtering.

Spatial and temporal filters

All three detectors outputs are combined into a control signal that determines the fading ratio between spatial and temporal filtering. For temporal filtering, either a standard field or frame comb-filter can be used. For spatial filtering, a median filter is used which operates on the chrominance derived from a band-pass filter. The median filter determines the least extreme value of the chrominance in the previous, current and next field lines as well as two averages. Outlying values, which are likely caused by decoding errors, are therefore omitted from the output. This is illustrated in Equation 2.1, with $C(\vec{x}, n)$ representing the modulated chrominance at sample position $\vec{x}$ in field n. Here, the required line delay d is either 1 for NTSC or 2 for PAL.

$$C_{med}(\vec{x}, n) = med \begin{pmatrix} -C(\vec{x} + \binom{0}{-d}, n), \\ C(\vec{x}, n), \\ -C(\vec{x} + \binom{0}{+d}, n), \\ \left(\frac{1}{2}C(\vec{x}, n) - \frac{1}{2}C(\vec{x} + \binom{0}{-d}, n)\right), \\ \left(\frac{1}{2}C(\vec{x}, n) - \frac{1}{2}C(\vec{x} + \binom{0}{+d}, n)\right) \end{pmatrix} \tag{2.1}$$

As the median filter operates on the modulated chrominance, an inversion of sign is required for the chrominance on the adjacent field lines to cancel the inverted subcarrier phase. Furthermore, the luminance is generated from the chrominance by subtraction from the CVBS signal.

The above 3D motion adaptive comb-filter is one example of present-day high-end 3D comb-filters. The basic principles are identical to the generic 3D motion adaptive filters, but various enhancements have been implemented in order to prevent artifacts in certain special situations, i.e. hanging dots and moving chrominance over stationary luminance.

2.4 3D motion compensated comb-filters

The idea behind motion compensated comb-filtering is that temporal comb-filters can yield perfect results in stationary areas. In case of movement, however, temporal filtering yields sub-optimal results and motion adaptive filters are forced to fall back to spatial filtering. In turn, spatial filtering is typically restricted to horizontal and vertical filtering, which is insufficient for the decoding of detailed areas.

By using motion compensation, moving areas can be virtually converted into stationary areas. As such, it promises the advantages of temporal filters even in areas of movement, therefore avoiding any fall-back to spatial filtering.

In practice, however, motion compensated comb-filtering is restricted by the phase requirement of the standard comb-filter kernel. Only if the motion compensated sample has an opposite phase with respect to the current sample, comb-filtering is possible. In all other cases, comb-filtering is not possible without additional measures. We will present two algorithms which address this problem for PAL and NTSC, respectively.

2.4.1 PAL filter

The graduation report of I.T. Briggeman [4] describes various approaches to motion compensated comb-filtering of PAL video signals, which can be divided in transversal and recursive filters. Furthermore, hybrid filter configurations are proposed that combine both filter types. For the transversal comb-filter, a standard comb-filter kernel is used as discussed in Chapter 2.1. It therefore requires an opposite relative phase for samples with equal V-switches and an opposite absolute phase for samples with unequal V-switches.

Vector mapping

An inherent problem of the standard comb-filter kernel is that few samples meet the required phase relationship. Typically, the motion vector will point to a sample which cannot be used for the standard comb-filter due to an unsuitable phase relation. If we only consider comb-filtering with an opposite relative phase, Figure 2.8 illustrates the samples with a suitable phase in the previous field in case the motion vector is zero. Only vectors which

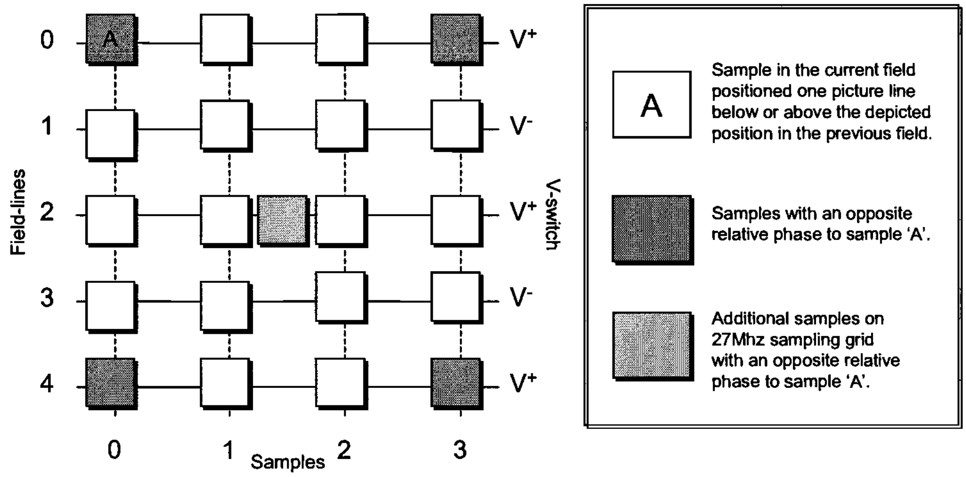
0
1
2
3
4
Field-lines
A
V+
V-
V+
V-
V+
V-switch
0
1
Samples
2
3
A
Sample in the current field positioned one picture line below or above the depicted position in the previous field.
Samples with an opposite relative phase to sample 'A'.
Additional samples on 27Mhz sampling grid with an opposite relative phase to sample 'A'.

Figure 2.8: Previous PAL field with suitable samples indicated, i.e. having an opposite relative phase to sample A in the current field.

point to these samples can be used, which is approximately only 20% of all vectors.

A straightforward solution for the remaining vectors is proposed, that consists of mapping the vectors that point to unsuitable samples to the nearest suitable vector. However, this results in an unacceptable loss of resolution and severe cross-talk. An improvement is achieved by up-sampling the composite video signal to a sampling grid of 27MHz, thereby introducing suitable samples on the remaining lines with equal V-switch as indicated in Figure 2.8. Although an increase in vertical resolution is achieved, the overall quality is still deemed unacceptable.

The possibility of using samples on the field lines with an opposite V-switch is investigated as well. These samples require an opposite absolute phase, which means that the relative location of these samples is dependent upon the current sample's phase. A scanning algorithm is proposed which determines and selects the nearest suitable sample. However, this introduces an annoying scanning pattern in the decoded image, which is considered to outweigh its benefits.

Vector-set expansion

Three more elaborate algorithms were proposed in order to expand the set of suitable vectors to the maximum set of all vectors. These consist of the following algorithms:

Interpolating-algorithm . This algorithm uses a weighted sum of two or more samples with an anti-phase relation to determine the value of all remaining samples. Unfortunately, artifacts appear around edges, as here interpolation across the edge can occur.

Gradient-algorithm . This algorithm improves upon the interpolation algorithm by interpolating along the direction of the edge, thereby preventing the interpolation across the edge. Four directions are considered, i.e. horizontal, vertical and two diagonals, and the interpolation is performed along the direction that yields the smallest gradient. The gradient itself consists of the difference between two composite sample values which meet the phase requirement. The decoded picture quality improves somewhat compared to the previous algorithm, however, the set of calculated gradients appears to be too limited in detailed areas.

Minimum-algorithm . In this algorithm the minimum color output of two or more field comb-filters adjacent to the motion vector is chosen, and the luminance is then derived from the chrominance by subtracting it from the CVBS signal. The positive aspect is a rather strong reduction of cross-color as the minimum color output is chosen. However, around chrominance edges, the selection of the minimum color means that a field comb-filter from across the edge can be selected, thereby introducing in artifacts in these areas.

Transversal filters

The filter configuration that is used for transversal comb-filtering is shown in Figure 2.9a. As the low frequencies contain luminance only, the filter operates on the high frequencies only, thereby preventing low frequency artifacts due to erroneous motion vectors. Depending upon the configuration, the motion vectors point at either the previous field, i.e. $n-1$, or the previous frame suitable for the frame comb-filter, i.e. $n-4$. The drawback of the latter is the increased temporal distance, which could make the estimation of large velocities more difficult. An advantage is the decoding of stationary areas with vertical detail, where a frame comb-filter yields superior results compared to a field comb-filter.

Recursive filters

Two recursive comb-filter configurations were proposed, which again operate on the chrominance only. The first configuration operates on modulated signals, where recursive filtering is possible with samples of equal phase. A similar problem as with transversal comb-filtering arises, i.e. the low density of vectors pointing to samples with a suitable phase. Again, both the interpolation and gradient algorithm can be used to increase the vector

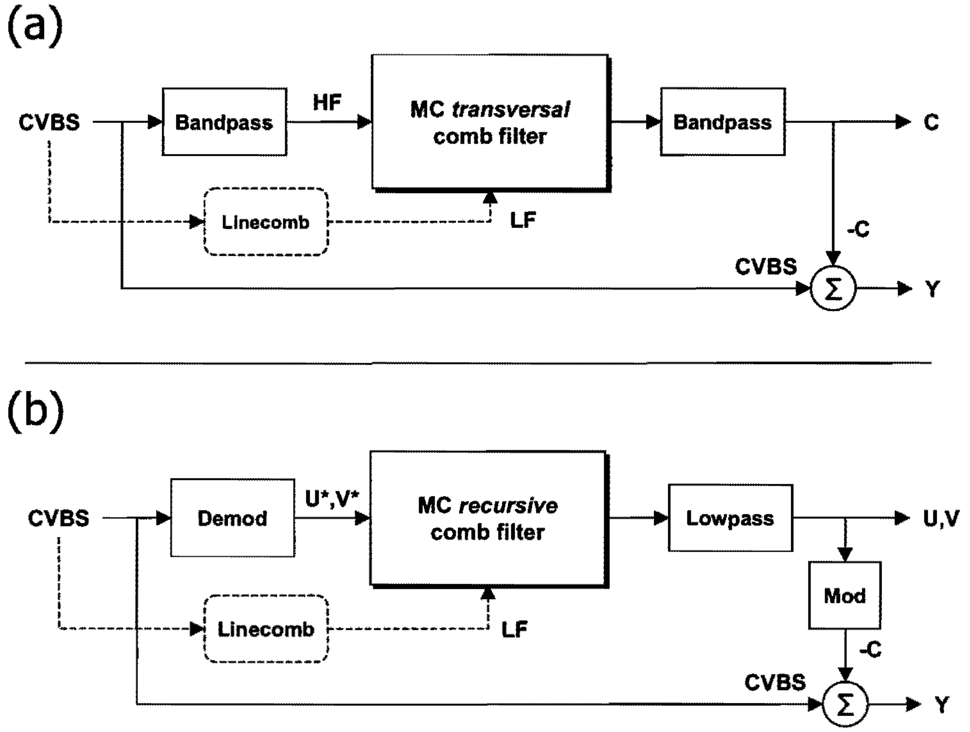

Figure 2.9: Motion compensated comb-filters: a) transversal filter, and b) recursive filter.

density. The minimum algorithm cannot be used, however, as it is based on field comb-filters which operate on samples with an opposite phase.

Above configuration is highly similar to the transversal filter depicted in Figure 2.9a, with the exception that the band-pass filter at the input is omitted. As the filter output is the mean value of a certain sample over a number of fields, the high frequency components of the luminance will be attenuated. The resulting signal at the output of the comb-filter is said to contain only low frequency luminance as well as the modulated chrominance, which can then be filtered out by a band-pass filter.

A baseband recursive comb-filter is shown in Figure 2.9b. Its advantage is the fact that there is no limitation of possible motion vectors as every sample can be used. In this configuration, the U and V chrominance components are recursively filtered, followed by a remodulation to obtain the luminance component. An additional advantage is the reduction in memory requirements of 33%, as the sampling frequency of each demodulated chrominance component is one third the sampling frequency of the modulated chrominance.

A general drawback of recursive filtering is the possible accumulation of vector errors. A proposed solution is the feedback adaptation of vector

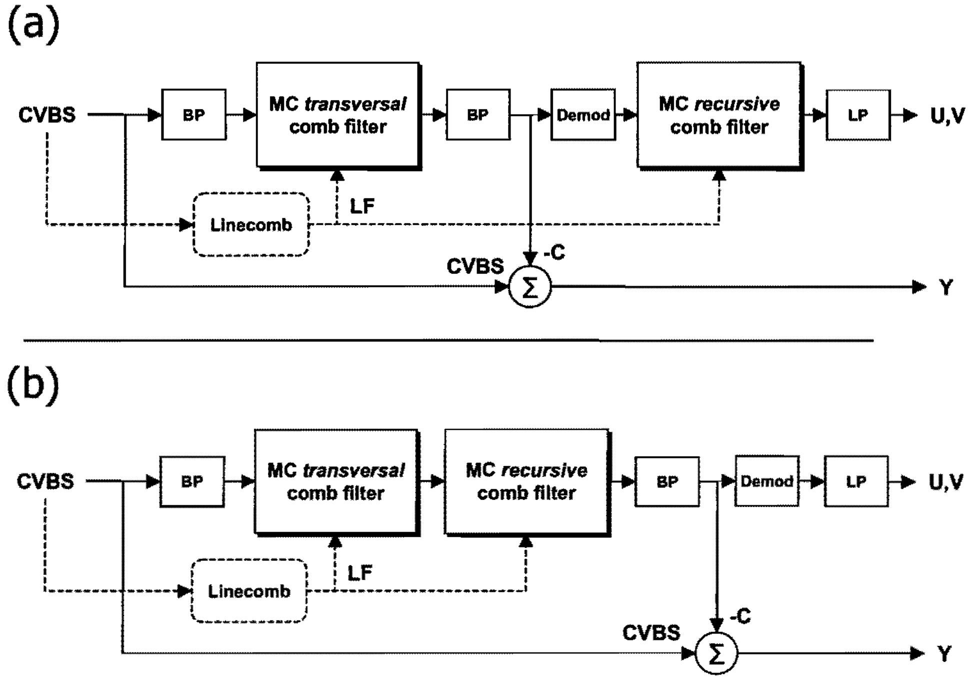
(a)
CVBS
BP
MC *transversal* comb filter
BP
Demod
MC *recursive* comb filter
LP
U,V
Linecomb
LF
-C
CVBS
Σ
Y
(b)
CVBS
BP
MC *transversal* comb filter
MC *recursive* comb filter
BP
Demod
LP
U,V
Linecomb
LF
-C
CVBS
Σ
Y

Figure 2.10: Motion compensated hybrid filter to a) reduce remaining cross color, and b) reduce remaining cross color and improve luminance resolution.

reliability, which means that the feedback factor is reduced if a motion vector is considered to be unreliable. As a possible indication of vector reliability, the match error between the sample in the current and previous field is proposed. However, the validity of this approach was not verified.

Hybrid filters

Furthermore, two hybrid configurations were proposed, that consist of the transversal comb-filtering of the chrominance, followed by the recursive filtering of either the modulated chrominance or the the baseband U and V chrominance components. These configurations are shown in Figures 2.10a and b, respectively. Both configurations yield a further reduction of cross-color artifacts compared to only transversal and recursive filtering. The configuration shown in Figure 2.10b results in an improved luminance signal as well by deriving it from the improved chrominance.

Evaluation

The evaluation of the proposed filters consisted of a subjective and an objective assessment. The latter was obtained by measuring the modulation depth of the decoded signal. Only one sequence was used for both tests, namely the *Rotating test circle* sequence, and the subjective results were based on the authors impressions. The standard PAL decoder and the line comb-filter were selected as reference filters.

Several conclusions could be drawn. First of all, the recursive filters alone and the transversal filters using interpolating or gradient algorithms do not achieve a significant improvement over the reference filters. Only an increase in horizontal resolution could be observed compared to the standard decoder, caused by the absence of a notch filter in the luminance path.

The transversal filter with minimum algorithm and the hybrid filters, however, do improve upon the reference filters. The largest gain could be achieved in cross-color suppression. Furthermore, the recursive and hybrid filters yield the best performance in tranquility, due to their inherent noise suppression characteristics.

Conclusions

From these results, the most promising approach seems to be either the transversal filter or hybrid filter, both using the minimum algorithm to obtain an improved chrominance. An improved luminance signal can then be generated by subtracting the chrominance from the composite video signal. Generally, the decoding quality of these configurations is superior to the standard decoder and the line comb-filter.

A number of recommendations were given, that include the adaptation of the motion estimator to the characteristics of the motion compensated comb-filter. This means that the generated vectors should point to samples which yield the lowest match error as well as exhibit the required phase relation. Also, it is suggested that recursive filters could benefit from a variable feedback factor which corresponds to the reliability of the motion vector. Finally, the gradient algorithm could be improved by including more directions, as well as calculating the gradient over more than two samples.

From this report, it can be concluded that the low density of suitable samples is an inherent drawback of the PAL video signal. Several methods have been proposed to improve the density, most of which perform significantly better than the simple mapping to the nearest suitable vector. A recursive baseband configuration has been discussed which is able to use all motion vectors, thereby avoiding the phase requirement and subsequent low density problem. However, the results are not as good as those obtained by transversal filtering or hybrid configurations.

Furthermore, even the best configurations do not yield a significant improvement over the reference filters in all possible aspects. We can therefore conclude that the low density of suitable samples is a fundamental problem for motion compensated PAL comb-filtering using the standard comb-filter kernel, and that the proposed filters do not solve this problem adequately.

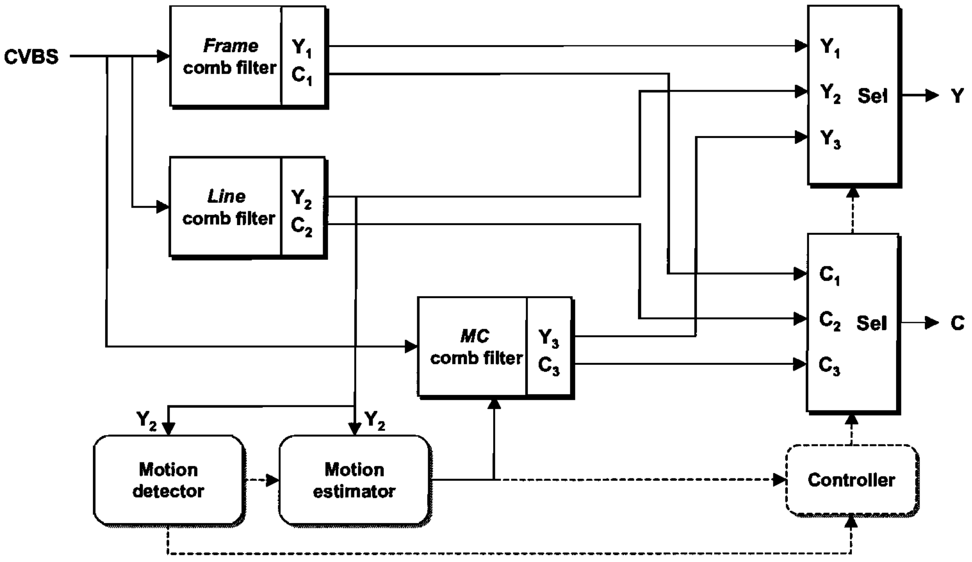

Figure 2.11: Motion compensated comb-filter for NTSC.

2.4.2 NTSC filter

A motion compensated comb-filter for NTSC was recently proposed by LG Electronics in References [5] and [10]. The fundamental difference between PAL and NTSC is that the latter lacks the V-switch, which for PAL meant that spatially adjoining field lines could not be used by standard comb-filters due to their opposite V-switch. The ability to use these field lines in NTSC, combined with the fact that the subcarrier phase is inverted every field line, means that motion compensated comb-filtering is expected to yield better results when applied to NTSC signals.

A simplified block diagram of the proposed algorithm is depicted in Figure 2.11. It can be seen that the algorithm switches between three comb-filters: the line comb-filter, the frame comb-filter and the motion compensated frame comb-filter. The filter selection is partly determined by the presence of movement, which in turn is detected by the motion detector.

Motion detection and estimation

The input to the motion detector is derived from the line comb-filter to prevent the subcarrier from being recognized as motion, as otherwise stationary chrominance would be undistinguishable from moving luminance. Any remaining cross-talk in the line comb-filtered signal is said to have a minimal effect on the motion detector.

The motion detector determines the match error of a 2 sample wide and 2 sample high (2x2) block in the current and previous frame. The classification in either motion or no motion is done by means of a fixed threshold. If the match error does not exceed the threshold, the block will be categorized as non-moving, and the algorithm will switch to the frame comb-filter as it produces the best results in stationary areas. However, if the match error does exceed the threshold, the block will be categorized as moving.

The motion estimator will now produce a vector describing the relative location of the current block in the previous frame. This vector is determined by a full search block matching algorithm, which again operates on a 2x2 block size. The general concept of the full search block matching algorithm is explained in Reference [7] (pp. 187-188). However, the reference block is moved by 2 samples horizontally and vertically when determining the match error, as opposed to common block matching algorithms where the movement is 1 sample horizontally and vertically at the maximum.

To determine the reliability of the motion vector, the match error is again compared to a threshold value. If the match error exceeds the threshold, the motion vector is considered to be unreliable. In this case the algorithm will fall back to spatial filtering by means of the line comb-filter. Otherwise, the motion vector is considered to be reliable, and the motion compensated frame comb-filter will be selected as output.

Vector mapping

The motion compensated comb-filter can now use the current and the motion compensated block to separate the luminance and chrominance components. When considering the motion vector of the 2x2 block, two situations can occur with respect to the relative phases of the current and matched block. These situations are illustrated in Figure 2.12a and b.

In the first situation, the horizontal component of the motion vector is an *odd multiple* of two, e.g. $1, 3, 5, \ldots$. The result is that the samples within the current and matched block have identical phases. In the second situation, the horizontal component is an *even multiple* of two, e.g. $0, 2, 4, \ldots$. Now, all samples within the current block have an opposite phase in the matched block. Clearly, the phase relationship is only dependent upon the horizontal and not the vertical component of the motion vector.

If the current and matched block have opposite relative phases, the Y and C components can be separated by adding and subtracting the composite values, i.e. using the standard comb-filter kernel. The same does not apply to identical phases, however, as here a separation is not possible. A solution is proposed where the upper and lower line in the matched block are swapped, after which the standard comb-filter kernel is applied. It is suggested that the signal correlation of the signals within the 2x2 block is sufficient to avoid significant errors due to the line swapping.

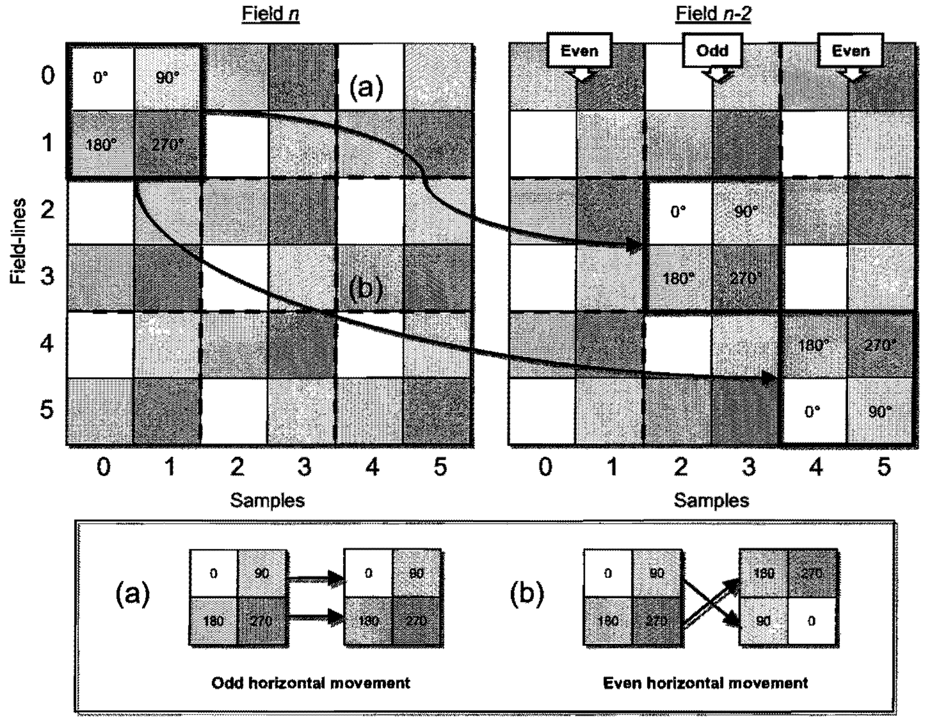

Figure 2.12: The phase relationship between the current and matched block depends only upon the horizontal component of the motion vector: a) odd horizontal motion results in an identical phase, and b) even horizontal motion results in an opposite phase.

Conclusions

A subjective evaluation was used to determine the performance of the proposed filter. For that purpose, the performance of a line comb-filter was compared to the proposed motion compensated filter. This comparison is valid, as the performance was only evaluated in the moving parts of the image where 3D motion adaptive filters are forced to fall back to spatial filtering. In these areas, the results are said to be far better than those of the line comb-filter, both in terms of resolution and cross-talk reduction. This is of particular interest for NTSC signals, as here the frame comb-filter has to be used as no field comb-filter is available. Due to the larger temporal distance, 3D adaptive filters are therefore forced to fall back earlier to spatial filtering than for PAL signals.

The promising results for motion compensated comb-filtering, as reported by the inventors, were expected as the density of suitable samples is far larger in NTSC than in PAL due to the lack of V-switch and the opposite phase of adjoining field lines. As such, motion compensated comb-filtering is better suited for NTSC signals than for PAL signals.

2.4.3 Conclusions

Although in theory, motion compensated comb-filtering promises a significant improvement over motion adaptive comb-filtering, the phase requirements of the standard comb-filter kernel restrict its application. In the case of PAL, the low density of suitable motion vectors results in a poor decoding quality. Various algorithms have been proposed to maximize the vector density, yet the overall performance is rather poor. Therefore, transversal motion compensated comb-filtering with the standard comb-filter kernel seems unsuitable for PAL signals.

More promising approaches include the application of a different filter kernel, as proposed in the next chapter, or the motion compensated baseband filtering. The latter is able to use all motion vectors as no phase requirements exist. However, as baseband filtering alone is not able to sufficiently suppress cross-talk, the combination with transversal comb-filters in a hybrid configuration is more desirable.

Generally, motion compensated comb-filtering is more suitable for NTSC. Even a fairly straightforward implementation using 2x2 blocks is said to yield significantly improved results in moving areas compared to motion adaptive filters. Further improvements may be possible as well. For example, instead of reversing the block lines if the phase of the current and matched block are identical, the filter could adaptively switch between the two adjacent lines with opposite phases depending upon the highest correlation. Also, the 2x2 block structure and corresponding motion estimation grid may limit the performance as well due to its coarseness.

2.5 Literature survey

We will conclude with a short summary of interesting 3D comb-filters found in publications and patents. Although various approaches to 3D comb-filtering have been published, neither of them has been found to be fundamentally different from the generic 3D motion adaptive comb-filter. The corresponding literature search procedures and complete list of references are shown in Appendix C.

- **3D motion adaptive comb-filter for PAL (Hitachi, 1992)** [1],[2]
  The proposed filter is a generic 3D motion adaptive comb-filter which distinguishes between a so-called moving and stationary mode. In the stationary mode, a frame comb-filter is used to filter along the temporal axis, whereas in the moving mode, a 2D adaptive filter is used. Of particular interest is the comparison of various motion detectors. A motion detector is proposed which uses two 1-frame differences, i.e. the differences of frames $(n, n-1)$ and $(n-1, n-2)$, and is said to yield the best performance.

- **Edge-based spatial filter and a sub-temporal filter for NTSC (Samsung, 1994)** [24] This filter operates temporally on the base-band chrominance components by demodulation and sub-sampling of the band-pass filtered chrominance. Its main advantage is the reduced memory requirements compared to temporal comb-filtering of modulated signals. For spatial filtering, an edge dependent filter is used which operates horizontally, vertically and in two diagonals. The edge direction is determined from combining the output of two pre-filters in the horizontal and vertical direction.

- **Study of scene change phenomena in PAL and NTSC (Japan Broadcasting Corporation, 1994-95)** [15][16] In this study, the performance of a number of motion detectors is compared for usage in 3D motion adaptive comb-filters. Various motion detectors are presented which operate on one and two frame difference signals. A simple luminance motion detector is proposed, which consists of the low-pass filtered difference between the next and previous field with basic post-processing. A corresponding chrominance motion detector is discussed as well, but the performance of the luminance detector was found to be sufficient for real-life video sequences. Generally, the proposed detector is said to achieve equal or superior performance to more elaborate motion detectors.

- **Patent: Motion adaptive comb-filter (Mitsubishi, 1994)** [18] This patent describes a generic motion adaptive comb-filter using a 2D adaptive spatial filter and a frame comb-filter, in which the output of the 2D adaptive spatial filter is used for motion detection instead of a commonly used simple 1D spatial filter.

- **Patent: Motion adaptive comb-filter (Fortel DTV, 2000)** [11] The described motion adaptive comb-filter uses both field and frame comb-filters. The output of the frame comb-filter is given priority in case no motion is detected from a 1-frame difference signal. Otherwise, the filter reverts to either the field comb-filter or spatial 2D adaptive filtering.

- **Patent: Motion and content adaptive comb-filter (Mitsubishi, 1994)** [22],[23] This filter uses frame comb-filtering if the detected motion is small. Otherwise, the smallest difference is determined between the current sample and sample points in the current and adjacent field with an identical chrominance phase. The smallest difference between samples corresponds to the highest correlation. Subsequently, the comb-filtering takes places in the spatial and/or temporal direction of the highest correlation.

- **Patent: Motion adaptive comb-filter using repeated motion detection (Matsushita, 1999) [17]** In this filter, a first motion detector is used as an input to a generic motion adaptive comb-filter. A second motion detector operates on the decoded luminance signal. In case both outputs differ, a 3D noise reduction is applied to the decoded luminance and chrominance.

- **Patent: Motion adaptive comb-filter operating on demodulated U,V (Toshiba, 1995) [12]** This patent describes a motion adaptive comb-filter operating on the baseband chrominance components for temporal filtering. Using sub-sampling followed by interpolation, the memory requirements can be reduced. A similar approach has been described in Reference [24].

Chapter 3

Novel decoding principle

As described in Chapter 2.1, a standard comb-filter kernel requires a pair of samples to either have an opposite *relative* subcarrier phase, i.e. ϕ and $\phi + 180^\circ$, or an opposite ***absolute*** subcarrier phase, i.e. ϕ and $-\phi$. An inherent drawback of this comb-filter kernel is the low density of candidate samples which both meet the required phase relationship, and are spatially and/or temporally adjacent. Due to this limited set of candidates, situations will occur where neither of the candidates exhibit sufficient correlation with respect to the current sample, therefore causing artifacts in the decoded video.

To increase the likelihood of obtaining highly correlated candidates, the candidate set needs to be expanded. One way of doing so is by taking into account the candidates with a non-opposite phase relationship with respect to the current sample. If these candidates could be used for comb-filtering, the candidate set could be greatly expanded without the increase in spatial and/or temporal distance and subsequent decrease in correlation.

This chapter discusses the possibility and feasibility of Y/C separation using non-opposite phases. Although the exact frequency response of the proposed filter has yet to be determined due to its complexity, we will from now on refer to it as comb-filter. Furthermore, we will focus on PAL video signals, as here the density of suitable samples is lower than for NTSC, and any expansion is more beneficial. However, the principles of the proposed comb-filter kernel for PAL samples with equal V-switches also apply to NTSC.

3.1 Principles

As a reminder, Equation 3.1 illustrates an encoder for PAL composite color video signals, where one CVBS sample is obtained by adding modulated U and V components to a baseband Y signal. Here, $\vec{x}$ indicates the pixel position in a given field n and ω equals $\pi \cdot F_{sc}$, where F_{sc} is the subcarrier frequency.

$$F_{cvbs}(\vec{x},n) = Y(\vec{x},n) + U(\vec{x},n) \cdot sin(\omega t) \pm V(\vec{x},n) \cdot cos(\omega t) \tag{3.1}$$

In the PAL decoder, a received CVBS sample, $F_{cvbs}(\vec{x},n)$, introduces three unknown variables, namely the values of $Y(\vec{x},n)$, $U(\vec{x},n)$ and $V(\vec{x},n)$, and one known value, i.e. the locally regenerated subcarrier phase ωt. Basic algebra shows that, given three linear equations, these three unknown variables can be solved. This means that three CVBS samples, encoded from *identical* Y, U and V values, can be used to separate the Y, U and V components exactly. In the situation that the CVBS samples were encoded from *non-identical* Y, U and V values, perfect separation is not possible and errors in the decoded values will occur.

To discuss the decoding of samples with non-opposite phases in more detail, two situation with respect to the V-switch of three CVBS samples should be considered:

- The V-switch of all three samples is identical.
- One of the three samples has an unequal V-switch with respect to the other samples.

We therefore distinguish between the decoding of samples with identical V-switches, and the decoding of samples with non-identical V-switches. For clarity, we will disregard the spatial and temporal location of the CVBS samples for the remainder of the chapter, which reduces Equation 3.1 to:

$$F_{cvbs} = Y + U \cdot sin(\omega t) \pm V \cdot cos(\omega t) \tag{3.2}$$

3.2 Identical V-switches

In case of identical V-switches, consider three CVBS samples encoded from the same Y, U and V values as shown in Equation 3.3. In order to obtain three independent equations, the phases were chosen to be unequal, i.e. $\alpha \neq \beta \neq \gamma$. Also, the V-switch of all V components is chosen to be positive. In case of all negative V-switches, the situation is identical expect for an inversion of the sign of the decoded V component.

$$\begin{aligned} F_{cvbs1} &= Y + U \cdot sin(\alpha) + V \cdot cos(\alpha) \\ F_{cvbs2} &= Y + U \cdot sin(\beta) + V \cdot cos(\beta) \\ F_{cvbs3} &= Y + U \cdot sin(\gamma) + V \cdot cos(\gamma) \end{aligned} \tag{3.3}$$

By solving these three linear equations for the Y, U and V components, the expressions in Equations 3.4 and 3.5 are obtained. Here, the Y, U and V components are expressed in terms of the three original CVBS samples and their corresponding subcarrier phase.

$$
\begin{aligned}
Y_n &= +F_{cvbs1} \cdot sin(\beta) \cdot cos(\gamma) - F_{cvbs1} \cdot sin(\gamma) \cdot cos(\beta) \\
&\quad +F_{cvbs2} \cdot sin(\gamma) \cdot cos(\alpha) - F_{cvbs2} \cdot sin(\alpha) \cdot cos(\gamma) \\
&\quad +F_{cvbs3} \cdot sin(\alpha) \cdot cos(\beta) - F_{cvbs3} \cdot sin(\beta) \cdot cos(\alpha) \\
U_n &= +F_{cvbs1} \cdot cos(\beta) - F_{cvbs1} \cdot cos(\gamma) + F_{cvbs2} \cdot cos(\gamma) \\
&\quad -F_{cvbs2} \cdot cos(\alpha) + F_{cvbs3} \cdot cos(\alpha) - F_{cvbs3} \cdot cos(\beta) \\
V_n &= +F_{cvbs1} \cdot sin(\gamma) - F_{cvbs1} \cdot sin(\beta) + F_{cvbs2} \cdot sin(\alpha) \\
&\quad -F_{cvbs2} \cdot sin(\gamma) + F_{cvbs3} \cdot sin(\beta) - F_{cvbs3} \cdot sin(\alpha) \\
D &= +sin(\alpha) \cdot cos(\beta) - sin(\alpha) \cdot cos(\gamma) \\
&\quad +sin(\beta) \cdot cos(\gamma) - sin(\beta) \cdot cos(\alpha) \\
&\quad +sin(\gamma) \cdot cos(\alpha) - sin(\gamma) \cdot cos(\beta)
\end{aligned}
\tag{3.4}
$$

with:

$$Y = \frac{Y_n}{D}, \qquad U = \frac{U_n}{D}, \qquad V = \frac{V_n}{D} \tag{3.5}$$

If no errors to due quantization occur, identical Y, U and V input values can be separated perfectly. In practice, however, spatially and/or temporarily adjacent samples rarely exhibit perfect correlation, and as such, the above decoding will result in errors. As such, the sensitivity of the decoder to any imperfect correlation is of particular interest. The non-perfect correlation can be interpreted as noise added to the input values of the encoder, as shown in Figure 3.1. Here, zero mean Gaussian noise is added to each of the Y, U and V input-values to represent the non-perfect correlation.

It is expected that the subcarrier phase of the samples affects the sensitivity of the decoder to the so-called *correlation noise.* This holds for the standard comb-filter kernel, where two samples are required to have the largest possible phase difference, i.e. 180°. With three samples, this difference amounts to 120°. We will therefore formulate the hypothesis that the decoder will attain the lowest noise sensitivity using CVBS samples at these relative phases.

To test this hypothesis and to determine the sensitivity to correlation noise for all possible phase combinations, noise was introduced to the original Y, U and V samples according to Equations 3.6 and 3.7. This is also depicted in Figure 3.1a, where the noise-corrupted (Y_1, U_1, V_1) values are encoded into F_{cvbs1} using subcarrier phase α. By encoding the noise corrupted (Y_2, U_2, V_2) and (Y_3, U_3, V_3) at subcarrier phases β and γ, respectively, we obtain three CVBS samples.

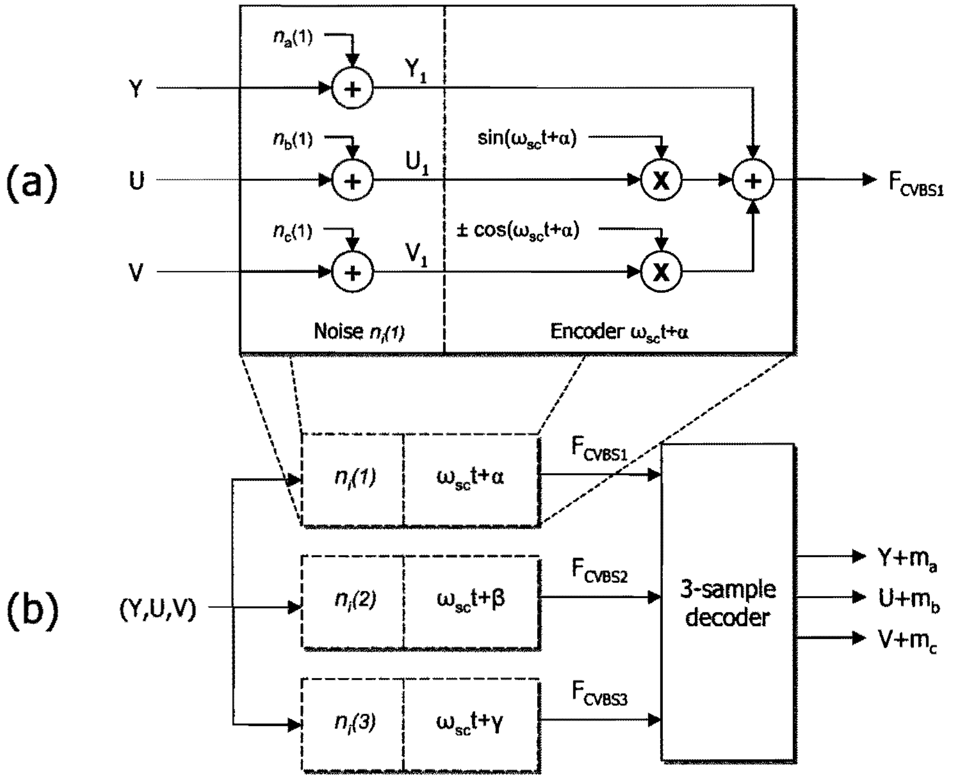
(a)
Y
U
V
$n_a(1)$
$n_b(1)$
$n_c(1)$
Y_1
U_1
V_1
sin(ω_sc t+α)
± cos(ω_sc t+α)
X
+
Noise $n_i(1)$
Encoder ω_sc t+α
F_CVBS1
(b)
(Y,U,V)
$n_i(1)$
$n_i(2)$
$n_i(3)$
ω_sc t+α
ω_sc t+β
ω_sc t+γ
F_CVBS1
F_CVBS2
F_CVBS3
3-sample decoder
Y+m_a
U+m_b
V+m_c

Figure 3.1: Noise to represent an imperfect correlation: a) addition of Gaussian noise and subsequent encoding into F_{cvbs1}, and b) decoding of F_{cvbs1}, F_{cvbs2} and F_{cvbs3}.

$$\begin{aligned} F_{cvbs1} &= Y_1 + U_1 \cdot sin(\alpha) + V_1 \cdot cos(\alpha) \\ F_{cvbs2} &= Y_2 + U_2 \cdot sin(\beta) + V_2 \cdot cos(\beta) \\ F_{cvbs3} &= Y_3 + U_3 \cdot sin(\gamma) + V_3 \cdot cos(\gamma) \end{aligned} \tag{3.6}$$

with, for $i \in \{1,2,3\}$:

$$\begin{aligned} Y_i &= \overline{Y} + n_a(i) \\ U_i &= \overline{U} + n_b(i) \\ V_i &= \overline{V} + n_c(i) \end{aligned} \tag{3.7}$$

Here, n_a, n_b and n_c are independent, zero mean Gaussian noise sources with variance $\sigma^2_{n_i} = 400$, whereas $\overline{Y}$, $\overline{U}$ and $\overline{V}$ were set to a value of 128[1].

---

[1] Within an 8-bit data representation, this minimizes the possibility of clipping, i.e. exceeding the maximum or minimum allowed value.

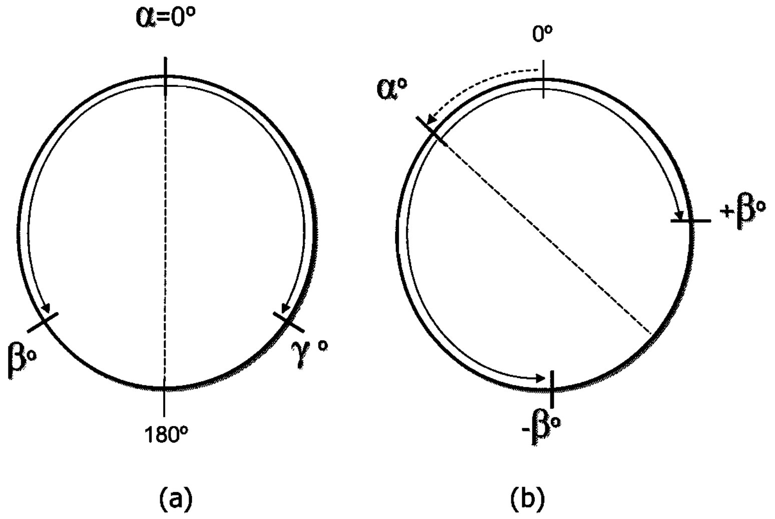

Figure 3.2: a) Varying relative phases β and γ with respect to a fixed absolute phase α of 0°, and b) varying relative phase β with respect to a varying absolute phase α.

The Signal-to-Noise Ratio (SNR) at the input of the encoder can now be determined, e.g. for the luminance path:

$$SNR(Y_{in}) = 10 \cdot log\frac{\overline{Y}^2}{\sigma^2_{n_a}}dB \approx 16.12dB \tag{3.8}$$

By decoding the resulting three CVBS samples, we obtain:

$$\begin{aligned} Y &= \overline{Y} + m_a \\ U &= \overline{U} + m_b \\ V &= \overline{V} + m_c \end{aligned} \tag{3.9}$$

where m_a, m_b and m_c are zero mean Gaussian noise sources, but with an unknown variance. By measuring the noise over a large enough number of samples, the corresponding variance can be determined. As such, we can calculate the amount of noise at the output of the PAL decoder for either Y, U or V. For the luminance path, the SNR is equal to:

$$SNR(Y_{out}) = 10 \cdot log\frac{\overline{Y}^2}{\sigma^2_{m_a}}dB \tag{3.10}$$

We would like to determine the optimum combination(s) of the subcarrier phases (α, β, γ), i.e. that yield the highest SNR at the output of the decoder. This can be accomplished by determining the optimum *relative* phases as well as any dependency upon the *absolute* phases of the CVBS samples:

- In order to determine the optimum *relative* phase combinations, the phase α of one of the three samples is set to 0°, whereas the phases β and γ of the remaining samples vary from 0° to 360°. This is illustrated in Figure 3.2a. By determining the relative phases at which the highest SNR occurs, the optimum combination(s) can be found.

- By calculating the SNR for a varying ***absolute*** phase α, any dependency upon the absolute phase of one of the samples can be determined. This situation is illustrated in Figure 3.2b, where the absolute phase α varies from 0° to 360° whereas the relative phase β of both remaining samples increases from 0° to 180°. Taking a relative phase of e.g. 120° will correspond with a relative phase of +120° for the second sample and −120° for the third. In case the SNR is independent from the absolute phase of one of the samples, the resulting SNR function will be independent of α.

Figure 3.3 shows the results of the first test, where the color intensity represents the SNR of the decoded luminance component at a given phase combination (β, γ). Clearly, for phase differences of 120°, the SNR measured at the output of the decoder equals the SNR at the input, i.e. 16.12dB, and there is no noise amplification. Also, if two out of three samples have an opposite phase, i.e. phase difference of 180°, the noise amplification will be zero as well.

From this one can deduct that there are two triangular regions for which there is no noise amplification. These are visible in Figure 3.3 as red triangles centered around phase differences of 120°. Outside these so-called ***stable regions***, decreasing relative phase differences will result in an increase in noise level at the output of the decoder.

Figure 3.4 shows the results of the second test. In this case, the SNR is not a function of the absolute phase α, as for every value of α the optimum relative phase β remains identical. For the chrominance components U and V, however, the stable regions are a function of α, as Figures 3.5 and 3.6 illustrate. This dependency can be characterized by an α-dependent offset on top of an average phase of 120°.

This means that, although the stable regions for the Y, U, and V components are not identical, the phase combination characterized by phase differences of 120° is always inside or at the edge of the stable regions. For identical V-switches, and taking into account the noise sensitivity for Y, U and V combined, we can therefore conclude that the hypothesis is true that the lowest noise sensitivity is obtained at phase differences of 120°. For each component separately though, there are extra phase combinations for which minimum noise sensitivity can be achieved.

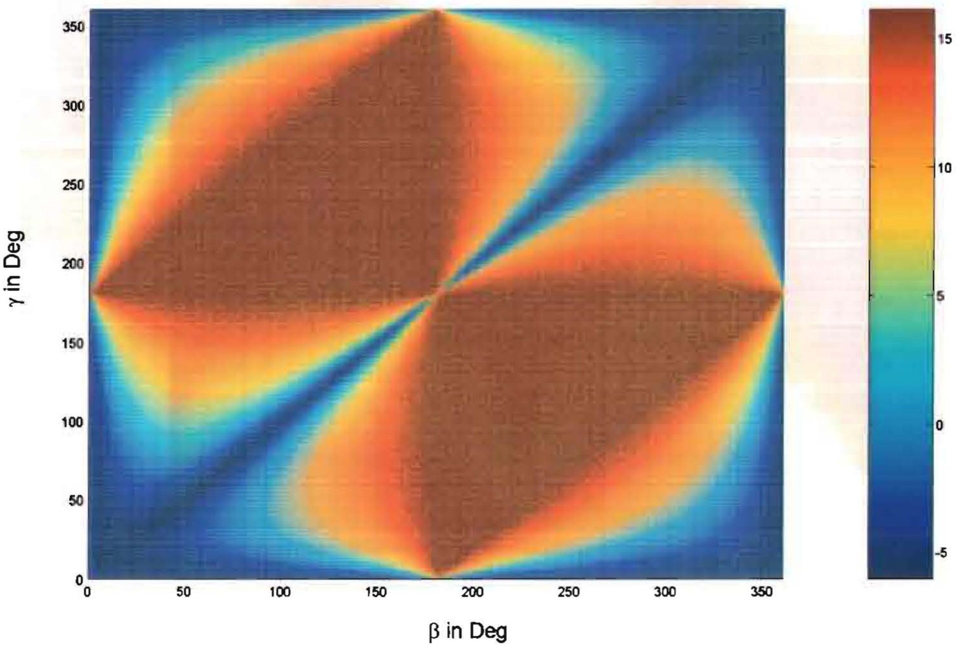

Figure 3.3: Identical V-switches: luminance SNR as function of relative phases β and γ with respect to a fixed absolute phase α of 0°.

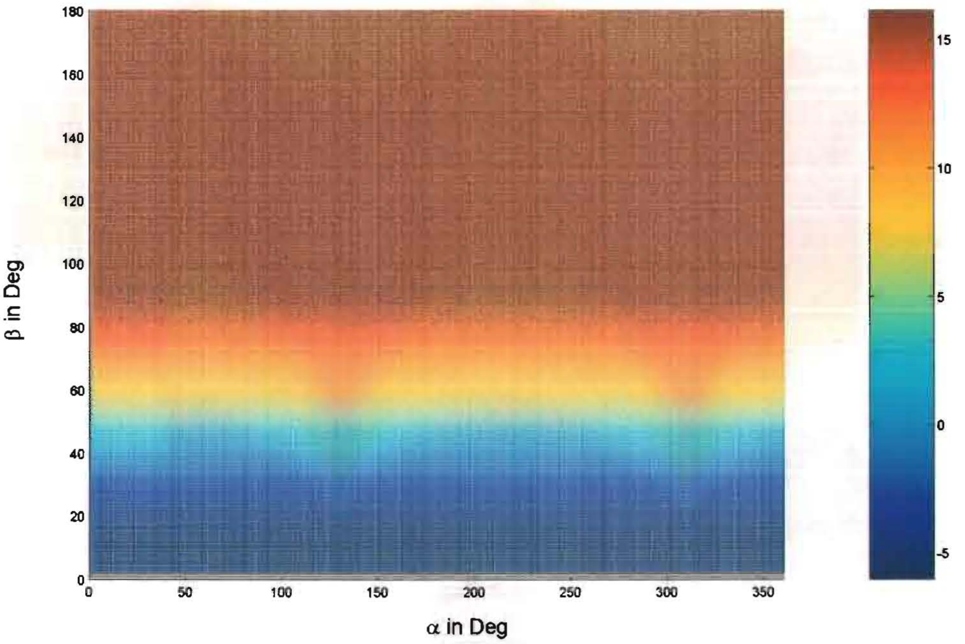

Figure 3.4: Identical V-switches: luminance SNR as function of absolute phase α and relative phase β.

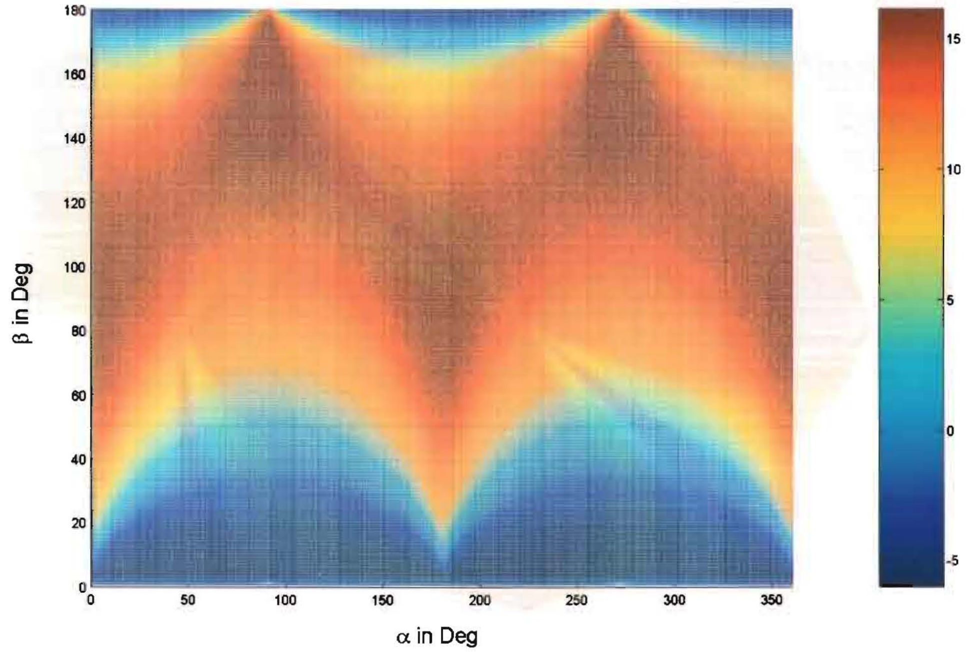

Figure 3.5: Identical V-switches: chrominance (U) SNR as function of absolute phase α and relative phase β.

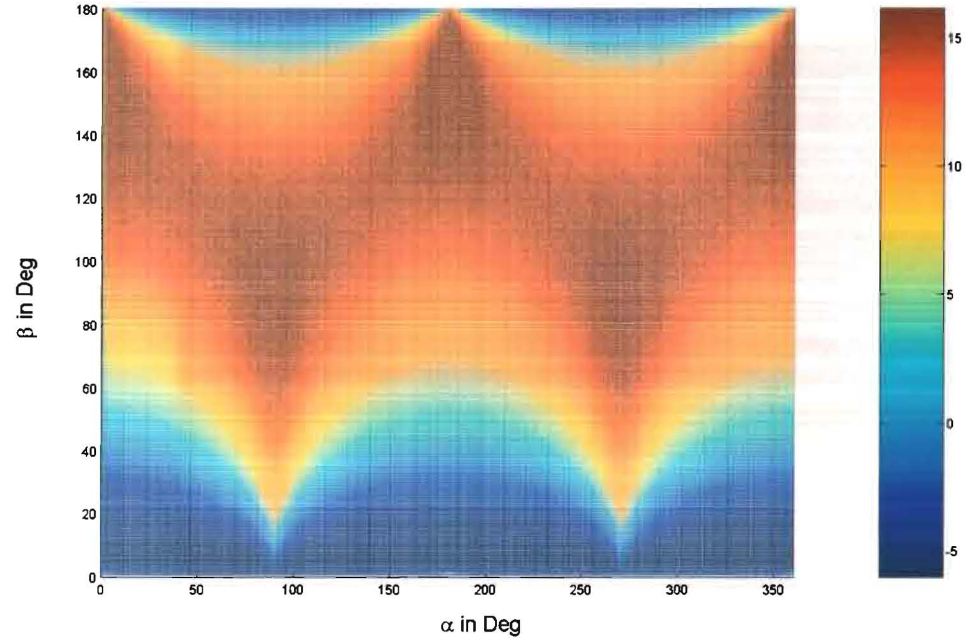

Figure 3.6: Identical V-switches: chrominance (V) SNR as function of absolute phase α and relative phase β.

3.3 Non-identical V-switches

In case of non-identical V-switches, we can distinguish two situations:

- The V-switch of one CVBS sample is positive, whereas the remaining samples have a negative V-switch.
- The V-switch of one CVBS sample is negative, whereas the remaining samples have a positive V-switch.

The first situation is depicted in Equation 3.11, whereas the second situation will not be covered, as it is identical except for an inversion in sign of the decoded V component.

$$\begin{aligned} F_{cvbs1} &= Y + U \cdot sin(\alpha) + V \cdot cos(\alpha) \\ F_{cvbs2} &= Y + U \cdot sin(\beta) - V \cdot cos(\beta) \\ F_{cvbs3} &= Y + U \cdot sin(\gamma) - V \cdot cos(\gamma) \end{aligned} \tag{3.11}$$

By solving these equations for the Y, U and V components, the expressions depicted in Equations 3.12 and 3.13 can be obtained.

$$\begin{aligned} Y_n &= +F_{cvbs1} \cdot sin(\beta) \cdot cos(\gamma) - F_{cvbs1} \cdot sin(\gamma) \cdot cos(\beta) \\ &\quad -F_{cvbs2} \cdot sin(\gamma) \cdot cos(\alpha) - F_{cvbs2} \cdot sin(\alpha) \cdot cos(\gamma) \\ &\quad +F_{cvbs3} \cdot sin(\alpha) \cdot cos(\beta) + F_{cvbs3} \cdot sin(\beta) \cdot cos(\alpha) \\ U_n &= +F_{cvbs1} \cdot cos(\beta) - F_{cvbs1} \cdot cos(\gamma) + F_{cvbs2} \cdot cos(\gamma) \\ &\quad +F_{cvbs2} \cdot cos(\alpha) - F_{cvbs3} \cdot cos(\alpha) - F_{cvbs3} \cdot cos(\beta) \\ V_n &= +F_{cvbs1} \cdot sin(\beta) - F_{cvbs1} \cdot sin(\gamma) + F_{cvbs2} \cdot sin(\gamma) \\ &\quad -F_{cvbs2} \cdot sin(\alpha) + F_{cvbs3} \cdot sin(\alpha) - F_{cvbs3} \cdot sin(\beta) \\ D &= +sin(\alpha) \cdot cos(\beta) - sin(\alpha) \cdot cos(\gamma) \\ &\quad +sin(\beta) \cdot cos(\gamma) + sin(\beta) \cdot cos(\alpha) \\ &\quad -sin(\gamma) \cdot cos(\alpha) - sin(\gamma) \cdot cos(\beta) \end{aligned} \tag{3.12}$$

with:

$$Y = \frac{Y_n}{D}, \qquad U = \frac{U_n}{D}, \qquad V = \frac{V_n}{D} \tag{3.13}$$

To test the stability as a function of the absolute and relative phase, zero mean Gaussian noise was added to the input of the PAL encoder. This situation was previously illustrated in Equations 3.6 and 3.7, except that now the sign of the V component is negative in two out of three samples.

For the luminance component, the stability as a function of the relative phase differences is shown in Figure 3.7. Here, the absolute phase α of the sample with the opposite V-switch is 0°, whereas the relative phases β and γ of the second and third sample vary from 0° to 360°.

It can be seen that if the phase difference between the two samples with identical V-switch equals 180°, there is no noise amplification. The resulting triangles are now centered around phase differences of 60°, i.e. $(\beta,\gamma) = (300°, 60°)$ and $(\beta,\gamma) = (60°, 300°)$. Compared to the stable regions in case of identical V-switches, the regions are of equal size yet centered around different relative phases.

In turn, Figure 3.8 was obtained by varying both the absolute phase α of the sample with opposite V-switch and the relative phase $\pm\beta$ of the remaining samples. Contrary to the situation with identical V-switches, the stable region of the luminance is now dependent upon the absolute phase α. This means that the optimum relative phase difference β varies as a function of the absolute phase α of the sample with the unequal V-switch.

For example, consider an absolute phase α of 90°. According to Figure 3.8, minimal noise amplification occurs at relative phase differences of approximately ±120°, i.e. $(\beta,\gamma) = (210°, 330°)$ or $(\beta,\gamma) = (330°, 210°)$. In case of an absolute phase α of 180°, the ideal relative phase differences now equal ±60°, i.e. $(\beta,\gamma) = (120°, 240°)$ or $(\beta,\gamma) = (240°, 120°)$.

The stability as a function of the absolute phase α is shown in Figures 3.9 and 3.10 for the chrominance components U and V, respectively. Although the stable regions do not match those of the luminance, there are distinct parts where all regions overlap. Whereas in the case of identical V-switches, the stability regions are centered around a relative phase difference of 120°, they now change position depending upon the absolute phase of the sample with an unequal V-switch.

3.4 Conclusions

We can conclude that comb-filtering using samples with non-opposite phases is possible with the proposed comb-filter kernel. In order to separate the Y, U and V components, three CVBS samples are required that are encoded at non-identical phases. As in practice these samples rarely exhibit perfect correlation, the sensitivity of the decoder to any imperfect correlation should be minimized.

The hypothesis that the lowest noise sensitivity is obtained at phase differences of 120° could only be validated for CVBS samples with an equal V-switch. For unequal V-switches, the optimum phase differences vary as a function of the absolute phase α of the sample with the unequal V-switch. In this case, Figures 3.8 through 3.10 are required to determine the optimum value of β for each value of α.

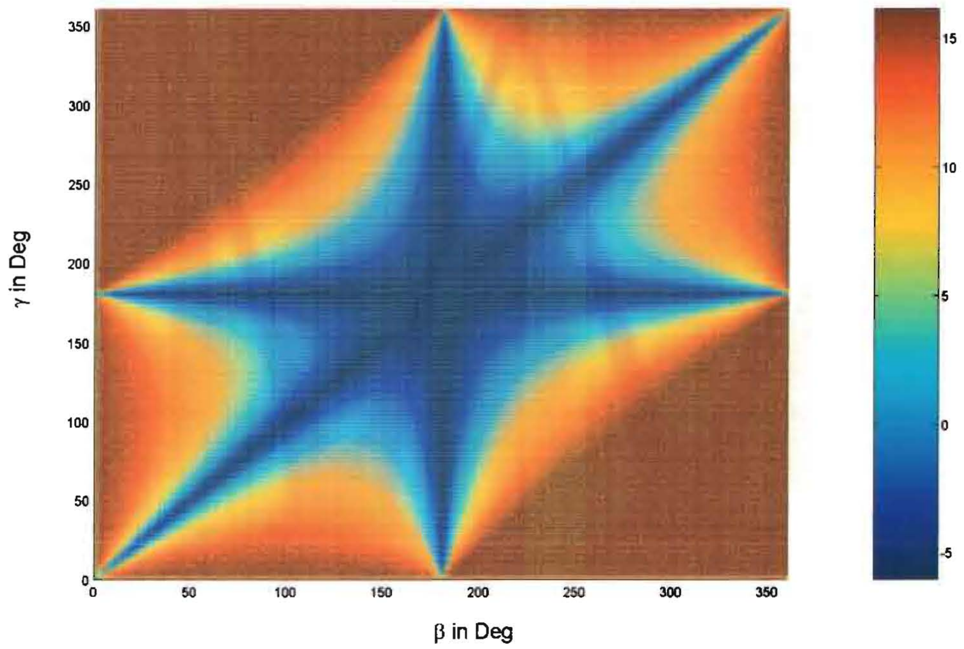

Figure 3.7: Non-identical V-switches: luminance SNR as function of relative phases β and γ with respect to a fixed absolute phase α of 0°.

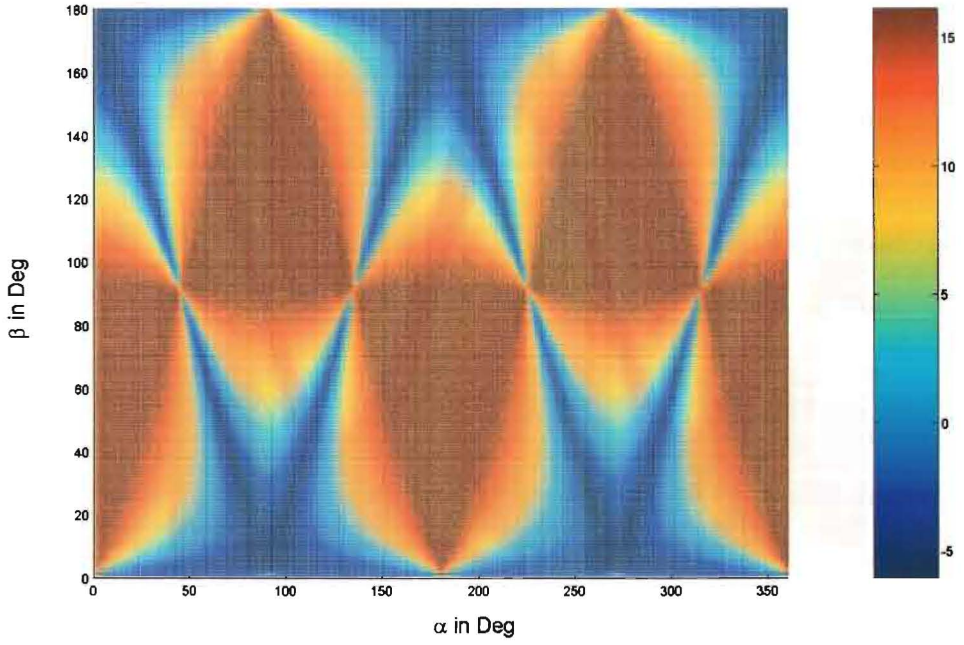

Figure 3.8: Non-identical V-switches: luminance SNR as function of absolute phase α and relative phase β.

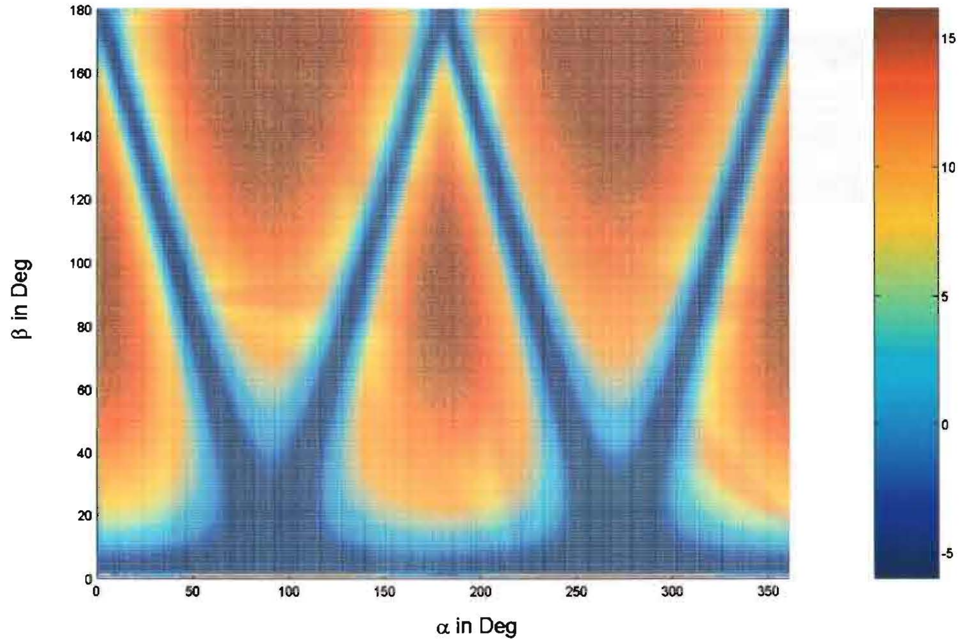

Figure 3.9: Non-identical V-switches: chrominance (U) SNR as function of absolute phase α and relative phase β.

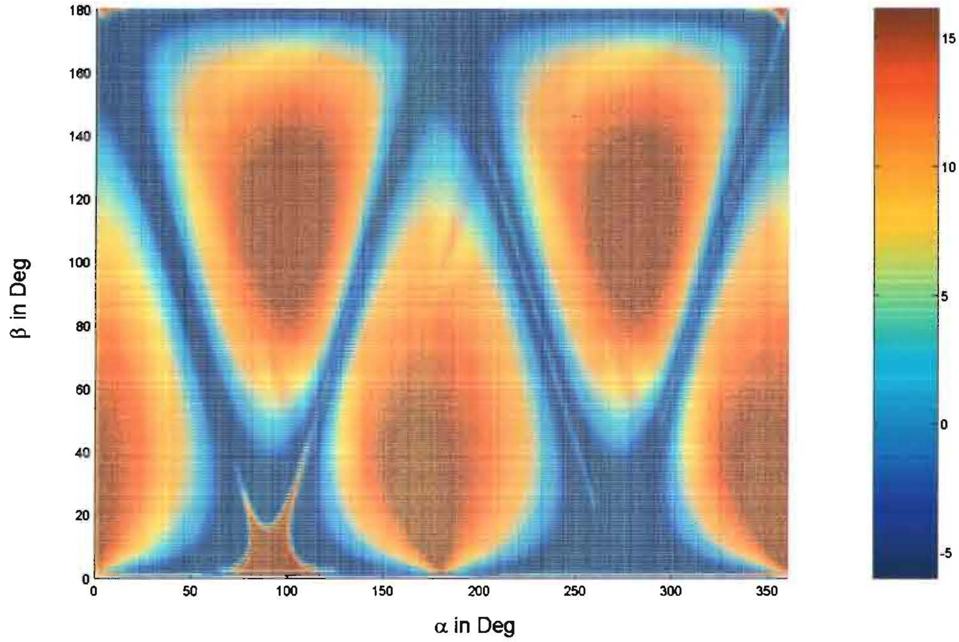

Figure 3.10: Non-identical V-switches: chrominance (V) SNR as function of absolute phase α and relative phase β.

Chapter 4

Implementations of the new decoder

We now have two kernels available for comb-filtering, i.e. using two samples, as described in Chapter 2.1, and a new method using three samples, as described in Chapter 3. Combining both methods promises an increase in decoding quality, as in some situations a three sample comb-filter is expected to yield better results than a two sample comb-filter and vice versa. By locally selecting the filter that yields superior results, an overall increase in quality is expected.

Decision rules are therefore required that, based upon local signal characteristics, select the most suitable comb-filter. In our approach, this decision is performed on a per-sample basis, i.e. for every CVBS sample to be decoded, the most suitable filter is chosen.

For each individual filter, the optimum samples should be selected as input to that filter. In order to ensure a minimal noise sensitivity, the decision rules should take into account the phase relationship between samples. In turn, the correlation noise itself should be minimized by selecting samples with the highest possible correlation. As such, the decision rules should find an optimum trade-off between the following requirements:

- *Optimum phase relationship between samples*, as an ideal phase relationship yields the lowest noise amplification.
- *Highest correlation between samples*, as a perfect correlation introduces no correlation noise.

Determining the optimum phase relationship between samples is straightforward, as the theoretical *stable regions* have been previously determined (see Chapter 3.2 and 3.3), and the phase is regenerated locally and therefore available to the comb-filter.

However, determining the correlation between samples constitutes a chicken-or-the-egg problem: in order to decode the composite video, one needs to know the correlation between samples, which in turn is only available after decoding.

To break this cycle, the comb-filter can be initialized by a simple separation, i.e. the band-pass and notch filters as depicted in Figure A.1. In the luminance path, the subcarrier is greatly attenuated, which prevents severe cross-luminance artifacts but reduces the luminance bandwidth. Even though this initial separation is far from perfect, we would like to investigate its suitability for this purpose, and eventually compare it to an initialization using more advanced separation methods.

Ideally, the correlation between samples should be determined by the correlation of luminance and chrominance. However, we will initially restrict ourselves to luminance correlation. This implicitly assumes that spatial and/or temporal changes in luminance value are accompanied by changes in chrominance value. If this assumption is proven invalid in real-life sequences, an additional chrominance adaptivity might be required.

4.1 Candidate selection

With both phase and correlation information available, a straightforward approach is to apply both criteria to spatially and/or temporally adjacent samples: the so-called *candidate set*. The optimum samples or *candidates* within that candidate set serve as input to either the two or three sample filter, thereby decoding the current CVBS sample.

In terms of candidate samples, spatially and/or temporally adjacent samples are generally expected to have a higher correlation to the current sample than non-adjacent samples. Therefore, larger spatial and/or temporal distances should be avoided, since the determined correlation might not be accurate in all situations due to the non-ideal initialization.

On the other hand, local signal characteristics can result in insufficient spatially and/or temporally adjacent samples which both meet the required phase relationship and exhibit sufficient correlation. As such, a larger number of candidates is preferred, as it will increase the amount of suitable candidates. This translates into considering samples with a larger spatial and/or temporal distance, and as such, seems to be contradictory to the previous claim.

4.1.1 Up-sampling

A possible solution to this problem is *up-sampling*, where an increased density of the sampling grid is achieved by means of interpolation. Within a certain spatial distance, now k times as many candidates are available in comparison to the original sampling grid (with k being the up-sampling factor). Therefore, the amount of candidates has increased, whereas a deterioration of correlation due to increased spatial distance has been avoided.

A straightforward way of up-sampling is the adding of zero-valued samples between the original samples, until the desired sampling frequency is achieved. For example, up-sampling by a factor of two is performed by the insertion of one zero between two original samples. By low-pass filtering the upsampled signal, any alias components above the original Nyquist frequency are removed. The following equations illustrate the zero-stuffing:

$$F_z(\vec{x}+\frac{a}{k},n)=\begin{cases} F(\vec{x},n) & \text{,if } \frac{a}{k}=1,2,3,\dots \\ 0 & \text{,else} \end{cases} \tag{4.1}$$

and the subsequent low-pass filtering of the upsampled signal, where h(a) equals the impulse response of the low-pass filter depicted in Figure A.4:

$$F_{up}(\vec{x},n)=\sum_a F_z(\vec{x}+\begin{pmatrix} a \\ 0 \end{pmatrix},n)\cdot h(a), \qquad a=\dots,-1,0,1,\dots \tag{4.2}$$

4.1.2 Dynamic window resizing

Another possible solution is the *dynamic resizing* of the candidate window. Basically, in flat areas, i.e. in case of highly correlated samples, the candidate window size will be decreased to avoid any errors due to inaccuracies in the initialization. This also preserves chrominance edges in areas devoid of luminance edges, as the filter will be forced to small spatial and/or temporal distances.

In highly detailed or textured areas, the candidate window size will increase to allow a minimum amount of candidates which meet both the phase requirements and exhibit sufficient correlation. This also prevents unnecessary use of resources as the window size is only increased if needed.

As such, a measure for the amount of detail or texture around the current sample is required. A straightforward solution is shown in Equation 4.3. Here, $T(\vec{x},n)$ is a measure for the amount of detail, or texture, in a region around pixel position $\vec{x}$ in field $n+m$. If $m=0$, the amount of detail is determined around the sample's position in the current field, i.e. the spatial correlation. If $m\neq 0$, the measure is determined in temporally adjacent fields around the same pixel position $\vec{x}$.

$$T(\vec{x},n+m)=\sum_{i=-N}^{N}\sum_{j=-M}^{M}\left|Y_{init}(F_{up}(\vec{x},n))-Y_{init}(F_{up}(\vec{x}+\begin{pmatrix} i \\ j \end{pmatrix},n+m))\right| \tag{4.3}$$

The measure itself consists of the summing of the absolute difference between the current sample's and the candidate's initial luminance values within a certain fixed spatial neighborhood. As previously stated, the initial luminance can be obtained by a notch filter, but more elaborate separations

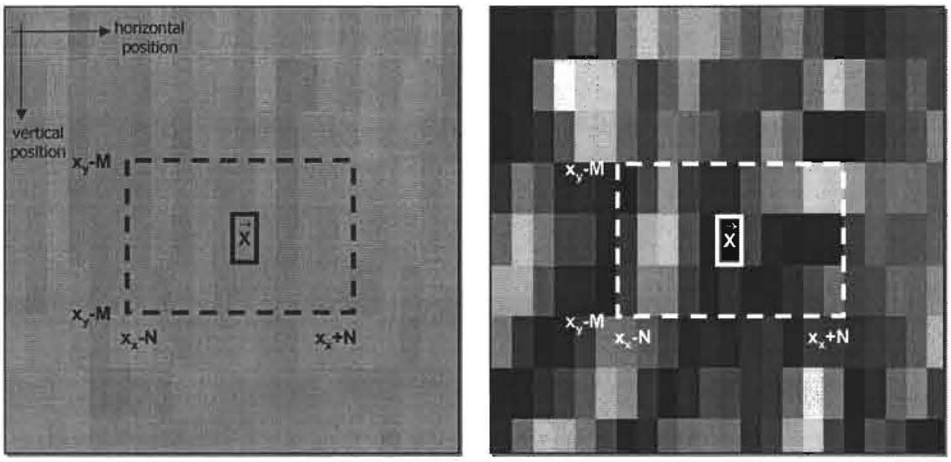

(a) (b)

Figure 4.1: Example of noise measurement in *Cross-color couple* sequence: a) flat region and b) detailed region.

are possible as well. The region is defined by a displacement N in horizontal direction, and a displacement M in vertical direction. Depending upon the horizontal up-sampling factor k, the horizontal displacement equals $\frac{N}{k}$ samples in the original sampling grid.

This approach is illustrated in Figure 4.1, where two segments of the *Cross-color couple* sequence are shown. It illustrates that within an identical noise measurement window, the samples in the flat region exhibit a significantly higher correlation with the current sample than in the detailed region.

Unfortunately, the detector is unable to distinguish between noise and detail. A flat area corrupted by noise of sufficient strength can yield the same measure as a detailed, non-noise corrupted area. Therefore, to be able to distinguish between noise and detail, a global noise adaptivity seems desirable, i.e. a measure for the noise on the whole image, which can be used to scales the results of the local measurement. This is explained in more detail in Reference [7] (pp. 65-68). In the implementation of the proposed comb-filter, this feature was not yet implemented.

4.1.3 Candidate set

From the measure $T(\vec{x}, n+m)$, horizontal and vertical boundaries t_x and t_y are derived, which are then scaled by a factor s_x and s_y respectively. These scaling factors translate the amount of detail in the measurement region into

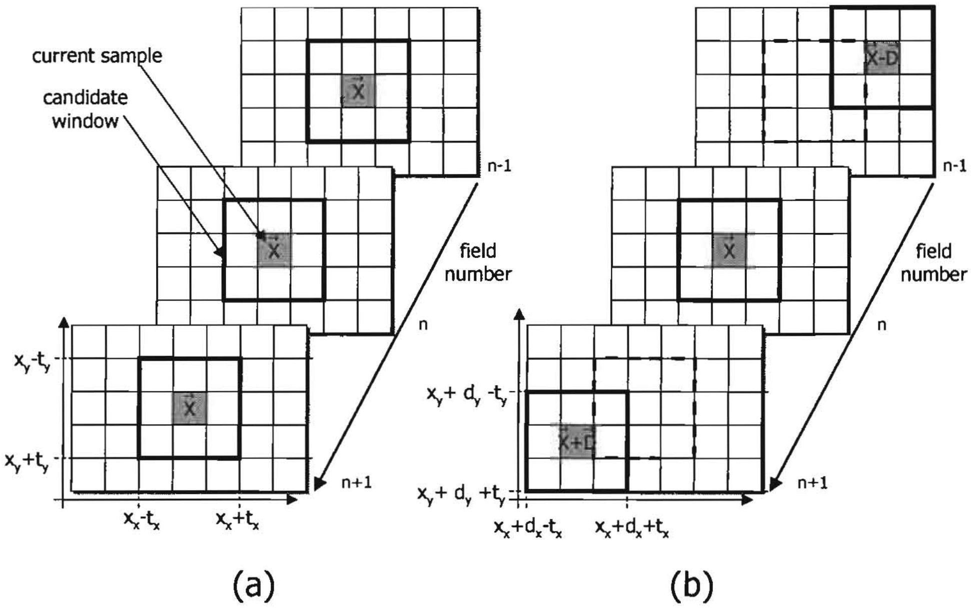
current sample
candidate window
$\vec{X}$
n-1
field number
n
n+1
x_y-t_y
x_y+t_y
x_x-t_x
x_x+t_x
(a)
$\vec{X}$-$\vec{D}$
$\vec{X}$
$\vec{X}$+$\vec{D}$
n-1
field number
n
n+1
x_y+ d_y -t_y
x_y+ d_y +t_y
x_x+d_x-t_x
x_x+d_x+t_x
(b)

Figure 4.2: Candidate windows in the next, current and previous fields at a) fixed position $\vec{x}$ and b) motion compensated positions $\vec{x} + D(\vec{x}, n)$, $\vec{x}$ and $\vec{x} - D(\vec{x}, n-1)$ respectively.

boundaries for the candidate set.

$$
\begin{aligned}
t_x &= \frac{1}{s_x} \cdot \frac{1}{(2N+1) \cdot (2M+1)} \cdot T(\vec{x}, n+m) \\
t_y &= \frac{1}{s_y} \cdot \frac{1}{(2N+1) \cdot (2M+1)} \cdot T(\vec{x}, n+m)
\end{aligned}
\tag{4.4}
$$

The size of the candidate window is then determined by the horizontal and vertical boundaries t_x and t_y:

$$
C(\vec{x}, n+m) = \left\{ F_{up}(\vec{x} + \begin{pmatrix} i \\ j \end{pmatrix}, n+m), i \in \{-t_x, \ldots, t_x\}, j \in \{-t_y, \ldots, t_y\} \right\}
\tag{4.5}
$$

If only spatial candidates are used, i.e. $m = 0$, this leads to Equation 4.6, i.e. the complete candidate set CS equals the spatial candidate set $C(\vec{x}, n)$.

$$
CS = \{C(\vec{x}, n)\}
\tag{4.6}
$$

However, the CS might be composed of spatial as well as temporal candidates. For example, consider the candidate set shown in Equation 4.7 and Figure 4.2a, where candidates originate from candidate windows in the previous, current and next field. Here, the size of the candidate window is

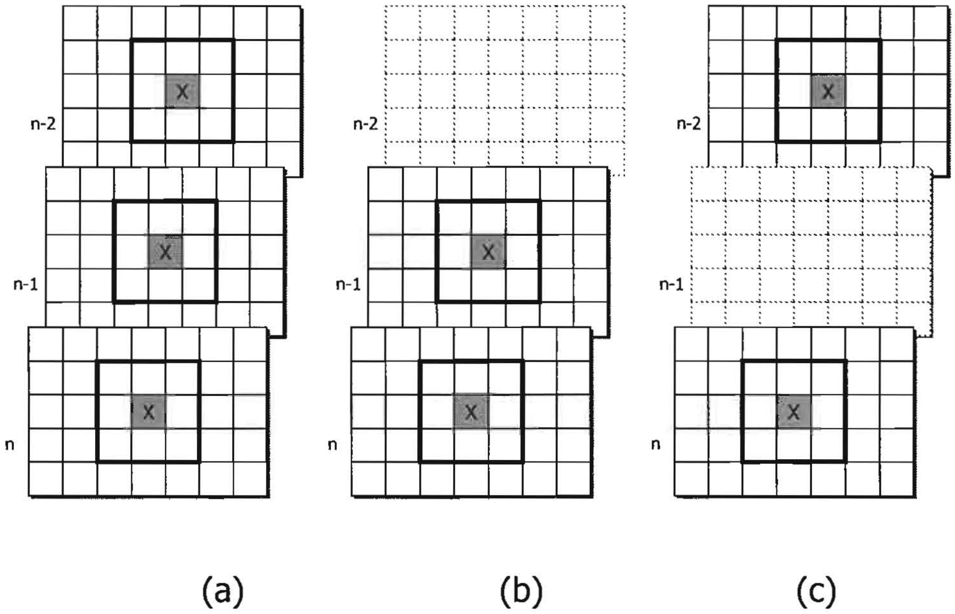

Figure 4.3: Temporal candidate sets: a) frame and field, b) field only and c) frame only.

adjust per field, i.e. the noise measure $T(\vec{x}, n+m)$ is determined for each field individually.

$$CS = \{C(\vec{x}, n+1) + C(\vec{x}, n) + C(\vec{x}, n-1)\} \tag{4.7}$$

As opposed to temporal windows centered around the current spatial position, motion compensation could be used to increase the correlation of temporal candidates by positioning the candidate windows along the motion axis. This is illustrated in Equation 4.8 and Figure 4.2b, where $D(\vec{x}, n)$ describes the displacement of the sample at pixel position $\vec{x}$ in field n to field $n+1$ (the displacement from field n to $n-1$ is assumed to be $-D(\vec{x}, n)$, i.e. linear movement).

$$CS = \{C(\vec{x} + D(\vec{x}, n), n+1) + C(\vec{x}, n) + C(\vec{x} - D(\vec{x}, n), n-1)\} \tag{4.8}$$

Due to the increase in latency, comb-filters using a next field can be undesirable. Therefore, various configurations are possible using only previous fields. Three examples are illustrated in Equations 4.9 through 4.11 and Figure 4.3a through 4.3c, where respectively frame and field, field only and frame only comb-filters are shown.

$$
\begin{aligned}
CS &= \{C(\vec{x},n) + C(\vec{x},n-1) + C(\vec{x},n-2)\} && (4.9)\\
CS &= \{C(\vec{x},n) + C(\vec{x},n-1)\} && (4.10)\\
CS &= \{C(\vec{x},n) + C(\vec{x},n-2)\} && (4.11)
\end{aligned}
$$

4.2 Penalty calculation

Given a candidate set *CS* of *CSMAX* candidates, a penalty value is assigned to each candidate as a function of both the phase relationship and the correlation to the current sample. This is shown in Equation 4.12, where the penalty ϵ_i is calculated for all candidates CS_i with $i \in \{1, \ldots, CSMAX\}$. The total penalty equals the weighted sum of the correlation penalty $L\,(CS_i, F_{cvbs1})$ and the phase penalty $P\,(CS_i)$, where α_1 and α_2 correspond to the respective weighting factors:

$$\epsilon_i(CS_i, F_{cvbs1}) = \alpha_1 \cdot L\,(CS_i, F_{cvbs1}) + \alpha_2 \cdot P\,(CS_i) \qquad (4.12)$$

with:

$$F_{cvbs1} = F_{up}(\vec{x}, n) \qquad (4.13)$$

The correlation penalty is calculated in a straightforward manner as the absolute difference of the initially separated luminance values, as shown in Equation 4.14. Experiments verified the validity of this approach, although improvements may be achieved by further optimization.

$$L\,(CS_i, F_{cvbs1}) = |Y_{init}(F_{cvbs1}) - Y_{init}(CS_i)| \qquad (4.14)$$

The basic idea behind the phase penalty is that the phase differences that result in no amplification of correlation noise should yield the lowest penalty. For the two sample decoder, this equals an opposite phase. For the three sample decoders, these equal the stability regions as calculated and illustrated in Chapters 3.2 and 3.3. If the phase difference exceeds these stable regions, the phase penalty should increase accordingly. The phase penalty should therefore be modelled around the phase stability regions described earlier. However, for our purposes these regions are approximated.

First, we will define $\angle(F_{cvbs1})$ as the subcarrier phase of F_{cvbs1}. The normalized phase difference β_n, which transforms the relative phase β from $[0, 2\pi]$ to $[-\pi, \pi]$, is determined according to:

$$
\begin{aligned}
\beta &= |\angle(CS_i) - \angle(F_{cvbs1})| && (4.15)\\
\beta_n &= \begin{cases} 2\pi - \beta & \text{,if } \beta > \pi \\ \beta & \text{,else} \end{cases} && (4.16)
\end{aligned}
$$

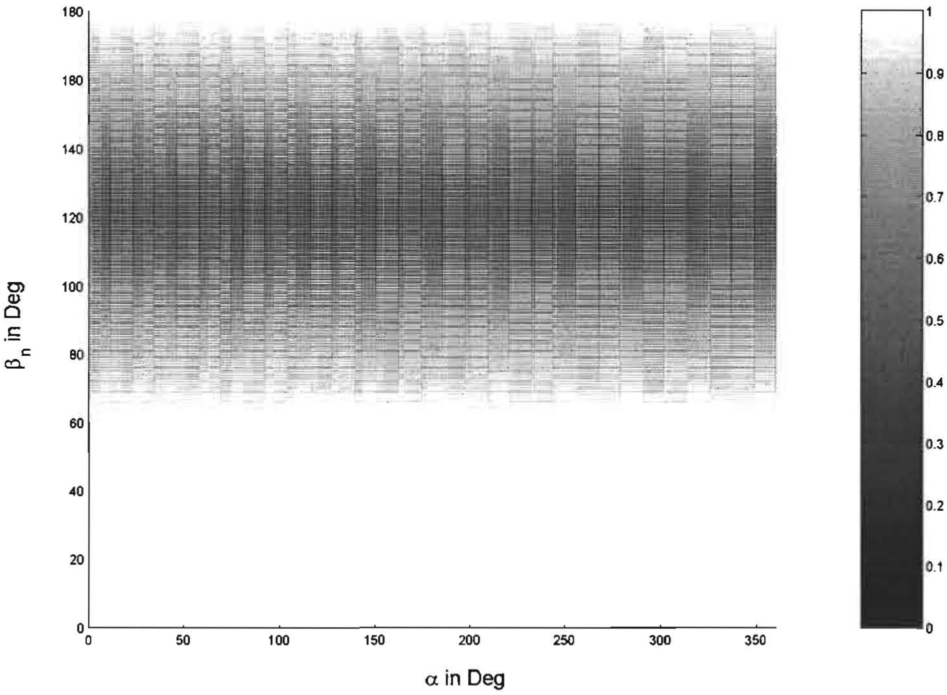

Figure 4.4: Identical V-switches: phase penalty as function of absolute phase α (i.e. $\angle(F_{cvbs1})$) and normalized phase difference β_n.

4.2.1 Identical V-switches

Again, we distinguish between identical and non-identical V-switches. In the first situation, a two sample comb-filter requires an opposite relative phase, whereas the stable regions for the three sample comb-filter are illustrated in Figure 3.3. As such, candidates with an opposite phase or phase difference of 120° yield the lowest phase penalty, whereas decreasing phase differences will result in increased penalties. Equation 4.17 and Figure 4.4 illustrate this approximation, which is clearly not dependent upon the absolute phase α of F_{cvbs1}.

$$P\left(CS_i\right) = \begin{cases} 0 & \text{,if } \beta_n = \pi \\ \frac{3\beta_n - 2\pi}{\pi} & \text{,if } \frac{2\pi}{3} < \beta_n < \pi \\ \frac{2\pi - 3\beta_n}{\pi} & \text{,if } \frac{\pi}{3} < \beta_n \leq \frac{2\pi}{3} \\ 1 & \text{,else} \end{cases} \tag{4.17}$$

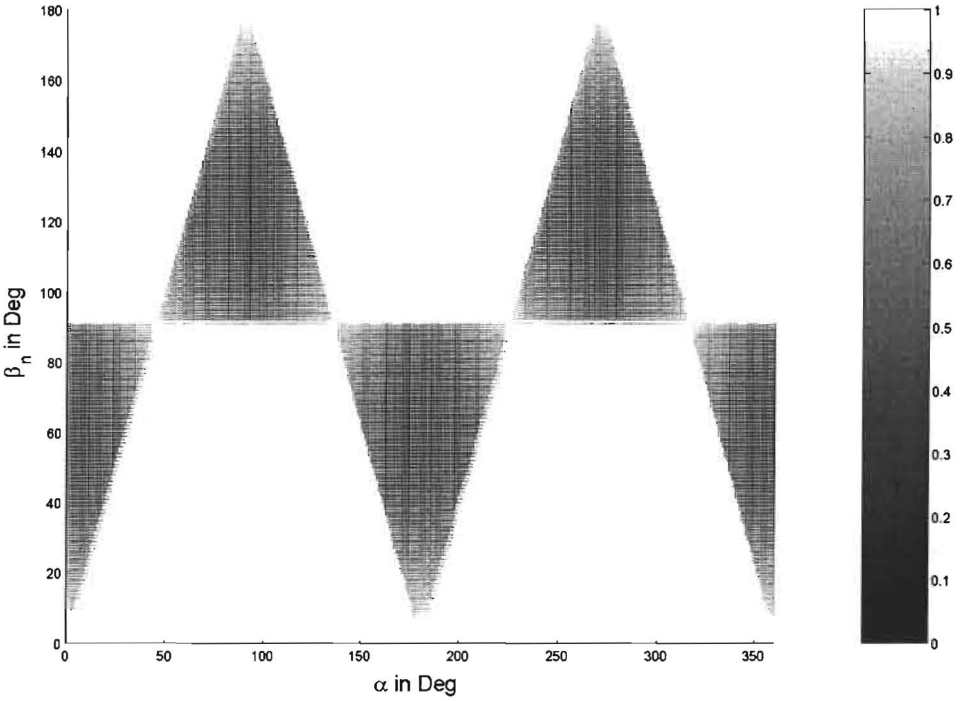

Figure 4.5: Non-identical V-switches: phase penalty as function of absolute phase α (i.e. $\angle(F_{cvbs1})$) and normalized phase difference β_n.

4.2.2 Non-identical V-switches

In case of non-identical V-switches, comb-filtering using two samples is only possible if the samples' absolute phases are opposite. When comb-filtering with three samples, the situation is more complicated, as the ideal phase difference is dependent upon the absolute phase of F_{cvbs1} (see Chapter 3.3). As such, the stable regions illustrated in Figure 3.8, 3.9 and 3.10 need to be approximated by the phase penalty function. Figure 4.5 shows this approximation, i.e. a phase penalty of zero in center of the stable regions, and a penalty of one outside the stable regions.

The corresponding equations are shown below, where again α is $\angle(F_{cvbs1})$ and β equals the phase difference with CS_i. Equation 4.19 shows the penalty for $0 < \alpha \leq \frac{\pi}{2}$, whereas the penalty for the other three quadrants, i.e. between $\frac{\pi}{2}, \pi, \frac{3\pi}{2}$ and 2π can be mapped to the first quadrant by means of α_n:

$$\alpha_n = \begin{cases} 2\pi - \alpha & \text{,if } \frac{3\pi}{2} < \alpha \leq 2\pi \\ \alpha - \pi & \text{,if } \pi < \alpha \leq \frac{3\pi}{2} \\ \pi - \alpha & \text{,if } \frac{\pi}{2} < \alpha \leq \pi \\ \alpha & \text{,else} \end{cases} \tag{4.18}$$

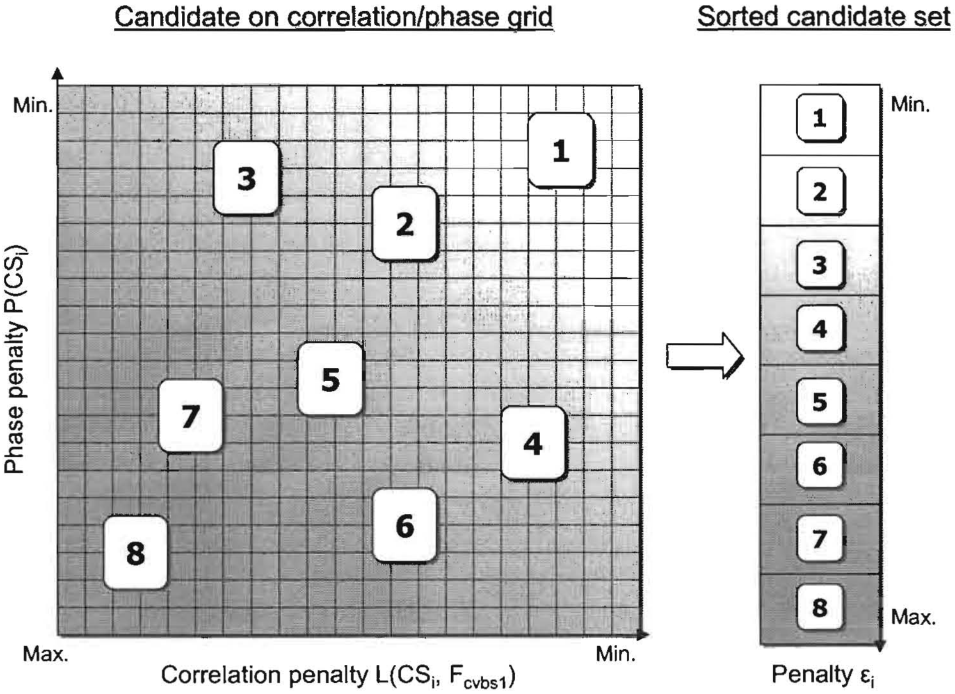
Candidate on correlation/phase grid
Sorted candidate set
Min.
Phase penalty P(CS$_i$)
Max.
Correlation penalty L(CS$_i$, F$_{cvbs1}$)
Min.
1
2
3
4
5
6
7
8
Min.
Max.
Penalty ε$_i$

Figure 4.6: Candidates on a 2D correlation/phase plane and the resulting sorted candidate set.

$$P(CS_i) = \begin{cases} 0 & ,\text{if } \angle(CS_i) = -\alpha \\ \left(\alpha_n^2 + (\beta_n - \frac{\pi}{3})^2\right)^2 & ,\text{if } \left(0 \leq \alpha_n < \frac{\pi}{4}\right) \wedge \left(2\alpha_n < \beta_n < \frac{\pi}{2}\right) \\ \left((\alpha_n - \frac{\pi}{2})^2 + (\beta_n - \frac{2\pi}{3})^2\right)^2 & ,\text{if } \left(\frac{\pi}{4} \leq \alpha_n \leq \frac{\pi}{2}\right) \wedge \left(\frac{\pi}{2} < \beta_n < 2\alpha_n\right) \\ 1 & ,\text{else} \end{cases} \tag{4.19}$$

Having determined the penalties for the $CSMAX$ candidates within candidate set CS, the optimum candidate, i.e. the one with the lowest penalty, will be chosen according to Equation 4.20. This is also shown in Figure 4.6, where a number of candidates are shown on a 2D correlation/phase plane, as well as the resulting sorted candidate set.

$$\begin{aligned} \exists j \in [1, \ldots, CSMAX] : \forall i &\in [1, \ldots, CSMAX] : \epsilon_j \leq \epsilon_i \\ F_{cvbs2} &= CS_j \end{aligned} \tag{4.20}$$

In the following two situations, both samples will be decoded by the two sample decoder:

- The V-switch of F_{cvbs1} and F_{cvbs2} is *equal*, and both samples have an opposite relative phase (i.e. phase difference 180°).

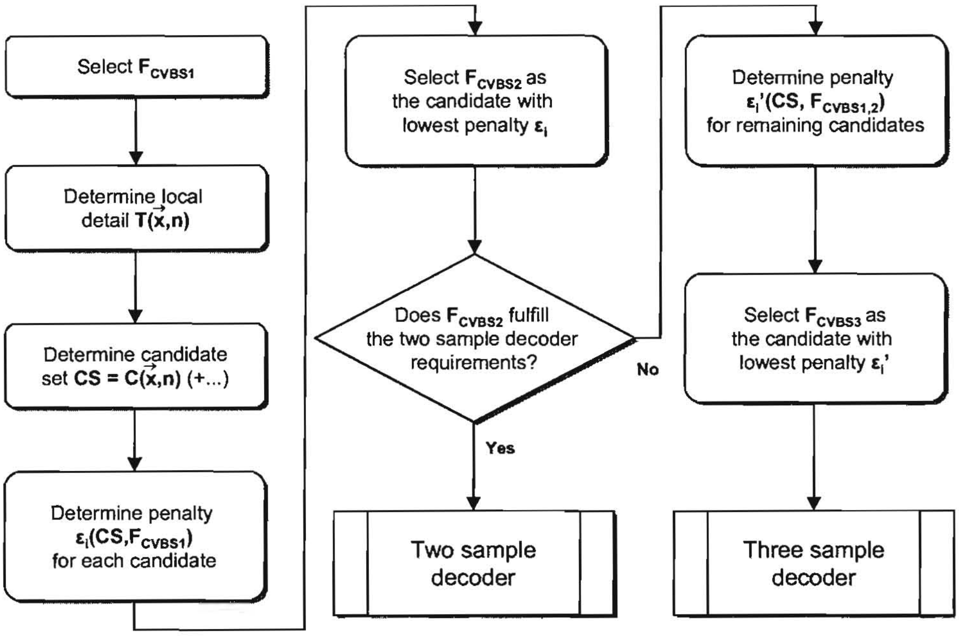
Select F_{CVBS1}
Determine local detail $T(\vec{x},n)$
Determine candidate set $CS = C(\vec{x},n)$ (+...)
Determine penalty $\varepsilon_i(CS, F_{CVBS1})$ for each candidate
Select F_{CVBS2} as the candidate with lowest penalty ε_i
Does F_{CVBS2} fulfill the two sample decoder requirements?
No
Yes
Two sample decoder
Determine penalty $\varepsilon_i'(CS, F_{CVBS1,2})$ for remaining candidates
Select F_{CVBS3} as the candidate with lowest penalty ε_i'
Three sample decoder

Figure 4.7: Flowchart of proposed comb-filter.

- The V-switch of F_{cvbs1} and F_{cvbs2} is *opposite*, and both samples have an opposite absolute phase.

4.2.3 Three sample decoder

In all other cases, no suitable candidates for the two sample decoder was available, and as such, F_{cvbs_2} has been optimized for the three sample decoder: a third sample is now required with an optimum phase relationship and correlation to both F_{cvbs1} and F_{cvbs2}. Therefore, the modified penalty ϵ_i' shown in Equation 4.21 is determined for all remaining candidates, after which F_{cvbs3} is selected as the candidate with the lowest penalty. This process is shown as a flowchart in Figure 4.7.

$$\epsilon_i'(CS_i, F_{cvbs1,2}) = \alpha_1 \cdot L\left(CS_i, F_{cvbs1}\right) + \alpha_2 \cdot P'\left(CS_i\right) \tag{4.21}$$

The correlation penalty remains identical, as again the absolute difference with F_{cvbs1} is determined. For the phase penalty calculation however, an extra step is necessary to ensure that the correct penalty is determined for all relative phases. As illustrated previously in Figure 3.2, if the optimum relative phase β between F_{cvbs1} and F_{cvbs2} is +120°, the optimum relative phase γ between F_{cvbs1} and F_{cvbs3} is −120°. Therefore, should β_n

be positive, γ_n should be negative and vice versa; F_{cvbs3} should be on the *oppposite side* of the phase circle as F_{cvbs2}.

As such, for all candidates for which γ_n and β_n have the same sign, the penalty is set to one. For all other candidates, the phase penalties is determined again by $P\left(CS_j\right)$.

$$P'\left(CS_j\right) = \begin{cases} 1 & \text{,if sign } (\beta_n) \neq \text{sign } (\gamma_n) \\ P\left(CS_j\right) & \text{,else} \end{cases} \tag{4.22}$$

with:

$$\begin{aligned} \beta &= \angle(F_{cvbs2}) - \angle(F_{cvbs1}) && (4.23) \\ \gamma &= \angle(CS_j) - \angle(F_{cvbs1}) && (4.24) \end{aligned}$$

and:

$$(\beta,\gamma)_n = \begin{cases} (\beta,\gamma) - 2\pi & \text{,if } (\beta,\gamma) > \pi \\ (\beta,\gamma) + 2\pi & \text{,if } (\beta,\gamma) < -\pi \\ (\beta,\gamma) & \text{,else} \end{cases} \tag{4.25}$$

Again, F_{cvbs3} will be chosen according to:

$$\begin{aligned} \exists j \in [1,\ldots,CSMAX] : \forall i &\in [1,\ldots,CSMAX] : \epsilon'_j \leq \epsilon'_i \\ F_{cvbs3} &= CS_j \end{aligned} \tag{4.26}$$

Conclusions

Above penalty calculation determines the penalty as a function of both the correlation as well as the phase difference. The optimum phase difference yields no phase penalty, whereas an unsuitable phase difference results in the maximum phase penalty. This ensures that candidates with the best correlation and optimum phase differences will be selected as F_{cvbs2}.

Depending upon the phase and V-switch of both F_{cvbs1} and F_{cvbs2}, both are either decoded by the two sample comb-filter, or a third sample is required for the three sample comb-filter. In the latter case, the penalty calculation is analogous to that of F_{cvbs2}, except that all candidates at the same relative side of F_{cvbs2} are assigned the maximum phase penalty. This ensures that both relative phases β and γ have an opposite sign, which in turn enables the re-use of the existing penalty functions.

A potential drawback of above candidate selection is that the suitability of a candidate for F_{cvbs2} determines the choice between the both decoders. Situations can occur where the three sample decoder is chosen due to a more suitable candidate for F_{cvbs2}, but where no suitable candidate for F_{cvbs3} can be found. In this case, the two sample decoder would have potentially yielded better decoding quality. This can be avoided by taking into account the correlation of all candidates. However, this is computationally expensive, as the (exhaustive) testing of all possible candidate combinations is required.

4.3 Decoder configurations

Having discussed the principles of the proposed comb-filter, various configurations are now possible within the PAL decoder. The standard configuration is shown in Figure 4.8a, where the luminance as well as the chrominance components are decoded by the proposed comb-filter. In the chrominance path, a low-pass filter (as depicted in Figure A.2) is present to suppress any frequency components above approximately 1.3MHz, as the chrominance has been bandlimited prior to encoding. As such, any high frequent decoding errors and/or noise can be suppressed, as clearly they cannot be part of the original chrominance signal.

Depending upon the implementation, the chrominance is then usually downsampled by a factor of two to arrive at half the luminance's sampling frequency (usually referred to as YUV-422, see Reference [9] pp. 19-24). As the signal has been bandlimited to below the new Nyquist frequency, a reduced memory storage requirement can be achieved without signal deterioration.

Instead of the PAL delay line used in a standard PAL decoder, a PAL median filter is applied to the chrominance U and V signals as developed by Philips PDSL and described in Reference [13]. Whereas the PAL delay line blurs vertical edges, the median filter preserves vertical chrominance edges and avoids the PAL delay line's vertical displacement of $\frac{1}{2}$ field line.

4.3.1 Selection techniques

As the initialization by a notch filter is far from perfect, decoding errors will occur. An improvement might be realized by selecting the top m best candidates for F_{cvbs2} (and subsequently F_{cvbs3} if F_{cvbs2} is unsuitable for the two sample decoder) instead of only the best one. This results in m comb-filter outputs, which then can be combined to form the decoded Y, U and V values.

Straightforward filters which can be used to combine the m outputs include *averaging*, *median filtering* and *vector median filtering*. Other approaches may be used as well, as e.g. the neighborhood selection techniques mentioned in Reference [7] (pp. 59-64). The *averaging filter* is the most basic approach, as illustrated in Equation 4.27 where three comb-filter outputs combined. Here, $CF_{y,1}$ corresponds to the luminance output of the first comb-filter. The main drawback is the inherent introduction of blurring if not all samples carry the same information. As such, extreme values

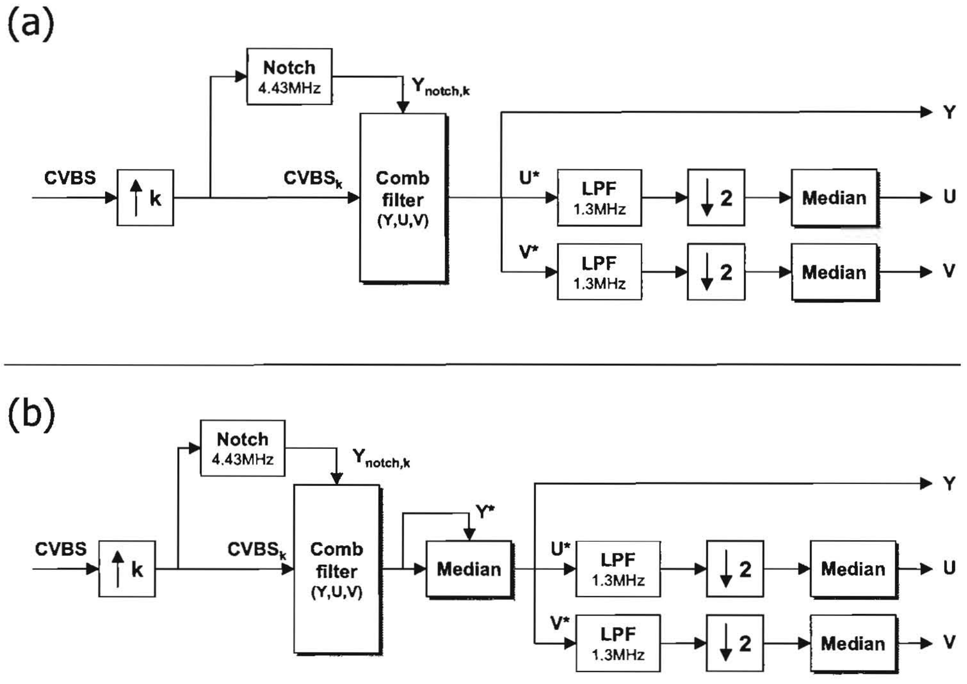
(a)
Notch
4.43MHz
Y_notch,k
Y
CVBS
↑k
CVBS_k
Comb
filter
(Y,U,V)
U*
LPF
1.3MHz
↓2
Median
U
V*
LPF
1.3MHz
↓2
Median
V
(b)
Notch
4.43MHz
Y_notch,k
Y
Y*
CVBS
↑k
CVBS_k
Comb
filter
(Y,U,V)
Median
U*
LPF
1.3MHz
↓2
Median
U
V*
LPF
1.3MHz
↓2
Median
V

Figure 4.8: a) Standard decoder configuration, and b) luminance median filter at the output.

caused by decoding errors have a significant contribution to the output of the decoder.

$$Y_d(\vec{x},n) = \frac{1}{3}\left(CF_{y,1}(\vec{x},n) + CF_{y,2}(\vec{x},n) + CF_{y,3}(\vec{x},n)\right) \quad (4.27)$$

$$U_d(\vec{x},n) = \frac{1}{3}\left(CF_{u,1}(\vec{x},n) + CF_{u,2}(\vec{x},n) + CF_{u,3}(\vec{x},n)\right) \quad (4.28)$$

$$V_d(\vec{x},n) = \frac{1}{3}\left(CF_{v,1}(\vec{x},n) + CF_{v,2}(\vec{x},n) + CF_{v,3}(\vec{x},n)\right) \quad (4.29)$$

The *median filter* avoids this problem in many instances, as the output of the decoder with the least extreme value is selected. As such, outliers are removed and do not contribute to the output. As the decoder output consists of a triplet of values, i.e. the Y, U and V values, median filtering is possible both on one of the values, e.g. the luminance, and on all three by means of a vector median.

The first approach is illustrated in Figure 4.8b, where the median filter operates on the luminance only. This means, that the least extreme luminance value is selected, along with the corresponding chrominance values. The latter however are not necessarily the least extreme values. The following equation illustrates the median filter, where sel_y selects the corresponding chrominance values to the selected luminance value:

$$
\begin{aligned}
Y_d(\vec{x},n) &= med_y\left(CF_{y,1}(\vec{x},n), CF_{y,2}(\vec{x},n), CF_{y,3}(\vec{x},n)\right) && (4.30)\\
U_d(\vec{x},n) &= sel_y\left(CF_{u,1}(\vec{x},n), CF_{u,2}(\vec{x},n), CF_{u,3}(\vec{x},n)\right) && (4.31)\\
V_d(\vec{x},n) &= sel_y\left(CF_{v,1}(\vec{x},n), CF_{v,2}(\vec{x},n), CF_{v,3}(\vec{x},n)\right) && (4.32)
\end{aligned}
$$

Another approach is the use of a *vector median filter*, as described in Reference [3], where the median operates on all three input values. As such, the resulting output is the least extreme combination of Y, U and V values:

$$
(Y,U,V)_d(\vec{x},n) = med_{(y,u,v)}\left(CF_1(\vec{x},n), CF_2(\vec{x},n), CF_3(\vec{x},n)\right) \qquad (4.33)
$$

However, for our purposes, this approach is unsuitable as the chrominance output of the two sample decoder contains alias components. As such, the chrominance has to be low-pass filtered prior to the vector median filtering, which in our case requires as many filters as there are combinations of selecting candidates for the two sample decoder within the candidate set. Due to its complexity, this approach could not be implemented.

4.3.2 Chrominance derived from luminance

Another possible improvement of the basic PAL decoder is the regeneration of the chrominance from the decoded luminance. For the two sample comb-filter, the chrominance is complementary to the luminance, as the summation of the decoded Y and C yields the original CVBS signal. However, for the three sample decoder, the luminance and chrominance are not necessarily complementary. This is caused by the fact that the stable regions for the Y, U and V components are not identical. As such, at phase combinations where the luminance component yields no noise amplification, this may not be the case for the chrominance components.

The approximated penalty functions, as previously illustrated in Figures 4.4 and 4.5, have been modelled from the luminance stability regions. This suggests that the decoded luminance is less noise susceptible than the decoded chrominance, and as such, an improved chrominance might be obtained by deriving it from the CVBS signal. This approach is illustrated in Figure 4.9a, where the chrominance is generated by subtracting the decoded luminance from the original CVBS signal. In turn, the U and V components are obtained by demodulating the resulting chrominance signal.

Furthermore, results similar to vector median filtering may be obtained by deriving the chrominance from the median filtered luminance. Any gain in luminance quality by means of median filtering will therefore result in a gain in chrominance quality.

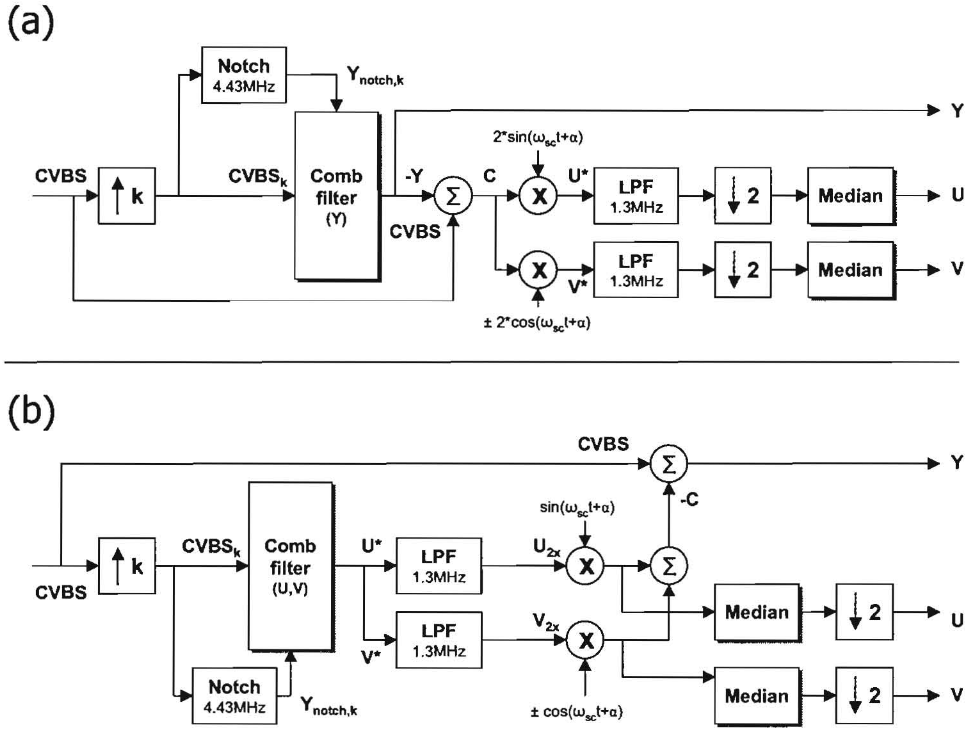
(a)
Notch
4.43MHz
Y_notch,k
CVBS
↑k
CVBS_k
Comb filter (Y)
-Y
CVBS
Σ
C
2*sin(ω_sc t+α)
X
U*
LPF 1.3MHz
↓2
Median
Y
U
X
V*
LPF 1.3MHz
↓2
Median
V
± 2*cos(ω_sc t+α)
(b)
CVBS
Σ
Y
-C
sin(ω_sc t+α)
CVBS
↑k
CVBS_k
Comb filter (U,V)
U*
LPF 1.3MHz
U_2x
X
Σ
Median
↓2
U
V*
LPF 1.3MHz
V_2x
X
Notch
4.43MHz
Y_notch,k
± cos(ω_sc t+α)
Median
↓2
V

Figure 4.9: a) Decoder with luminance comb-filter and derived chrominance, and b) decoder with chrominance comb-filter and derived luminance.

4.3.3 Luminance derived from chrominance

Another improvement may be achieved by the opposite approach: regenerating the luminance by subtracting the decoded chrominance from the CVBS signal. Unlike the luminance signal, the chrominance signal was strictly bandlimited prior to encoding. As such, any high-frequency components are caused by decoding errors and/or noise, and can be suppressed by applying a low-pass filter. The obtained clean chrominance signal can then used to obtain an improved luminance signal, as illustrated in Figure 4.9b.

A possible drawback, however, is the fact that strong low-frequent cross-color artifacts in the chrominance signal will appear in the derived luminance signal as well, hence causing cross-luminance artifacts. This means that cross-luminance artifacts will occur simultaneously with cross-color artifacts, possibly reducing the achieved gain.

Finally, the largest improvement is expected from the combination of all proposed improvements, i.e. the median filtering to reduce the contribution of decoding errors, the subsequent generation and filtering of the improved chrominance, and finally deriving the complementary luminance.

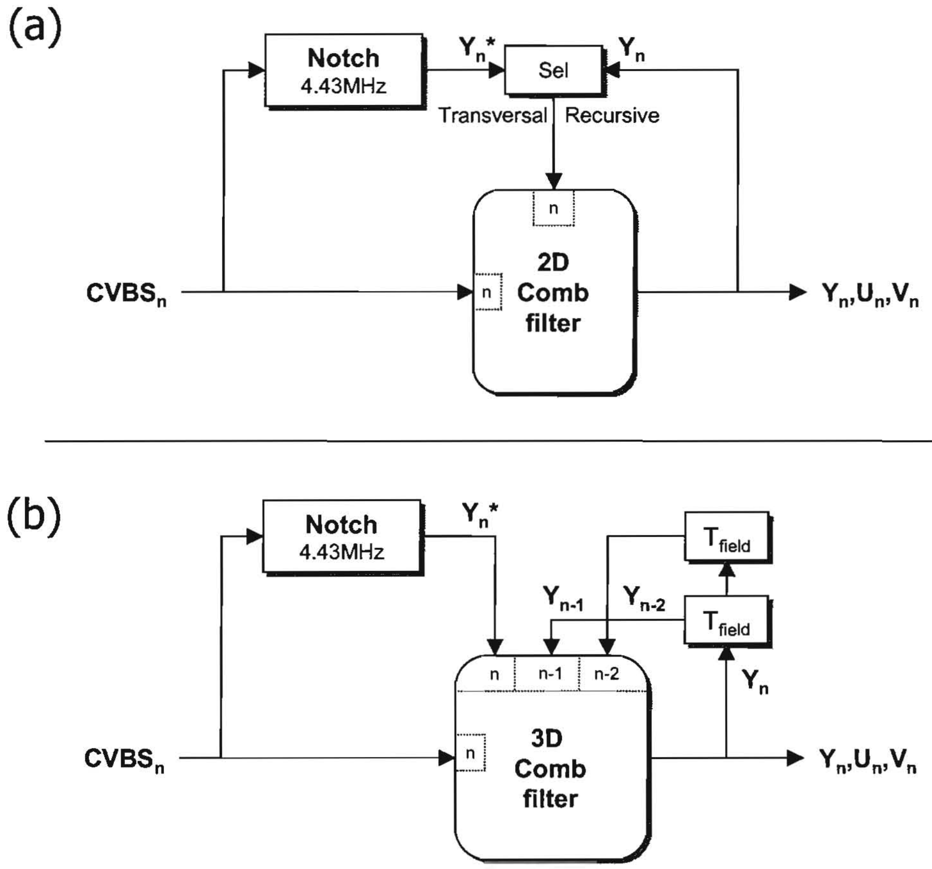
(a)
Notch
4.43MHz
Y*n
Sel
Yn
Transversal
Recursive
n
2D
Comb
filter
CVBSn
n
Yn,Un,Vn
(b)
Notch
4.43MHz
Y*n
Tfield
Yn-1
Yn-2
Tfield
n
n-1
n-2
Yn
3D
Comb
filter
CVBSn
n
Yn,Un,Vn

Figure 4.10: Decoder configuration for a) recursive 2D comb-filtering, and b) recursive 3D comb-filtering.

4.3.4 Recursive comb-filtering

As the notch-filter initialization is far from perfect, a significant improvement in decoding quality is expected by using a more elaborate filter. One way of doing so is *recursive comb-filtering*, where the previous comb-filter output is used to initialize repeated decoding passes. However, due to the required causality, the notch filtered CVBS signal is still used as the first initialization.

Figure 4.10a illustrates this approach for a 2D comb-filter. Here, the gradient is determined from either the notch-filtered input or the decoded luminance signal. A 3D recursive comb-filter configuration is also possible, as depicted in Figure 4.10b. Due to the causality requirement, the 3D comb-filter cannot use next fields, i.e. $n + 1$. The gradient for the current field n is determined from the notch-filtered input, whereas for $n - 1$ and $n - 2$, the gradient is determined from the 1 or 2 field delayed output of the comb-filter.

Chapter 5

Evaluation of the new decoder

The quality assessment of certain design choices is possible by means of *subjective* as well as *objective* quality measures. Whereas the objective quality measures translate certain signal characteristics into quantitative measures, the subjective measures describe opinions of observers (see Reference [14] pp. 31-32). Both quality measures were used in the evaluation of the previously described comb-filter configurations.

For the objective assessment, the Mean Square Error (MSE) was used as criterion to measures the difference between the reference and the decoded image. The measurement setup is shown in Figure 5.1, where the MSE between the decoded signal F_{dec} and the reference signal F_{ref} is defined as:

$$MSE(n) = \frac{1}{N} \sum_{\vec{x}} (F_{ref}(\vec{x}, n) - F_{dec}(\vec{x}, n))^2 \tag{5.1}$$

with N being the number of pixels within a field n and $\vec{x}$ the current sample's position. Typically, the MSE is determined for both the luminance and the chrominance, and averaged over multiple fields. As the pre-filtered signals prior to encoding were chosen as a reference, an ideal comb-filter will yield a zero MSE.

The subjective assessment was primarily done by split-screen comparisons of moving sequences on a 21" CRT and a 18" LCD computer-monitor. Here, motion adaptive de-interlacing was used to display the interlaced sequences on the progressive displays. Also, still fields were used in the subjective assessment. As the evaluation was an initial subjective test, it is not compliant to any standard testing procedure (i.e. ITU-R BT.500-10). In the evaluation of most design steps, the MSE was the primary criterion as often changing one of the many possible parameters did not result in clearly visible changes on the screen. The subjective evaluation was preferred during the comparison of the final comb-filter designs, because at this stage in

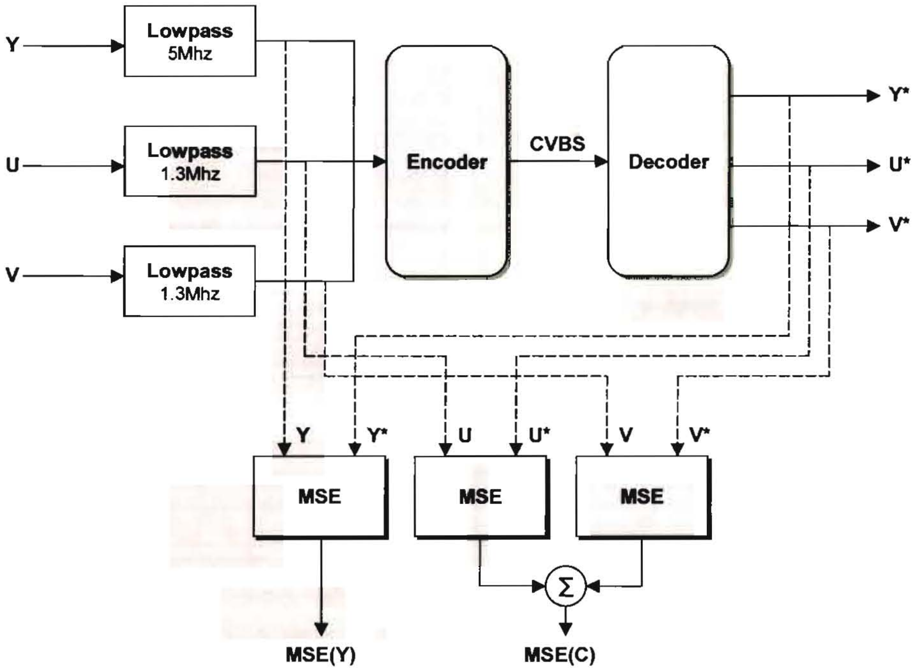

Figure 5.1: Calculation of MSE for luminance and chrominance.

the design process, the differences were visible.

A number of test sequences were selected to evaluate the performance of the comb-filters using the mentioned assessment methods. Ideally, the content of these test sequences should be representative for common broadcast video. However, as this requires an extensive set of sequences, the choice was limited to those where severe cross-talk artifacts were expected to occur. This excludes sequences containing little high-frequency content, e.g. blurry or smooth images. For the evaluation, the following sequences as depicted in Figure 5.2 were selected:

Mobcal contains both highly detailed luminance texture, as for instance in the depicted sheep and calendar's letters, and highly saturated colors. Therefore, both severe cross-color and cross-luminance artifacts are expected to occur. As the sequence contains many moving areas, the temporal correlation will be reduced compared to stationary areas.

Cross-color couple was specifically designed to contain strong high-frequency luminance textures, thereby causing severe cross-color artifacts. Also, any attenuation of high-frequency luminance due to comb-filtering is expected to be visible. As few saturated colors are present, cross-luminance artifacts are less likely to occur. Both stationary as well as fast moving luminance detail is present.

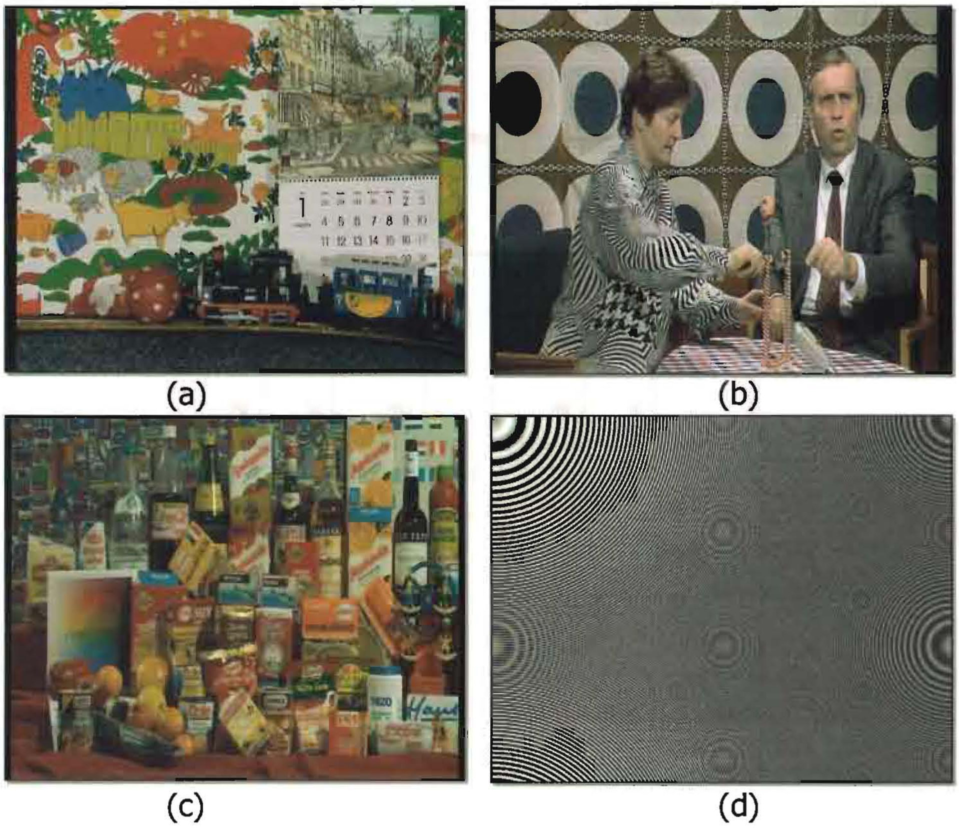

Figure 5.2: Snapshots of the test sequences: a) *Mobcal*, b) *Cross-color couple*, c) *Shopping zoom* and d) *Moving zoneplate* (visible alias is due to printing, and not part of the actual sequence).

Shopping zoom with its strong chrominance edges as well as highly saturated colors is expected to suffer from severe cross-luminance artifacts. Often these edges do not coincide with strong luminance edges, thereby causing problems with comb-filters that use luminance motion detection. The movement consists of a slow zoom towards the center of the image.

Moving zoneplate is an artificially generated sequence, that contains increasing horizontal, vertical and diagonal luminance frequencies starting at the upper-left corner. Therefore, the luminance bandwidth and cross-color suppression characteristics of the comb-filter can be determined from the decoded sequence. As the phase of the generated sine-wave is increased each field, movement is present throughout the sequence.

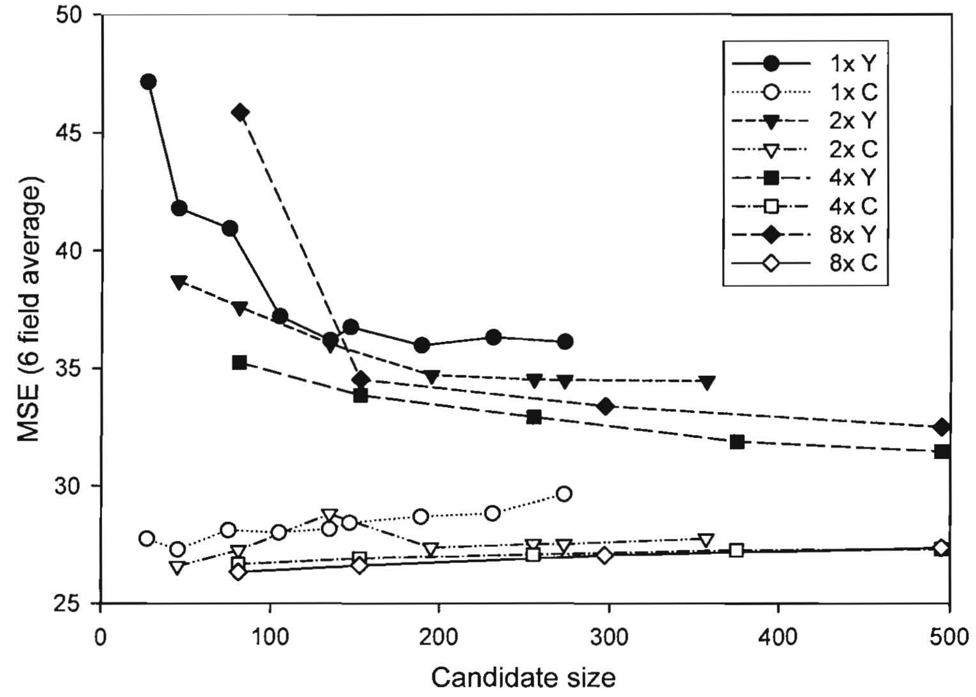

Figure 5.3: *MSE* of Y and C as a function of the candidate set size for up-sampling factors of 1,2,4 and 8.

Chapter 5.1 outlines the results of the objective evaluation of several comb-filter parameters, as they have been previously described in Chapter 4. In turn, Chapter 5.2 compares the objective and subjective performance of the proposed comb-filter to the reference filters described in Chapter 2.

5.1 Decoder parameters

5.1.1 Up-sampling and window size

As discussed in Chapter 4.1, the candidate set size can be increased to ensure that sufficient suitable candidates are available. For that purpose, the window size and/or the up-sampling factor can be altered. It was expected that a too small candidate set limits the number of suitable candidates, whereas a too large candidate set increases the susceptibility to an erroneous initialization.

To verify these assumptions, the luminance and chrominance *MSE* has been determined for various window sizes at up-sampling factors of 1, 2, 4 and 8 times. The results have been depicted in Figure 5.3, where the *MSE* is plotted as a function of the candidate set size and the up-sampling factor. At a given candidate set size, a higher up-sampling factor corresponds to a

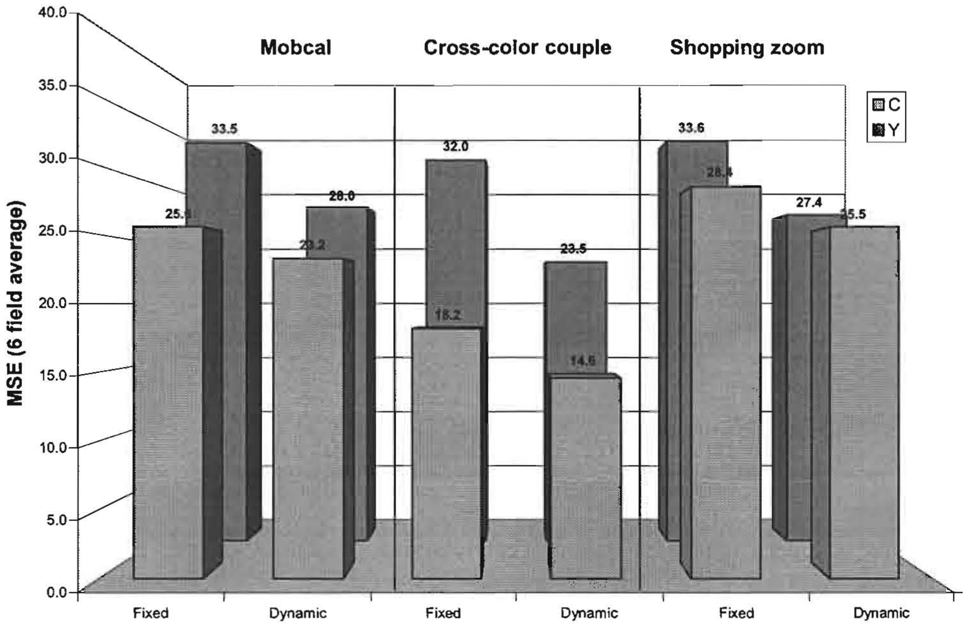

Figure 5.4: MSE of Y and C for fixed and dynamic window sizes.

smaller spatial window on the original sampling grid.

Two conclusions can be drawn from these results. First of all, an increase in candidate set size generally results in a decreased MSE and therefore increased decoding quality. This confirms the assumption that larger candidate set sizes contain more suitable candidates. However, an increased susceptibility to erroneous initialization could only be observed at the original sampling grid, as here the MSE increases above a certain candidate set size. For all upsampled signals, the advantages of more candidates seem to outweigh its drawbacks, as the MSE declines monotonously.

Furthermore, we can conclude that an increasing up-sampling factor up until a certain boundary yields a decreasing MSE. If the up-sampling factor exceeds this boundary, the window size on the original sampling grid becomes too small to contain sufficient suitable candidates which meet the phase requirement. This results in a reduction in decoding quality, and can be observed at an up-sampling factor of 8x where the performance has decreased compared to 4x up-sampling. The best results are therefore achieved at 4x up-sampling.

5.1.2 Dynamic window resizing

Next to up-sampling, dynamic window resizing was also expected to result in an increased decoding quality. Therefore, a candidate window with fixed dimensions was compared to one using dynamic window resizing. The quality

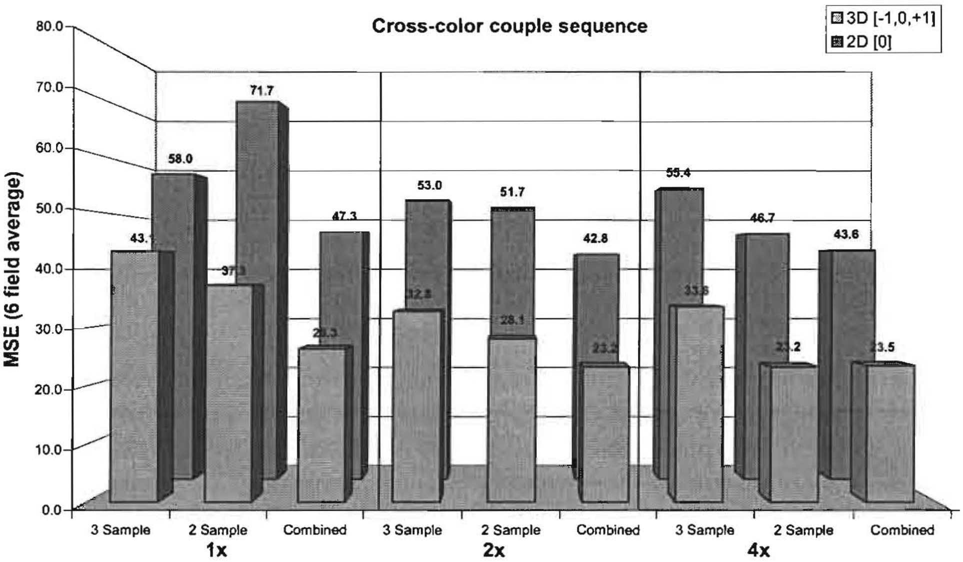

Figure 5.5: *MSE* of a 2D and 3D comb-filter as a function of the comb-filter type (two sample, three sample, combined) and window size (1,2 and 4).

assessment was performed for three sequences using an up-sampling factor of 4. Only resizing along the horizontal axis took place in this initial test. The fixed window dimensions were $t_x = 8$ and $t_y = 2$, whereas the dynamic window dimensions were $t_x = [1, \ldots, 12]$ and $t_y = 2$.

Figure 5.4 shows the result of this comparison. Clearly, dynamic window resizing results in an overall reduction in luminance *MSE* of approximately 20%. The subjective increase in decoding quality was significant as well, as e.g. in the *Cross-color couple* sequence, certain cross-color artifacts disappeared completely.

As dynamic window resizing leads to, on the average, smaller window sizes, this results in a significant computational reduction. Although no formal verification was performed, the implemented algorithm's running time decreased approximately 50-75% when using dynamic instead of fixed window sizes. In addition, the decoding quality is improved. Dynamic window resizing along the vertical axis is expected to result in further improvements.

5.1.3 Individual versus combined comb-filter kernels

The proposed comb-filter adaptively combines the standard (two sample) and the proposed (three sample) comb-filter kernels by locally selecting the kernel that is expected to yield the best results. By doing so, an increase in decoding quality is expected over filters that are restricted to either individual kernel. To test this assumption, we can evaluate the performance of the proposed comb-filter in three configurations:

- Restricted to the *standard* comb-filter kernel that uses *two samples of opposite phase.*
- Restricted to the *proposed* comb-filter kernel that uses *three samples of non-opposite phase.*
- Default configuration that *adaptively combines* both comb-filter kernels.

For the default configuration, an initial experimental validation was used to determine the optimum ratio between both filters. The best results were obtained by decoding approximately 30% of all composite samples with the proposed comb-filter kernel, and the remainder with the standard comb-filter kernel. However, further optimization is recommended to achieve better results.

Figure 5.5 shows the result of this comparison for the *Cross-color couple* sequence. In order to determine the effect of varying candidate set sizes, three horizontal scaling factors ($s_x = 1, 2, 4$) for the dynamic window resizing were used. This resulted in three candidate windows with relative sizes of 1, 2 and 4. Furthermore, all tests were performed for a 2D and a 3D comb-filter configuration. The depicted MSE is for the luminance only; the chrominance shows similar characteristics.

For the 3D comb-filter, the adaptive combination of both kernels results in a significantly improved performance at the smallest window size. To achieve similar performance, a comb-filter using only the standard kernel would require more than double the window size. At the largest window size, however, the gain has disappeared. The candidate window apparently contains sufficient optimal candidates with an opposite phase, therefore not benefiting from the additional candidates offered by the three sample decoder.

Similar observations can be made for the 2D comb-filter configuration. The largest gain in performance is achieved at the smallest window size. Remarkable is the poor performance of the two sample decoder, as only at this window size, the three sample decoder alone achieves better results. It appears that few spatial decoding options are available for the two sample decoder at this window size. For increasing window sizes, the gain decreases to ultimately less than 10%.

Several conclusions can be drawn. First of all, a comb-filter restricted to the three sample comb-filter generally performs worse than one using the two sample decoder. Secondly, the adaptive comb-filter is able to profit from the additional decoding options, which results in significantly improved results for smaller window sizes. Finally, the combined comb-filter achieves similar results to the two sample decoder at half the window size. This can

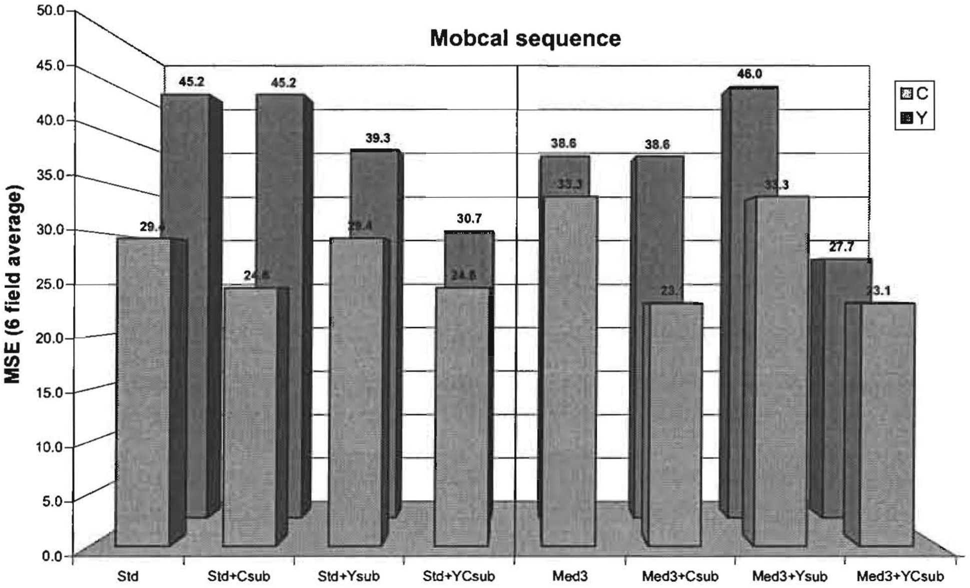

Figure 5.6: MSE for the standard (*Std*) and the median filter (*Med*3) configurations with derived chrominance C_{sub}, derived luminance Y_{sub}, and the combination of both.

be advantagous, as it reduces the computational cost and, as proven later, the susceptibility to noise.

5.1.4 Median filtering and Y/C derivation

As discussed in Chapter 4.3, a median filter can be applied to the decoded luminance to attenuate the influence of decoding errors. It is suggested that further improvements may be realized by post-processing, i.e. deriving the luminance and/or chrominance by subtraction from the original composite signal. In order to test these assumptions, the performance of the standard and the median comb-filter was evaluated using the following post-processing:

- No post-processing.
- C_{sub}: deriving the chrominance from the decoded luminance.
- Y_{sub}: deriving the luminance from the low-pass filtered decoded chrominance.
- YC_{sub}: deriving the chrominance from the decoded luminance, and subsequently deriving the luminance from the low-pass filtered chrominance C_{sub}.

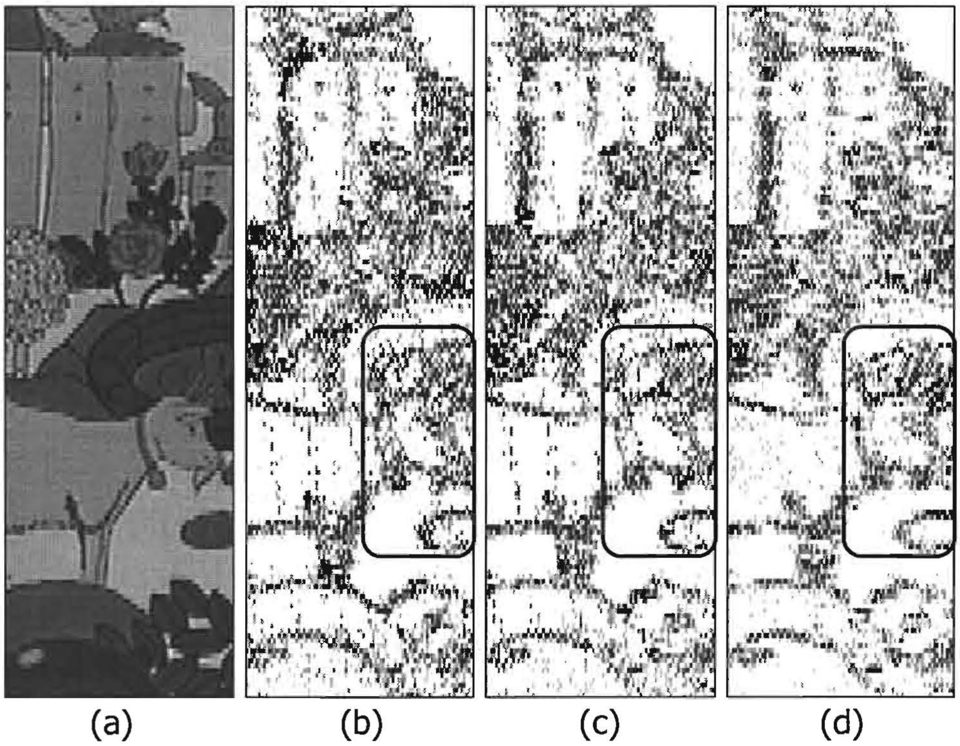

Figure 5.7: a) Original *Mobcal* and absolute difference with output of b) standard decoder, c) median filter, and d) median filter using derived luminance and derived chrominance (YC_{sub}).

The results are shown in Figure 5.6, where a 3D comb-filter was used with 4x up-sampling and dynamic window resizing. We can make several observations. First of all, median filtering results in a improved luminance but worsened chrominance. This was expected, as the median filter operates on the luminance only.

Secondly, the derived chrominance C_{sub} gives a better performance on the MSE score, as the MSE decreases by 17% and 30% for the standard and median configuration, respectively. As the decoded luminance of the median filter is superior to that of the standard decoder, its derived chrominance is superior as well. Furthermore, the earlier assumption is confirmed that the decoded chrominance of the comb-filter is not complementary to its decoded luminance, as otherwise the chrominance performance would not have improved.

Thirdly, the derived luminance Y_{sub} from the decoded chrominance does not necessarily result in an improvement. For the median filter, the luminance deteriorates due to the poor quality of the decoded chrominance.

The standard decoder, however, is able to achieve a reduction of 13% in luminance MSE.

Finally, the best performance is obtained when deriving the luminance from the derived chrominance C_{sub}. For the standard and median filter, the luminance gain is approximately 30% when compared to the filters without post-processing. Now, the improvement due to median filtering is 6% for the chrominance and 9% for the luminance.

Figure 5.7 depicts the error in decoded luminance of three comb-filter configurations. Clearly, the median filter yields little visible improvement over the standard decoder. Furthermore, it can be seen that post-processing by using YC_{sub} results in the smallest decoding error, as e.g. visible in the highlighted area.

Less visible in the depicted snapshots is a reduction in noise artifacts around the edges, that are primarily visible in moving sequences. These are caused by the fact that the decoder instantaneously switches between various filters on a per-sample basis, and therefore loses spatial and temporal consistency. As these high-frequency artifacts are severely attenuated in the low-pass filtered C_{sub}, the derived luminance Y_{sub} is nearly devoid of these artifacts.

We can conclude that the best objective and subjective performance is achieved by the combination of median filtering and YC_{sub}, i.e. derived luminance and chrominance. However, as the additional gain of median filtering is minimal, it can be omitted in order to reduce the computational cost.

5.1.5 Candidate set configurations

The proposed comb-filter can use various temporal candidate set configurations. A number of these configurations have been previously depicted in Figure 4.2 and 4.3, where one spatial filter (2D[0]), two two-field filters (3D$[-1,0]$ and 3D$[-2,0]$) and three three-field filters (3D$[-1,0,+1]$, 3D MC$[-1,0,+1]$, and 3D$[-2,-1,0]$)[1] are shown.

The objective and subjective assessment of above configurations was performed on the sequences depicted in Figures 5.2a, b and c. The optimum comb-filter parameters were used, i.e. 4x up-sampling, median filtering and derived chrominance and derived luminance. Furthermore, the size of each spatial window was inversely proportionate to the number of windows used. For example, the candidate window of the 2D[0] filter is three times as large as each individual window of the 3D$[-1,0,+1]$ filter. This ensures that an equal number of candidates was available to each filter.

For the objective assessment, the MSE of the 3D$[-1,0]$ filter was used as a reference for all other filters, as it represents a compromise in terms of

---

[1] The index refers to the fields used by the comb-filter. For example, the 3D$[-1,0,+1]$ comb-filter obtains candidates from the previous, current and next fields.

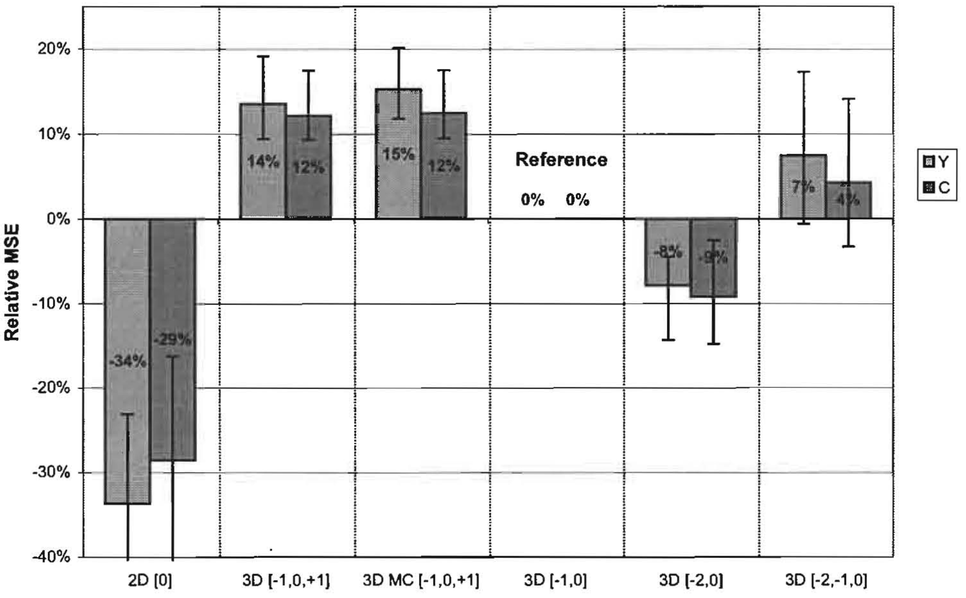

Figure 5.8: Relative MSE as function of various candidate set configurations with respect to the 3D$[-1, 0]$ comb-filter.

memory requirements between the spatial and the three-field comb-filters. Equation 5.2 shows how the relative performance is calculated when comparing filter F to the reference filter G.

$$MSE_{rel}(F) = -100\% \cdot \frac{MSE(F) - MSE(G)}{MSE(G)} \tag{5.2}$$

The relative MSE was then averaged over the three sequences, as each filter showed highly similar characteristics for each sequence. Figure 5.8 shows the results of the objective assessment, where the error bars represent the minimum and maximum and the solid bar the average value.

Clearly, the spatial 2D[0] comb-filter yields the lowest performance. This was expected, as especially in stationary or slowly moving detailed areas, the temporal correlation is generally higher than the spatial correlation.

The 3D$[-1, 0, +1]$ and 3D MC$[-1, 0, +1]$ filters achieve the best performance, as their candidates originate from the current and both temporally adjacent fields. Only a marginal improvement is realized by the 3D MC$[-1, 0, +1]$ filter, where the candidate windows are placed along the motion axis. Motion compensation might be more advantageous in fast moving sequences, though artifacts will appear to be less significant anyway because of motion blurring of either the display or a non-tracking observer (see Reference [7] pp. 107-109).

Furthermore, the 3D$[-2, 0]$ filter performs worse than the reference 3D$[-1, 0]$

filter. Apparently, the reduction in temporal correlation due to the increased temporal distance is not accompanied by additional advantageous decoding options for the two and/or three sample decoder. The two sample decoder would benefit from a 3D$[-4, 0]$ configuration, as here frame comb-filtering is possible. However, it was not included in the initial tests as its drawbacks due to the very large temporal distance were expected to outweigh its advantages in stationary areas.

In turn, the 3D$[-2, -1, 0]$ filter performs slightly worse than the 3D$[-1, 0, +1]$ filter. However, as no next field is used, its decreased latency is advantageous for a potential real-time implementation.

The subjective impressions correspond to the results of the objective evaluation. The best performance is achieved by the three-field comb-filters, with no significant differences in between them. The two-field filters yield a slight increase in artifacts, which is primarily visible in stills and sequences with little movement. Only for the 3D$[-2, 0]$ filter, an increase in cross-luminance in the *Shopping zoom* sequence was more prominently visible. This could be observed around strong chrominance edges, where subcarrier breakthrough became visible.

For the spatial comb-filter, the decoding artifacts are more significant. Compared to the 3D filters, a clear increase in cross-luminance artifacts was visible in the *Shopping zoom* sequence. This can be seen in the highlighted area in Figure 5.9a. Cross-color artifacts are more visible as well, as illustrated in snapshot of the *Cross-color couple* sequence in Figure 5.9b.

In conclusion, the best performance is achieved by the three-field comb-filters, of which the 3D$[-2, -1, 0]$ filter is preferred due to its reduced latency. Motion compensation is not required for the proposed comb-filters, as it only realizes marginal improvements. Finally, the 3D$[-1, 0]$ constitutes a good compromise between memory requirements and performance.

5.1.6 Recursive comb-filtering

The 2D$[0]$ and 3D$[-2, -1, 0]$ comb-filters can be used in a transversal and recursive configuration, as previously shown in Figure 4.10. Figure 5.10 shows the results of the comparison between the transversal and the first recursive filtering step for both filters.

For the *Mobcal* and *Cross-color couple* sequences, the recursive filtering yields better results than the initial transversal filtering. The largest gain is achieved by the 2D comb-filter, with an improvement in MSE of up to 20%. The 3D comb-filter does not benefit as much, with an improvement of up to 10%. This is due to the fact that during the recursive filtering, the current field is still initialized by the notch filter. An improved initialization by for instance a spatial comb-filter is likely to achieve further improvements.

In the *Shopping zoom* sequence, however, the gain in decoding quality is minimal or even negative for the 2D and 3D comb-filter, respectively. This

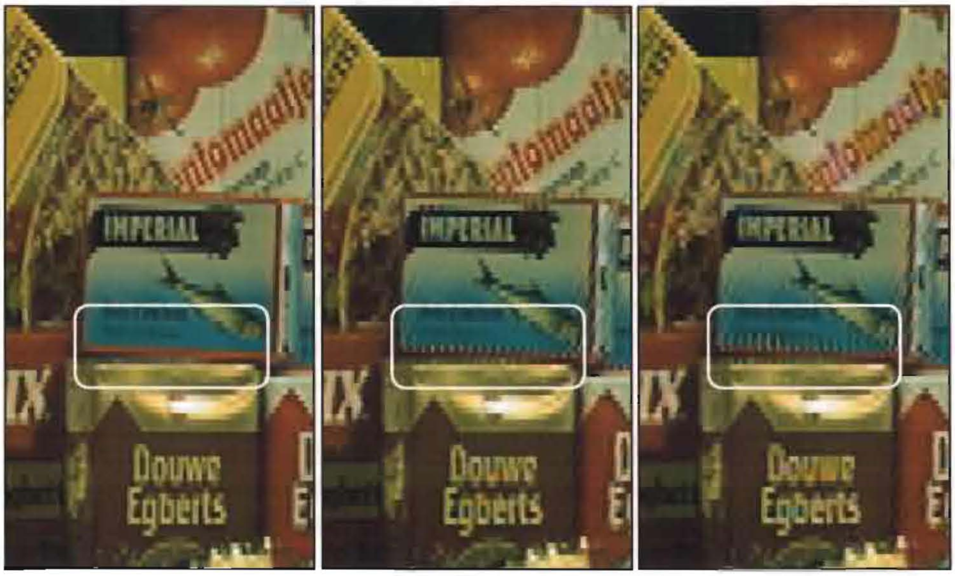
IMPERIAL
Douwe
Egberts

(a) Original 3D[-1,0,+1] 2D[0]

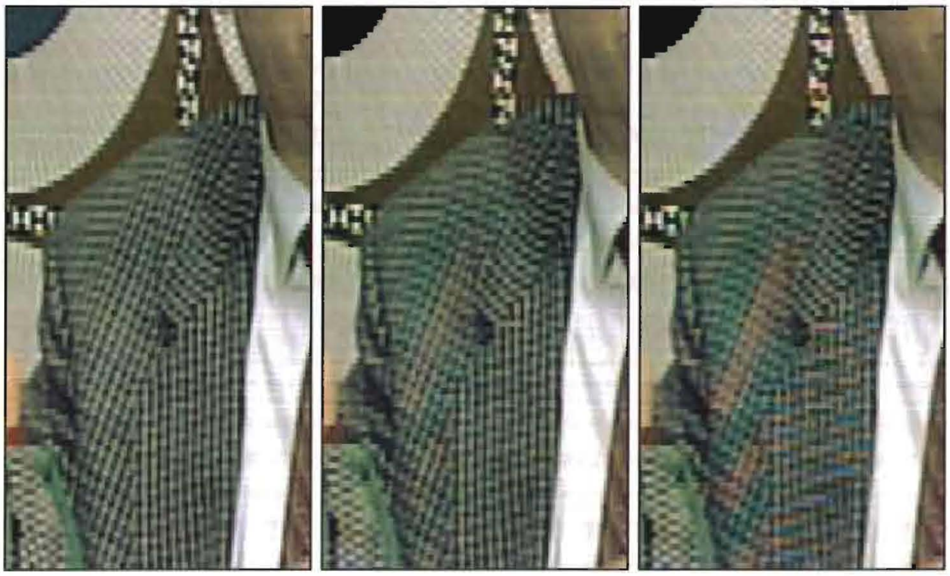

(b) Original 3D[-1,0,+1] 2D[0]

Figure 5.9: a) Cross-luminance artifacts in the *Shopping zoom* sequence, and b) cross-color artifacts in the *Cross-color couple* sequence.

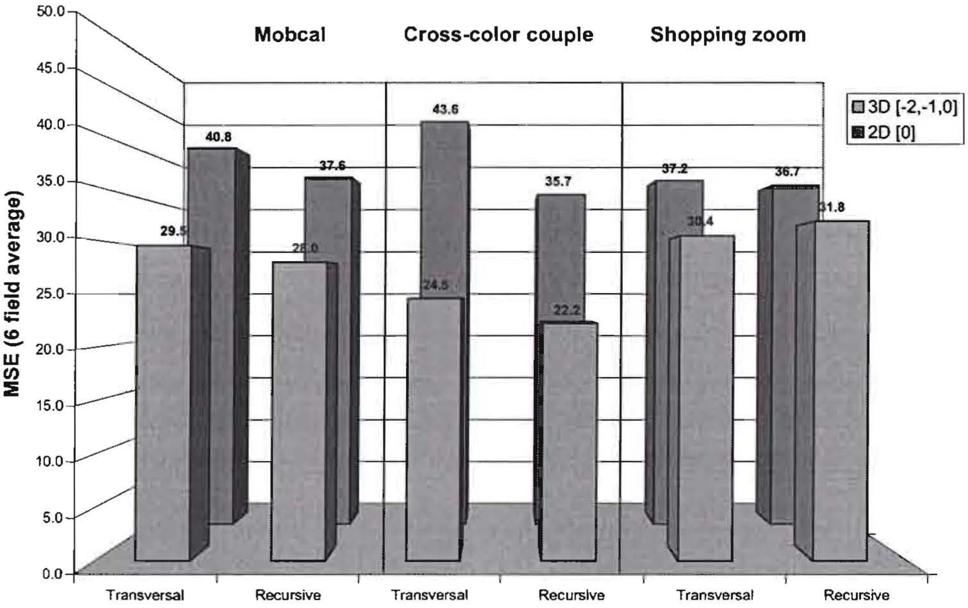

Figure 5.10: *MSE* of the transversal and recursive configuration of a 2D and 3D comb-filter.

was not expected, as transversal filtering yields a significant improvement in *MSE* over the notch filter; subsequent recursive filtering was expected to benefit from this improved initialization.

However, due to the many strong chrominance edges in the *Shopping zoom* sequence, the notch-filter initialization contains severe cross-luminance artifacts. If these artifacts are of sufficient strength, the transversal filtering step will preserve these artifacts by filtering along their gradients. This was previously shown in Figure 5.9a. Recursive comb-filtering can therefore result in the preservation or possibly slight amplification of severe cross-luminance artifacts.

Typically, cross-luminance artifacts are not as severe as in the *Shopping zoom* sequence, and recursive filtering will yield an improved Y/C separation. Recursive comb-filtering seems most promising in case of 2D comb-filtering, as here the highest gain is achieved. Repeated recursive filtering steps may yield further improvements, although the gain will be limited as initial experiments have shown.

5.2 Comparison to reference filters

In order to benchmark the performance of the proposed comb-filter, a number of reference comb-filters were selected for comparison. First of all, a standard PAL decoder using band-pass/notch filters was included, as it is the most common Y/C separation method. Furthermore, several configurations of the Philips comb-filter presented in Chapter 2.3 were selected, as they are representative of current high-end comb-filters. The following configurations were selected, as they were available in a *comb-filter Simulator* software developed at Philips CE-PDSL:

- Spatial median filter (2D[0]), as illustrated in Equation 2.1, which is restricted to spatial filtering only.
- Field-based motion adaptive filter (3D[$-1, 0$]), as depicted in Figure 2.7, which uses a field-comb-filter for temporal filtering.
- Field-based motion adaptive filter (3D[$-4, 0$]), as depicted in Figure 2.7, which uses a frame-comb-filter for temporal filtering.

Motion compensated comb-filters were not included in the comparison, as the algorithms available for PAL do not achieve competitive results. A more promising approach for NTSC was described in Chapter 2.4, but was omitted as this initial test was restricted to PAL.

The proposed comb-filter configurations were previously illustrated in Figure 5.8. Their parameters were set to the optimal settings determined so far, i.e. 4x up-sampling, dynamic window resizing, median filtering and derived luminance and derived chrominance. However, optimization of for instance weighting and scaling factors may yield further improvements.

All comb-filters were restricted to transversal filtering, i.e. no recursive configurations. It was aimed to keep all parameters which were not comb-filter specific identical, which means that the following common filters were used:

- *Pre-filters* for the luminance and chrominance components were selected according to Figure A.3, which results in the bandwidth limitation to approximately 5MHz and 1.3MHz, respectively.
- *Channel filters* were not used, which resulted in an ideal transmission channel without bandwidth limitation.
- *Post-filters* were applied to the chrominance components in order to suppress any alias components due to demodulation as well as high-frequency decoding errors and/or noise. The used low-pass filter is depicted in Figure A.2. Subsequently, a *PAL median filter* was applied as described in Reference [13] (pp. 33).

However, various parameters may not be identical to those of the reference comb-filter. For instance, the composite signal is represented as a 9-bit signal within the reference comb-filter, whereas the proposed filter uses a

8-bit representation. The impact of those parameters on the test results is expected to be insignificant though, as initial tests using modified parameters yielded little change in performance.

For the comparison, the subjective and objective assessment with the MSE as criterion were used. Again, the test sequences depicted in Figure 5.2 were selected as input, and the comparison was performed on the decoded sequences of each comb-filter. The results of the objective evaluation are shown in Figures 5.2a through c for the *Mobcal*, *Cross-color couple* and *Shopping zoom* sequences, respectively.

5.2.1 Evaluation of reference filters

Several observations can be made when comparing the performance of the reference filters. First of all, the standard decoder yields the worst performance in all sequences, as it suffers from severe cross-talk artifacts and loss of sharpness.

Furthermore, the relatively poor performance of the 3D$[-4,0]$ filter is surprising. It was expected that its near-perfect results in stationary areas would make up for its poor performance in moving areas, where it has to fall back to spatial filtering. However, in the *Mobcal* and the *Shopping zoom* sequences, its objective performance was worse than both the 3D$[-1,0]$ and 2D$[0]$ filters. The subjective assessment confirmed this result, as a clear reduction in sharpness and increase in cross-talk was visible.

The most probable cause is that both sequences contain primarily slow movement, which apparently is insufficient to cause the filter to fall back to spatial filtering. This is supported by the fact that, if the filter had fallen back to spatial filtering, its performance would match that of the spatial filter. As it performs significantly worse, the 3D$[-4,0]$ must at least partially apply temporal filtering. A faster fall-back to spatial filtering may improve the results in these sequences, yet may yield worse results in others.

In both sequences, a significant improvement was achieved by the 3D$[-1,0]$ filter due to its decreased temporal distance and thereby increased correlation. Only in the *Cross-color couple* sequence, the 3D$[-4,0]$ filter could improve upon the 3D$[-1,0]$ filter. This sequence contains a stationary background with vertical detail, where due to interlacing, the temporal correlation of candidates is larger in field $n-4$ than in field $n-1$. The 3D$[-4,0]$ was therefore able achieve near-perfect decoding of the stationary background, as opposed to the 3D$[-1,0]$ which is often restricted to spatial filtering.

We can conclude that in the test sequences the advantages of the 3D$[-4,0]$ filter do not outweigh its disadvantages. The objective and subjective improvements in stationary areas cannot make up for the artifacts and loss in sharpness in (slightly) moving areas. Overall, the 3D$[-1,0]$ filter can be seen as a compromise, as it is superior to the spatial 2D$[0]$ filter in stationary areas and improves upon the 3D$[-4,0]$ filter in moving areas.

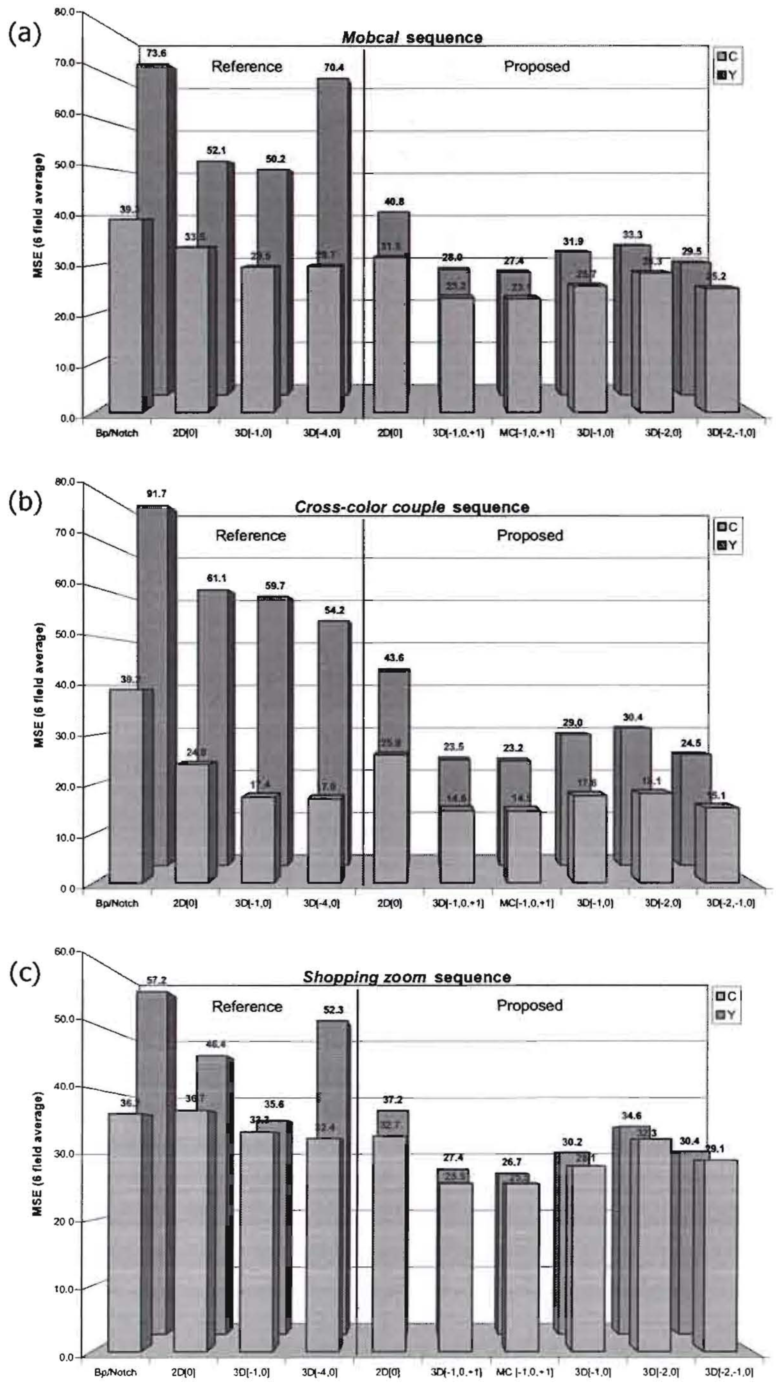

Figure 5.11: *MSE* comparison using a) *Mobcal*, b) *Cross-color couple* and c) *Shopping zoom* sequences.

5.2.2 Comparison on noise-free sequences

We can now compare the performance of the proposed comb-filters to the above references for the three test sequences.

Mobcal sequence

For this sequence, the best proposed filter (3D$[-1, 0, +1]$) improves upon the best reference filter (3D$[-1, 0]$) by 44% and 21% in luminance and chrominance MSE, respectively. This was confirmed by the subjective evaluation, where an increase in sharpness and reduction in ringing around strong edges could be seen. Furthermore, an increase in chrominance resolution was noticeable in still pictures, as chrominance edges were blurred in the decoded output of the reference filters.

When comparing filters of equal memory usage such as the 3D$[-1, 0]$ filters, the luminance and chrominance gain was 36% and 13%, respectively. Even the spatial 2D$[0]$ filter outperformed the best reference 3D comb-filter, although the subjective gain was significantly reduced. An increase in sharpness was still visible in still pictures, but cross-talk artifacts were equally prominent in both filters.

Cross-color couple sequence

For this sequence, an even larger increase in objective luminance performance could be achieved, as the luminance MSE improves by 57%. In the subjective evaluation, an increase in sharpness and slight reduction in cross-color artifacts was visible, as illustrated by the highlighted areas in Figure 5.12b. However, the subjective gain was not as large as the decrease in MSE suggests, as the largest gain occurs in areas of already high luminance contrast where its visibility is reduced.

As expected, the best decoding quality of the stationary background was achieved by the reference 3D$[-4, 0]$ filter, as frame comb-filtering yields perfect results here. All other filters suffered from cross-color artifacts that were primarily visible in still pictures. Furthermore, the proposed spatial filter was not able to achieve the same performance as the 3D reference filters for this sequence, as its decoded output contained more cross-color artifacts.

Shopping zoom sequence

For this sequence, the performance gap between the proposed and reference comb-filters is the smallest of all sequences. This is caused by the fact that strong chrominance edges are present without accompanying luminance edges. As the proposed comb-filter is color-blind, i.e. luminance adaptive only, it can cause severe cross-luminance artifacts by filtering across

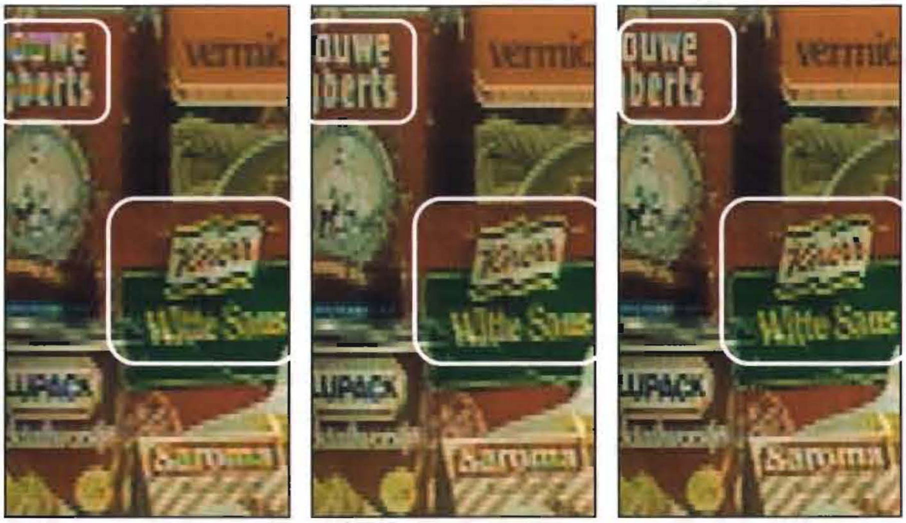

(a) Bandpass/Notch Reference 3D [-1,0] Proposed 3D [-1,0]

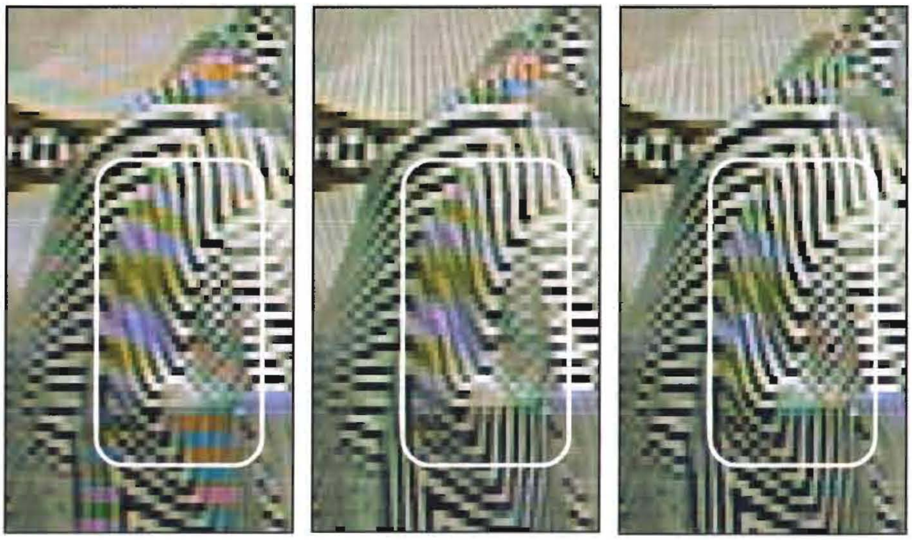

(b) Bandpass/Notch Reference 3D [-1,0] Proposed 3D [-1,0]

Figure 5.12: Extract of a) the *Shopping zoom* sequence and b) the *Cross-color couple* sequence.

chrominance edges. The reference comb-filters, however, are luminance and chrominance adaptive, and therefore less likely to cause artifacts in these areas.

Nevertheless, all proposed 3D comb-filters achieve a better objective performance than the best reference filter (3D$[-1,0]$), and the proposed 2D[0] filter only trails by 4% in the luminance and 1% in the chrominance. The results of the subjective assessment were ambiguous though, as severe cross-luminance artifacts were present in all comb-filter outputs. Although the proposed filters achieved a reduction in cross-luminance artifacts in some areas, an increase could be seen in others.

Overall, cross-luminance artifacts seemed to be slightly more prominent in the decoded output of the proposed comb-filters. However, an increase in sharpness could be achieved, as illustrated by the characters 'Saus' and 'Vermic(elli)' in Figure 5.12a. Furthermore, cross-color artifacts were slightly reduced, as for example in the '(D)ouwe (Eg)berts' characters.

Conclusions

From above results, we can conclude that the proposed filters achieve an increase in sharpness and reduction of cross-color artifacts. The gain in cross-luminance reduction, however, is less significant due to the filter's color-blindness, which particularly results in artifacts around strong chrominance edges without accompanying luminance transition. As chrominance edges typically do coincide with luminance edges, the above situation is unlikely to occur in common broadcast video.

However, the subjective gain is not always as large as the decrease in MSE suggests. This is partly caused by the fact that relatively small computer-monitors were used instead of larger high-resolution television displays. Furthermore, de-interlacing was used to display the interlaced sequences on the progressive displays, which may also influence the visibility of artifacts. Lastly, it is known that objective quality measures such as the MSE do not completely correspond to the opinion of human observers, and as such, a perfect correlation between the objective and subjective gain cannot be expected.

5.2.3 Comparison on noise-corrupted sequences

It is desirable to determine the noise sensitivity of comb-filters, as real-life composite video signals are always corrupted by noise of varying magnitudes. Therefore, the objective performance of various filters was determined for noise levels of -40dB, -30dB, -26dB and -23dB. The noise was introduced as additive white Gaussian noise to the CVBS signal prior to decoding. Only the luminance performance was considered, as any impact on the chrominance was less significant due to its limited bandwidth. The relative MSE

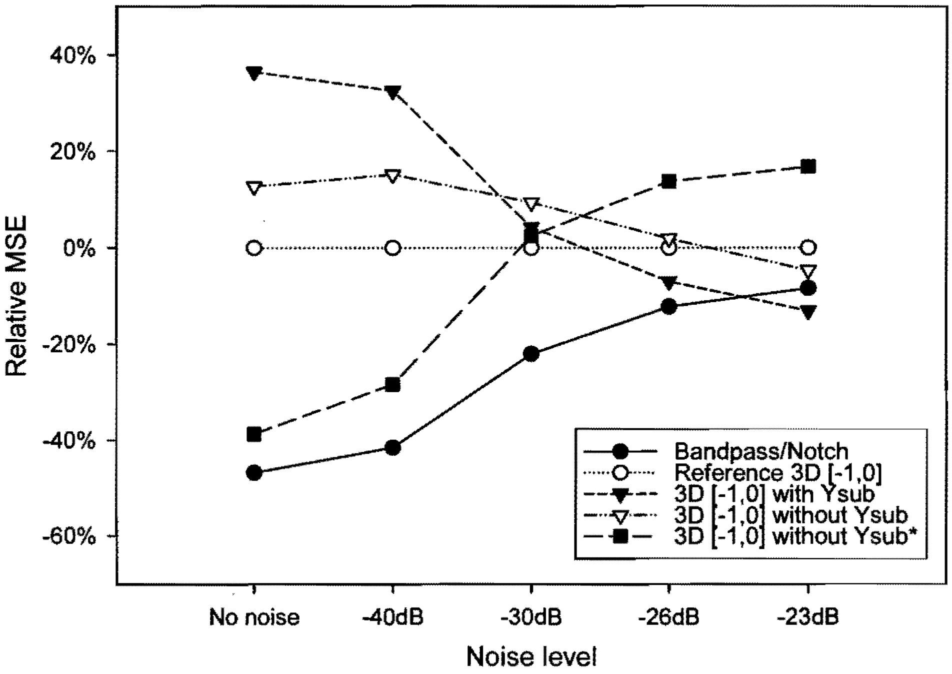

Figure 5.13: Relative MSE of various comb-filters as function of noise level (the asterisk denotes a 50% reduction in relative window size).

was determined with respect to the reference 3D$[-1,0]$ filter according to Equation 5.2.

Comb-filter configurations

First of all, a standard decoder using band-pass/notch filters was included as a reference. Furthermore, three configurations of the proposed 3D$[-1,0]$ filter were included. The first configuration is a comb-filter using the optimum settings as previously determined for noise-free sequences.

The second configuration is identical, except that now the luminance is directly decoded by the comb-filter instead of using the derived luminance Y_{sub}. By deriving the luminance from the low-pass filtered chrominance, the low-frequency noise in the composite signal will be preserved in the derived luminance Y_{sub}. As comb-filtering inherently works as an averaging filter, deriving the luminance directly from the comb-filter may therefore result in an attenuation of noise.

The third configuration is identical to the previous one, i.e. directly decoding the luminance, but uses half the original relative window size. As the comb-filter initialization becomes noise-corrupted at high noise levels, it is not a reliable indication of the candidate's correlation anymore. Generally, the correlation of adjacent samples is higher than the correlation of distant samples. By restricting the window size, the filtering of distant and thereby potentially uncorrelated samples is prevented.

Results

The results of the objective assessment are depicted in Figure 5.13. At low noise levels, the proposed 3D$[-1,0]$ filter using Y_{sub} clearly yields the best results, followed by the filter without Y_{sub}. The proposed filter with reduced window size shows poor performance, only improving slightly upon the band-pass/notch filter.

At higher noise levels, a convergence of all filters is noticeable, as the MSE is increasingly determined by the noise itself. Both proposed filters using normal window sizes now experience a decline in relative performance. In particular, the 3D$[-1,0]$ filter using Y_{sub} declines rapidly, and performs even worse than the band-pass/notch at the highest noise level.

The same filter without Y_{sub} experiences a more moderate decline, and still performs better than the reference until a noise level of -26dB. Furthermore, the filter using relative smaller windows improves in relative performance at increasing noise levels, resulting in the best performance at the highest noise level.

Discussions

Above results generally correspond to the previous expectations. Due to the flexibility of the proposed filters in selecting candidates, a noise corrupted input sample will result in the selection of additional samples with equal characteristics. This results in the preservation of noise. Filters with limited flexibility, as e.g. the reference filters, will be forced to select less suitable candidates, therefore attenuating the influence of noise by acting as an averaging filter. By limiting the flexibility of the proposed comb-filter, for instance by reducing the window size, its performance can be improved for increasing noise levels.

However, the question arises if comb-filters should incorporate noise suppression. Instead of having comb-filters with noise suppressing characteristics, a better approach might be the combination of the proposed filters with more advanced noise suppression methods. This is supported by the fact that averaging itself is inferior in terms of noise suppression to various other methods, as mentioned in Reference [7] (pp. 55-64). However, due to time constraints, the feasibility of this approach could not be verified.

5.2.4 *Moving zoneplate* comparison

An evaluation of the decoded *Moving zoneplate* sequence is of particular interest, as the presence of predefined spatial and temporal frequencies enables a characterization of the comb-filter's luminance resolution and cross-color suppression.

A snapshot of the original *Moving zoneplate* sequence is depicted in Figure B.1a, where the spatial location of the modulated chrominance components is indicated. Ideally, any decoder output should consist of luminance only. However, all tested decoders suffer from varying degrees of cross-color artifacts, typically centered around the location of the chrominance components.

Spatial (comb) filters

The output of the standard PAL decoder is depicted in Figure B.2a as a reference. Clearly, all horizontal frequency components centered around the subcarrier frequency of 4.43MHz are erroneously decoded as chrominance. The luminance is almost completely attenuated due to the notch filter, as shown by the luminance error on the right hand.

Figure B.2b shows the output of the reference 2D[0] filter. It can be seen that a reduction in cross-color artifacts and increase in luminance bandwidth can be achieved compared to the standard decoder. Figure B.2c shows the output of the proposed 2D[0] filter, which further improves upon the reference filter. However, the drawback of deriving the luminance from the chrominance becomes visible, as the cross-color artifacts have resulted in complementary cross-luminance artifacts.

Field-based 3D comb-filters

The decoded output of the reference and the proposed 3D[$-1, 0$] filters is shown in Figures B.3a and b, respectively. It can be seen that the reference filter falls back to spatial filtering in certain areas, which results in the eye-shaped area with increased cross-color and cross-luminance artifacts.

The comparison of cross-color performance is difficult, as artifacts around the V chrominance component have increased somewhat whereas those around the U chrominance component have been reduced. A clearly improved luminance bandwidth could be achieved though, while avoiding the strong cross-luminance artifacts of the proposed 2D[0] filter.

Figure B.3c shows the decoded output of the proposed 3D[$-1, 0, +1$], which clearly yields the best performance so far. Compared to the proposed 3D[$-1, 0$] filter, the extra field has resulted in a further reduction of cross-color and cross-luminance artifacts.

Frame-based 3D comb-filters

The reference 3D[$-4, 0$] and proposed 3D[$-2, 0$] filter are shown in Figures B.4a and b, respectively. As no stationary areas are present, the reference 3D[$-4, 0$] suffers from its increased temporal distance. The proposed filter yields a superior luminance and less significant improvement in cross-color suppression. Compared to the proposed 3D$[-1,0]$, an increase in cross-luminance and cross-color artifacts can be observed.

In turn, the proposed 3D$[-2,-1,0]$ filter depicted in Figure B.4c yields better performance than the 3D$[-2,0]$ and the 3D$[-4,0]$ filters, yet slightly worse performance than the proposed 3D$[-1,0,+1]$. If next fields cannot be used due to latency requirements, this filter achieves the best results.

Conclusions

We can conclude that the overall performance of the proposed filters is superior to that of the reference filters for the *Moving zoneplate* sequence. The reduction in cross-color artifacts and increase in luminance bandwidth are clearly visible, with the best performance achieved by the three-field comb-filters. Furthermore, a drawback of deriving the luminance from the chrominance can be seen, as cross-luminance artifacts appear where severe cross-color artifacts occur. This is particularly the case for the spatial and two-field comb-filters, as they exhibit stronger cross-color artifacts than the three-field comb-filters.

Chapter 6

Conclusions and recommendations

6.1 Conclusions

Several conclusions can be drawn. First of all, it was shown that the proposed comb-filter kernel enables the Y/C separation of samples with non-opposite chrominance phases. This provides additional decoding options to comb-filters. The proposed kernel differs for samples with identical and non-identical V-switches, as the decoding of the latter is significantly more complicated.

A comb-filter was proposed that adaptively combines the standard and the proposed filter kernels. It was shown that the combination of both kernels yields better results than each kernel individually. Various techniques have been proposed to increase the decoding quality, such as dynamic window resizing and the successive derivation of chrominance and luminance.

Using experimentally determined parameters, it was shown that an improvement of more than 50% and 25% in luminance and chrominance MSE, respectively, is possible over current high-end comb-filters. A significant improvement is maintained even when the comb-filter is restricted to the standard comb-filter kernel. Subjective assessment confirmed an increase in decoding quality, although it was not always as significant on the used monitors as the MSE suggests.

Furthermore, it was determined that a restriction to only luminance adaptivity can result in increased cross-luminance artifacts in certain situations. An extreme example is the *Shopping zoom sequence*, in which the proposed filter suffered slightly more from cross-luminance artifacts than the reference comb-filters. In typical broadcast video, however, these extreme situations are unlikely to occur.

6.2 Recommendations

Several things remain to be done. First of all, an analysis of the computational cost of the proposed filter kernel is required to determine its feasibility as part of future comb-filters. Although it has been established that the inclusion of the proposed kernel yields improved decoding quality, the implementation costs should be balanced against the achievable quality gain. For that purpose, further optimization of the comb-filter is suggested to enable the most effective usage of the additional decoding options.

Secondly, the comb-filter should be evaluated for other test sequences which are known to cause severe cross-talk artifacts. Although the used test sequences contain a number of the most extreme situations that can be encountered, some situations remain untested. In particular, the performance on sequences that contain fast moving chrominance over stationary luminance should be evaluated, as here luminance-only adaptive comb-filters potentially cause artifacts due to temporal filtering. From these results, it can be determined if luminance adaptivity is sufficient for real-life video sequences, or if the addition of chrominance adaptivity is required.

Moreover, the performance of the proposed comb-filters in combination with advanced noise suppression techniques could be evaluated. In theory, this could improve the performance at high noise levels, where until now, filters with limited flexibility yield better performance. However, it remains to be verified if this indeed holds in practice.

In addition, it is recommended to include high-end large-screen television displays in the subjective assessment, as it was previously limited to small-screen CRT and LCD computer-monitors. The visibility of artifacts is expected to increase on larger CRT televisions and emerging high-resolution displays such as LCoS. Any improvement in decoding quality will therefore be more significant on these displays.

Finally, the proposed comb-filter could be adapted to NTSC signals and compared to current high-end NTSC comb-filters. As NTSC lacks the sign inversion of the V chrominance component, the comb-filter can be simplified as the proposed comb-filter kernel becomes far less complicated. The reduced computational cost should be taken into account when considering the feasibility of applying the proposed comb-filter to NTSC signals.

Bibliography

[1] Achiha, M.
Bewegungsadaptiver Qualitätsdecoder und Up-Konverter für PAL-Signale,
Fernseh- und Kino-Technik, Vol. 46 (1992), No. 2, pp. 98-104.

[2] Achiha, M. and M. Kishihara
Luminance/chrominance signal separation circuit for PAL color television signal.
Applicant: Hitachi, 1989.
EU Patent Application EP0364967.

[3] Astola, J. and P. Haavisto, Y. Neuvo
Vector Median Filters,
Proceedings of the IEEE, Vol. 78 (1990), No. 4, pp. 678-689.

[4] Briggeman, I.T.
Motion-compensated Y/C-separation of the composite PAL video signal.
Delft: Delft University of Technology, 1990.
Graduation Thesis.

[5] Choi, S. and S. Kwon, H. Kim, Y. Kwon, Y. Ha
Motion adaptive 3D Y/C separation algorithm using motion estimation and motion compensation,
IEEE Trans. Consumer Electron., Vol. 47 (2001), No. 4, pp. 770-778.

[6] Drewery, J.O.
Encoding and decoding of composite video.
Applicant: BBC, 1997.
WO Patent Application WO9742769.

[7] Haan, G. de
Video processing for multimedia systems.
Eindhoven: University Press Facilities Eindhoven, 2000.
ISBN 90-9014015-8.

[8] Hentschel, C.
Video-Signalverarbeitung.

Stuttgart: Teubner, 1998.
ISBN 3-519-06250-X.

[9] Jack, K.
Video demystified: a handbook for the digital engineer, 3rd ed.
Eagle Rock: LLH Technical Publishing, 2001.
ISBN 1-878707-56-6.

[10] Kim, J.W. and W.J. Song
Luminance/chrominance signal separating device.
Applicant: LG Electronics, 1997.
US Patent Application US5990978.

[11] Lowe, V.L. and J.W. Curtis
Digital comb-filter for decoding composite video signals.
Applicant: Fortel DTV, 2000.
US Patent Application US6278495.

[12] Mawatari, M. et al.
Luminance/chrominance separating apparatus.
Applicant: Toshiba, 1995.
EU Patent Application EP0485165.

[13] Nieuwenhuizen, M.
3D comb-filter for Columbus and Spider, technical description.
PDSL Lab Eindhoven, Philips Consumer Electronics, 2002.
Internal Report (Draft).

[14] Puttenstein, J.G.
Quality of noise measurement in TV-systems.
Eindhoven: Eindhoven University of Technology, 2001.
Graduation Thesis.

[15] Shin-Etsu, I.
A study of digital Y/C separation in NTSC or PAL color television,
IEEE Trans. Consumer Electron., Vol. 40 (1994), No. 4, pp. 963-968.

[16] Shin-Etsu, I.
Scene change phenomena and optimum control of the digital Y/C separation circuit,
IEEE Trans. Consumer Electron., Vol. 41 (1995), No. 2, pp. 282-287.

[17] Takeshima, M.
Video signal processing circuit and video signal processing method.
Applicant: Matsushita Electric, 1999.
US Patent Application US6400762.

[18] Takuji, K. et al.
Chrominance-luminance separation method and filter performing selective spatial filter based on detected spatial correlation.
Applicant: Mitsubishi, 1994.
US Patent Application US5502509.

[19] Teichner, D.
Quality improvement by adaptive inter-/intraframe processing in PAL TV receivers,
IEEE Trans. Consumer Electron., Vol. 31 (1985), No. 3, pp. 226-239.

[20] Teichner, D.
Adaptive filter techniques for separation of luminance and chrominance in PAL TV signals,
IEEE Trans. Consumer Electron., Vol. 32 (1986), No. 3, pp. 241-250.

[21] Teichner, D.
Three-dimensional pre- and post-filtering for PAL TV signals,
IEEE Trans. Consumer Electron., Vol. 34 (1988), No. 1, pp. 205-227.

[22] Yamaguchi, N. et al.
Motion adaptive luminance signal/chrominance signal separation filter.
Applicant: Mitsubishi, 1994.
US Patent Application US5500686.

[23] Yamaguchi, N. et al.
Motion adaptive luminance signal and color signal separation filter.
Applicant: Mitsubishi, 1995.
US Patent Application US5541669.

[24] Yeong-Taeg, K. and L. Hyun-Kyu, H. Humor
A new 3-D Y/C separation algorithm using an edge-based spatial filter and a sub-temporal filter,
Digest of the ICCE'94, June 1994, pp. 352-353.

[25] Zon, K. van
Software TV system study on color decoding: NTSC and PAL decoding
Philips Research Laboratories Eindhoven, 1994.
Internal Report, NL-RWB-516-IR-94020.

Appendix A

Filters

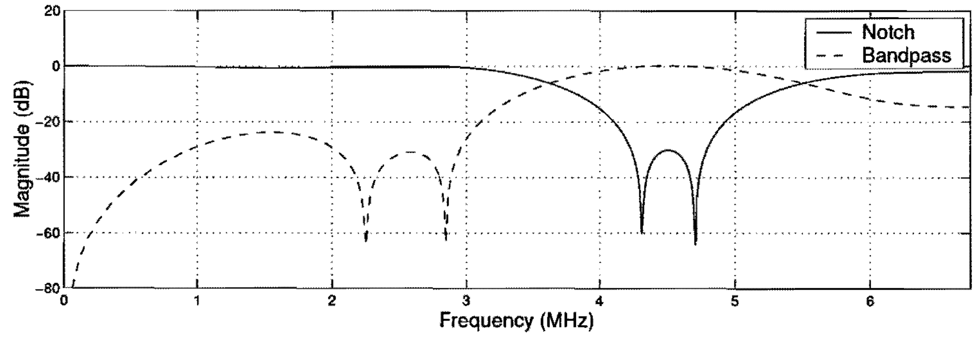

Figure A.1: Luminance notch and chrominance band-pass filter.

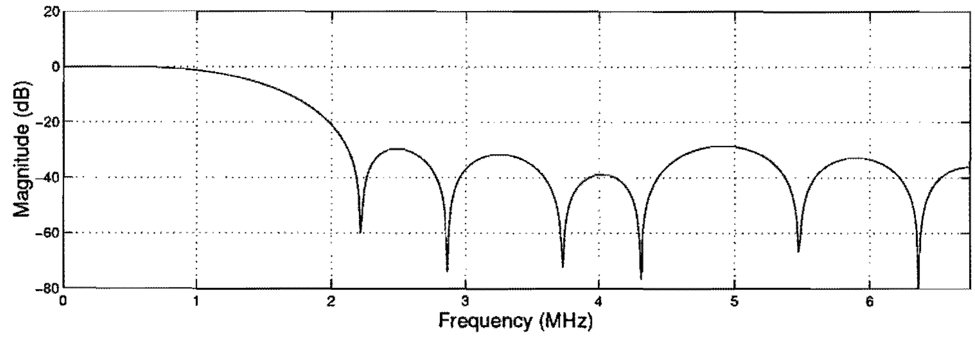

Figure A.2: U and V low-pass filter.

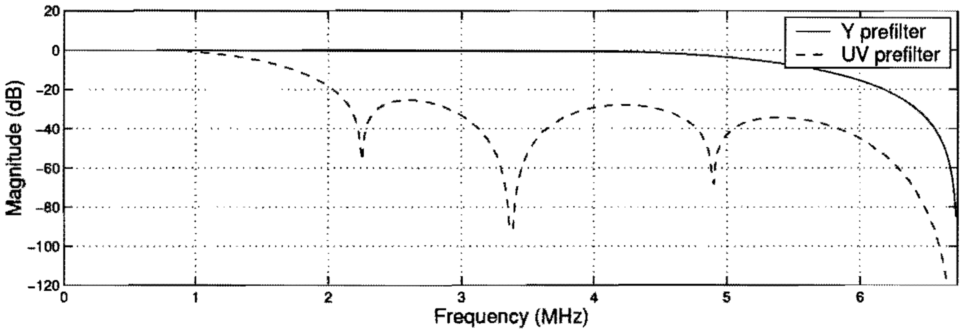

Figure A.3: Luminance and chrominance low-pass pre-filter.

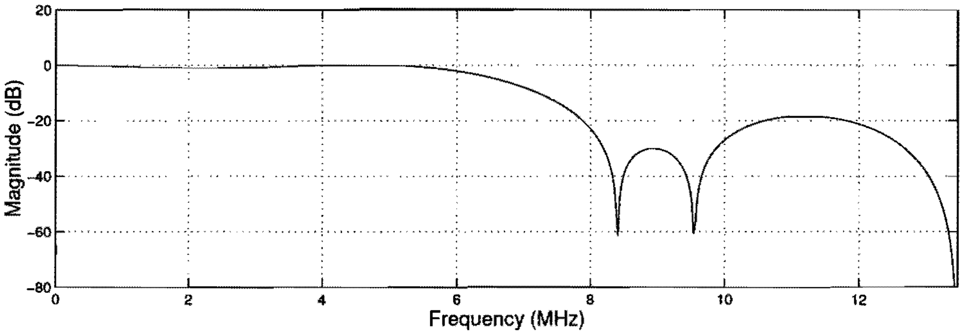

Figure A.4: CVBS up-sampling low-pass filter.

Filter type	Filter coefficients
Y notch	$\frac{1}{64}\cdot$[-2,3,4,-10,5,10,44,10,5,-10,4,3,-2]
C band-pass	$\frac{1}{64}\cdot$[2,-3,-4,10,-5,-10,20,-10,-5,10,-4,-3,2]
Y low-pass	$\frac{1}{64}\cdot$[-1,4,-8,12,50,12,-8,4,-1]
C low-pass	$\frac{1}{64}\cdot$[-1,-2,-1,1,5,10,13,14,13,10,5,1,-1,-2,-1]
U,V low-pass	$\frac{1}{256}\cdot$[-6,-6,-3,6,22,37,50,56,50,37,22,6,-3,-6,-6]
CVBS low-pass	$\frac{1}{32}\cdot$[2,0,-3,0,9,16,9,0,-3,0,2]

Table A.1: Filter coefficients.

Appendix B

Decoded *Moving zoneplate*

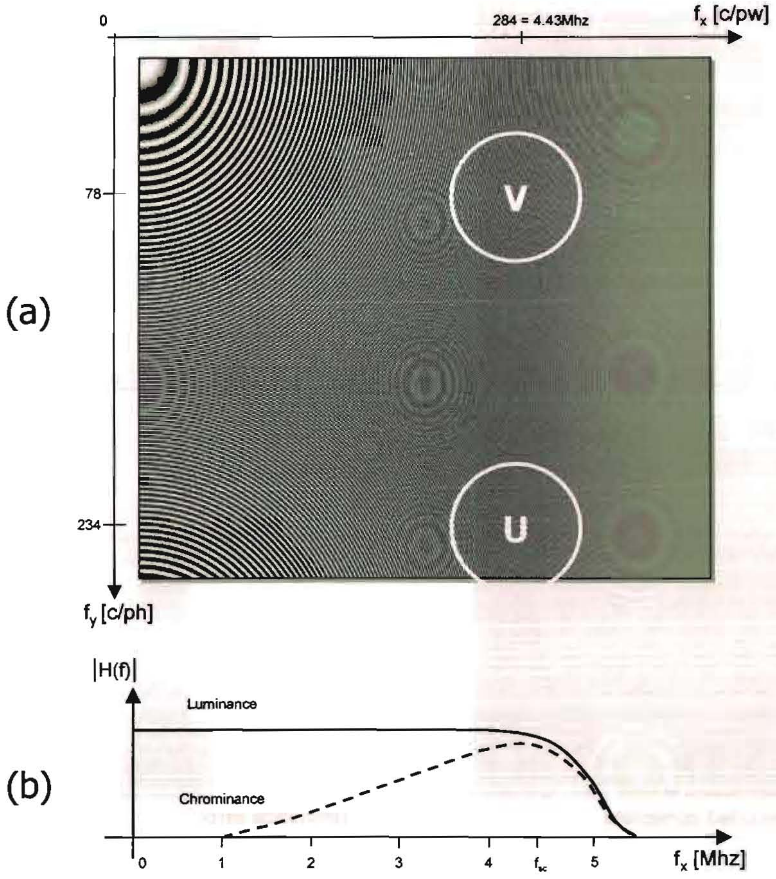
(a)
0
284 = 4.43Mhz
f_x [c/pw]
78
V
U
234
f_y [c/ph]
(b)
|H(f)|
Luminance
Chrominance
0
1
2
3
4
f_sc
5
f_x [Mhz]

Figure B.1: a) Location of chrominance components in original *Moving zoneplate*, and b) luminance and chrominance components of composite PAL signal.

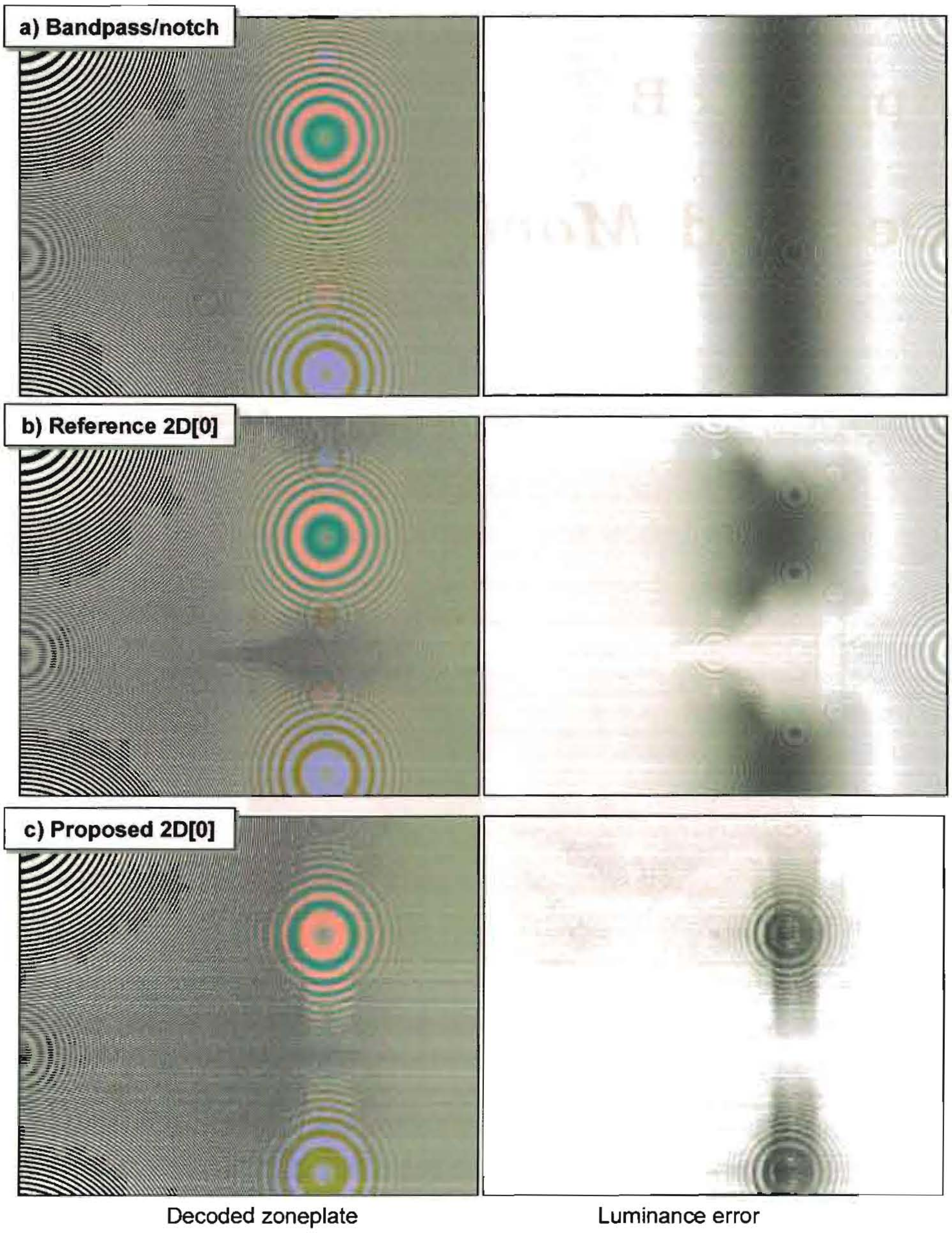
a) Bandpass/notch
b) Reference 2D[0]
c) Proposed 2D[0]
Decoded zoneplate
Luminance error

Figure B.2: Decoded *Moving zoneplate* of standard decoder and 2D comb-filters.

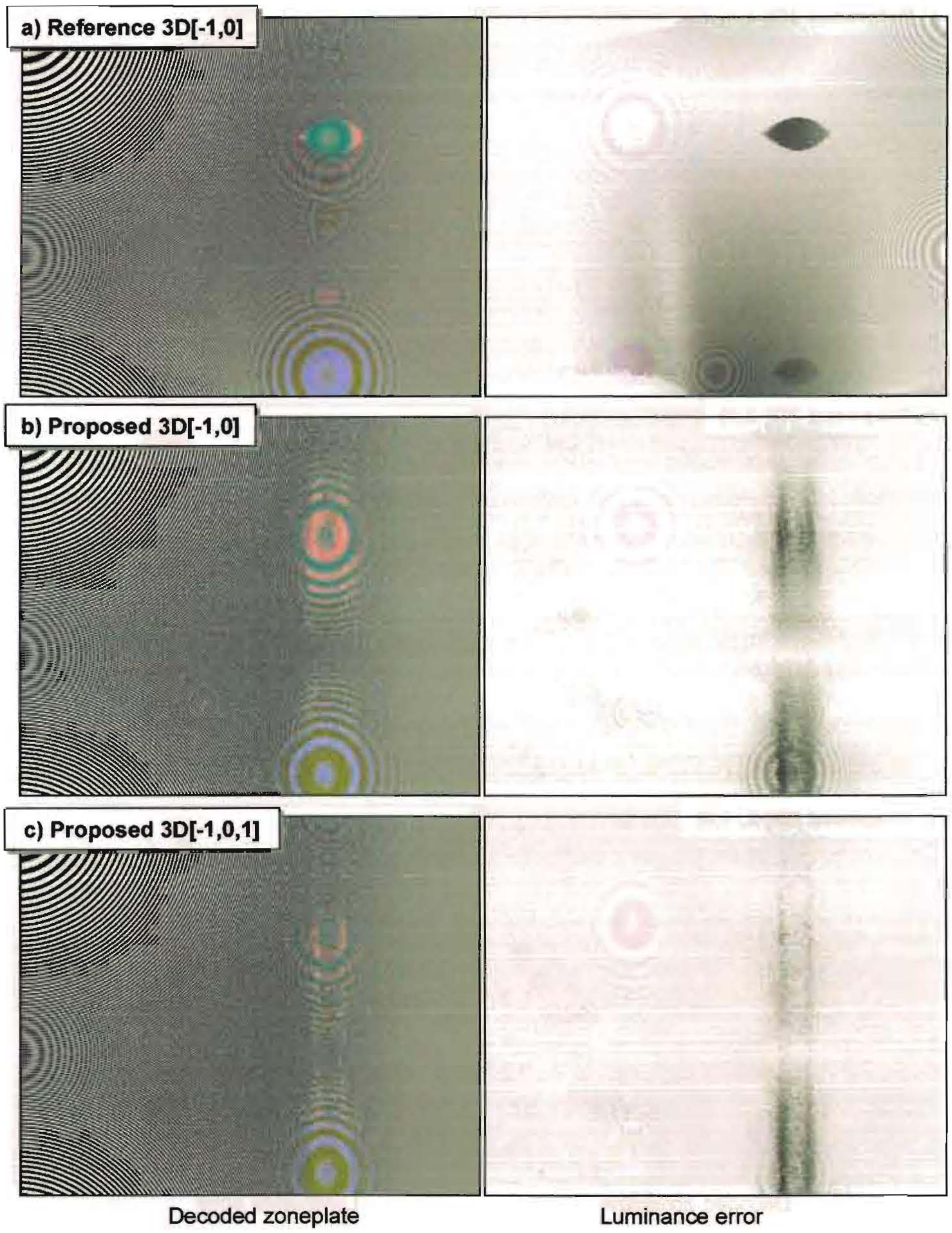
a) Reference 3D[-1,0]
b) Proposed 3D[-1,0]
c) Proposed 3D[-1,0,1]
Decoded zoneplate
Luminance error

Figure B.3: Decoded *Moving zoneplate* of field-based 3D comb-filters.

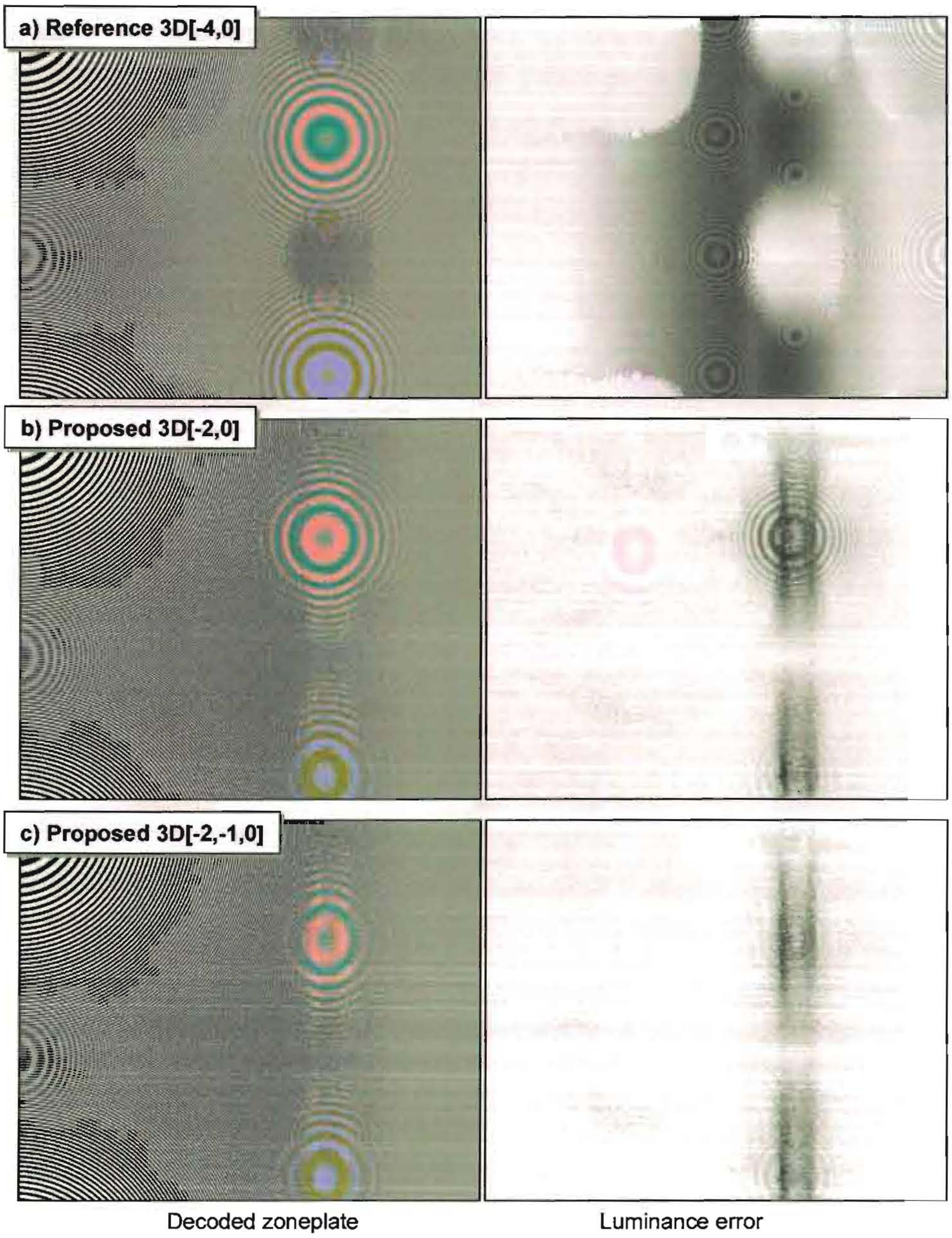
a) Reference 3D[-4,0]
b) Proposed 3D[-2,0]
c) Proposed 3D[-2,-1,0]
Decoded zoneplate
Luminance error

Figure B.4: Decoded *Moving zoneplate* of frame-based 3D comb-filters.

Appendix C

Literature research

The goal of the literature research was to obtain an overview of the different methods for Y/C separation. The focus was on so-called three dimensional comb-filters, i.e. methods that adaptively switch between spatial and temporal comb-filters. Also, literature describing further developments, as e.g. motion compensated comb-filters, was of particular interest. For that purpose, two search methods were applied, i.e. the snowball and the citation method.

C.1 Snowball method

The snowball method uses references to search for related literature. As starting points, references (1) and (2) were chosen. Both are recent publications discussing two different approaches to three-dimensional comb-filtering. The resulting diagram is depicted in Figure C.1, whereas the corresponding references are listed below.

1. Choi, S. and S. Kwon, H. Kim, Y. Kwon, Y. Ha
   Motion adaptive 3D Y/C separation algorithm using motion estimation and motion compensation,
   IEEE Trans. Consumer Electron., Vol. 47 (2001), No. 4, pp. 770-778.

2. Ding, Y. and X. Gao, K. Yi
   Effective simple Y-C separator for PAL and NTSC TV signals,
   Electron. Lett., Vol. 32 (1996), No. 5, pp. 426-428.

3. Yoshida, T. and K. Ashizawa, A. Nishihara
   Design and implementation of multidimensional Y-C separation filters for NTSC signals,
   IEEE Trans. Circuits Syst. Video Technol., Vol. 2 (1992), No. 4, pp. 373-380.

4. Dubois, E. and W.F. Schreiber
   Improvements to NTSC by multidimensional filtering,
   SMPTE J., Vol. 97 (1988), No. 6, pp. 446-463.

5. Teichner, D.
   Three-dimensional pre- and post-filtering for PAL TV signals,
   IEEE Trans. Consumer Electron., Vol. 34 (1988), No. 1, pp. 205-227.

6. Schreiber, W.F.
   Improved television systems: NTSC and beyond,
   SMPTE J., Vol. 96 (1987), No. 8, pp. 734-744.

7. Faroudja, Y. and J. Roizen
   Improving NTSC to achieve near-RGB performance,
   SMPTE J., Vol. 96 (1987), No. 8, pp. 750-761.

8. Strolle, C.H.
   Cooperative processing for improved NTSC chrominance/luminance separation,
   SMPTE J., Vol. 95 (1986), No. 8, pp. 782-789.

9. Teichner, D.
   Adaptive filter techniques for separation of luminance and chrominance in PAL TV signals,
   IEEE Trans. Consumer Electron., Vol. 32 (1986), No. 3, pp. 241-250.

10. Teichner, D.
    Quality improvement by adaptive inter-/intraframe processing in PAL TV receivers,
    IEEE Trans. Consumer Electron., Vol. 31 (1985), No. 3, pp. 226-239.

11. Dubois, E. and M.S. Sabri, J.Y. Ouellet
    Three-dimensional spectrum and processing of digital NTSC color signals,
    SMPTE J., Vol. 91 (1982), No. 4, pp. 372-378.

12. Turner, R.
    Some thoughts on using comb-filters in the broadcast television transmitter and at the receiver,
    IEEE Trans. Consumer Electron., Vol. 23 (1977), No. 3, pp. 248-257.

13. Drewery, J.O.
    The filtering of luminance and chrominance signals to avoid cross-colour in a PAL colour system,
    BBC Eng., Sept. 1976, pp. 8-39.

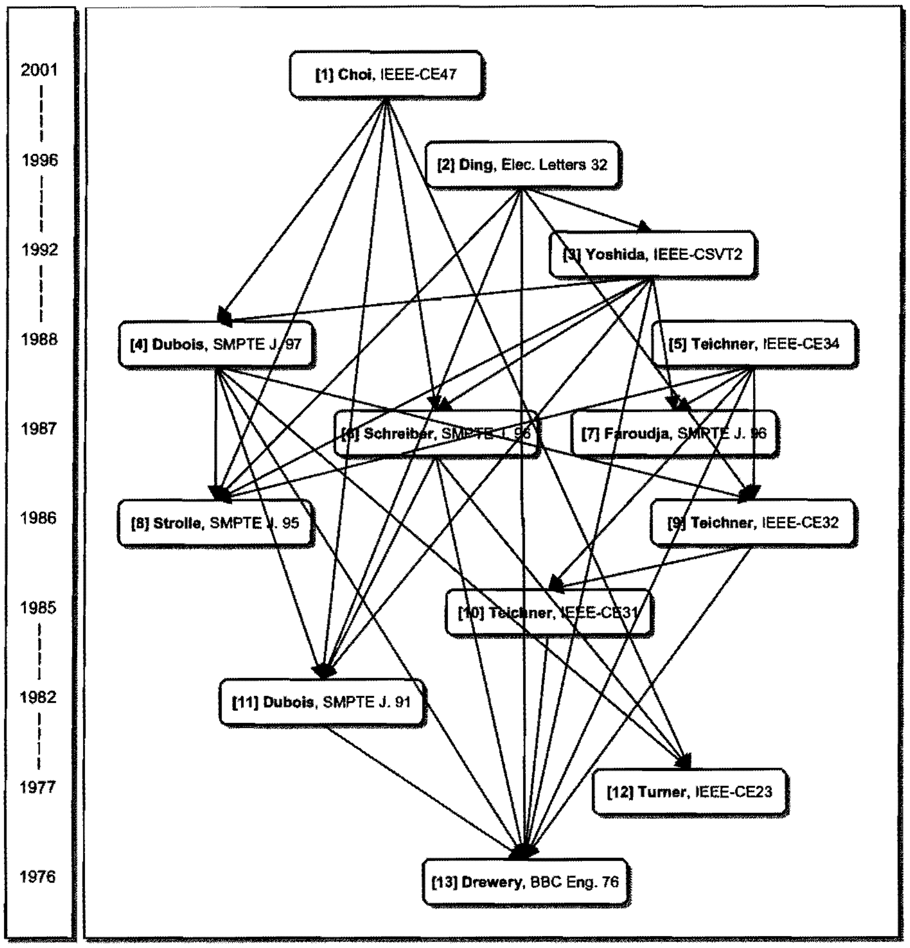
2001
1996
1992
1988
1987
1986
1985
1982
1977
1976
[1] Choi, IEEE-CE47
[2] Ding, Elec. Letters 32
[3] Yoshida, IEEE-CSVT2
[4] Dubois, SMPTE J. 97
[5] Teichner, IEEE-CE34
[6] Schreiber, SMPTE J. 96
[7] Faroudja, SMPTE J. 96
[8] Strolle, SMPTE J. 95
[9] Teichner, IEEE-CE32
[10] Teichner, IEEE-CE31
[11] Dubois, SMPTE J. 91
[12] Turner, IEEE-CE23
[13] Drewery, BBC Eng. 76

Figure C.1: Snowball method

C.2 Citation method

The citation method consists of finding newer papers referring to a given reference paper. As starting point, reference (1) was chosen, as it is a comprehensive publication discussing nearly all methods of comb-filtering known at the time. The resulting diagram is depicted in Figure C.2, whereas the corresponding references are listed below.

1. Teichner, D.
   Adaptive filter techniques for separation of luminance and chrominance in PAL TV signals,
   IEEE Trans. Consumer Electron., Vol. 32 (1986), No. 3, pp. 241-250.

2. Teichner, D.
   Three-dimensional pre- and post-filtering for PAL TV signals,

IEEE Trans. Consumer Electron., Vol. 34 (1988), No. 1, pp. 205-227.

3. Dubois, E. and W.F. Schreiber
   Improvements to NTSC by multidimensional filtering,
   SMPTE J., Vol. 97 (1988), No. 6, pp. 446-463.

4. Ito, S.E. and R. Lowlor, N. Ebihara
   Development of a crosstalk measurement type 3-dimensional digital color decoder,
   IEEE Trans. Consumer Electron., Vol. 39 (1993), No. 2, pp. 63-70.

5. Ito, S.
   A study of digital Y/C separation in NTSC or PAL color-television,
   IEEE Trans. Consumer Electron., Vol. 40 (1994), No. 4, pp. 963-968.

6. Taylor, K. and C. Careysmith, I. Goodwin
   A simulation environment utilizing 3-dimensional frequency-spectra for the analysis of television coding techniques,
   SMPTE J., Vol. 104 (1995), No. 11, pp. 735-741.

7. Ding, Y. and X. Gao, K. Yi
   Effective simple Y-C separator for PAL and NTSC TV signals,
   Electron. Lett., Vol. 32 (1996), No. 5, pp. 426-428.

8. Taylor, K. and D.P. Taylor
   Analyzing television coding techniques using three-dimensional signal analysis,
   IEEE Trans. Circuits Syst. II Analog Digit. Signal Process., Vol 46 (1999), No. 4, pp. 414-427.

9. Choi, S. and S. Kwon, H. Kim, Y. Kwon, Y. Ha
   Motion adaptive 3D Y/C separation algorithm using motion estimation and motion compensation,
   IEEE Trans. Consumer Electron., Vol. 47 (2001), No. 4, pp. 770-778.

C.3 Conclusions

The problem of Y/C separation is inherent to current backwards compatible color television standards. As such, literature discussing the problem and various basic approaches to resolving it started to appear in the early seventies.

As the quality and size of televisions increased, cross-color and cross-luminance artifacts became more visible. Hence, during the eighties, the amount of research and publications on Y/C separation increased as well.

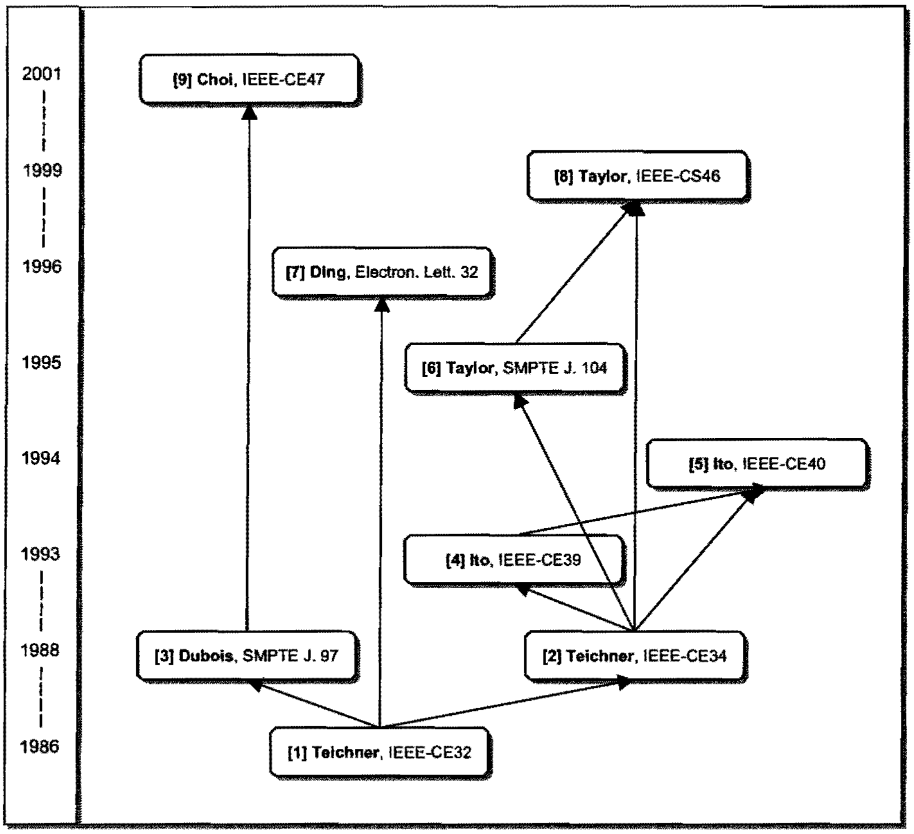
2001
1999
1996
1995
1994
1993
1988
1986
[9] Choi, IEEE-CE47
[8] Taylor, IEEE-CS46
[7] Ding, Electron. Lett. 32
[6] Taylor, SMPTE J. 104
[5] Ito, IEEE-CE40
[4] Ito, IEEE-CE39
[3] Dubois, SMPTE J. 97
[2] Teichner, IEEE-CE34
[1] Teichner, IEEE-CE32

Figure C.2: Citation method

During that period, the more advanced content- and motion-adaptive algorithms were developed. From then on until the late nineties, most publications were on the subject of alterations and improvements of existing adaptive algorithms.

Only recently, advances in technology made new methods of Y/C separation possible, of which motion-compensated comb-filtering is the most important example. As such, only one publication and one patent on the subject have been found, as well as an earlier graduation thesis on the feasibility of this type of comb-filtering.

As expected, most publications on the subject were either papers or patents. However, although many patents described algorithms which were not published in papers, they were mostly minor variations or improvements of methods more extensively described in other literature. In terms of books, only few publications of interest were found. The books included in the bibliography were recommended by research staff as good general background information on the television standard.